Frequency Stability Study of Interconnected Power Systems with High Penetration of Renewable Energy in the Restructured Environment: Emulation and Control of Virtual Inertia Using Intelligent Techniques

Anuoluwapo Oluwatobiloba Aluko

219071286

A thesis submitted to
the University of KwaZulu-Natal,
College of Agriculture, Engineering and Science,
in partial fulfillment of the requirements for the degree of

Doctor of Philosophy

Supervisor: Dr. Rudiren Pillay Carpanen
Co-Supervisor 1: Prof. David G. Dorrell
Co-Supervisor 2: Dr. Evans E. Ojo

School of Engineering

University of KwaZulu-Natal

April 2021

I, Anuoluwapo Oluwatobiloba Aluko , declare that:

(i) The research reported in this thesis, except where otherwise indicated, is my original research.

(ii) This thesis has not been submitted for any degree or examination at any other university.

(iii) This thesis does not contain other persons' data, pictures, graphs or other information, unless specifically acknowledged as being sourced from other persons.

(iv) This thesis does not contain other persons' writing, unless specifically acknowledged as being sourced from other researchers. Where other written sources have been quoted, then:

   a) their words have been re-written but the general information attributed to them has been referenced:

   b) where their exact words have been used, their writing has been placed inside quotation marks, and referenced.

(v) This thesis does not contain text, graphics or tables copied and pasted from the Internet, unless specifically acknowledged, and the source being detailed in the dissertation/thesis and in the References sections.

Candidate: Anuoluwapo Oluwatobiloba Aluko

Signature: ____________________________________

As the candidate's supervisors, we agree to the submission of this thesis

Supervisor: Dr. Rudiren Pillay Carpanen

Signature: ____________________________

Co-Supervisor 1: Prof. David G. Dorrell

Signature: ____________________________

Co-Supervisor 2: Dr. Evans E. Ojo

Signature: ____________________________

ABSTRACT

Frequency Stability Study of Interconnected Power Systems with High Penetration of Renewable Energy in the Restructured Environment: Emulation and Control of Virtual Inertia Using Intelligent Techniques

Anuoluwapo Oluwatobiloba Aluko
School of Engineering
Doctor of Philosophy

The main aim of power system operations and control is to ensure reliability and quality of power supply, a key action that helps in achieving this aim is frequency control. Frequency control in power systems is the ability to maintain the system frequency within specified operating limits, i.e., proper coordination between generation and load. The task of frequency control, more importantly, load frequency control (LFC) is becoming a complex control problem in the design and operation of modern electric power systems due to its growing size, changing market structure, newly emerging distributed renewable energy sources with little or no inertia support, evolving regulatory requirements and the increasing interconnectedness of power systems. These developments can lead to a reduction in the active overall inertia in the power system which reduces its frequency response capability by increasing the amplitude of frequency deviation, continuous frequency oscillations and increased settling time after a power mismatch in the system. The potential role of virtual inertia in the task of frequency control has been identified as an integral part of modern power systems. Therefore, in this thesis, novel methods for implementing virtual inertia using intelligent control techniques are proposed in the LFC framework of a multi-area interconnected system with high penetration of renewable energy in the deregulated environment. The first method proposes the novel application of the artificial bee colony (ABC) optimization algorithm in the design of the virtual inertial control in a grid-connected wind energy conversion system (WECS). The WECS operates below the maximum power point to reserve a fraction of active power for frequency response. The proposed ABC-based control method minimizes the first frequency undershoot and active power transients compared to the classical optimization method. Due to the non-storable and variable nature of renewable energy sources, the first method may not be accessible when needed. To tackle this challenge, the second method proposes the application of an energy storage system (ESS) and the type-II fuzzy logic control (FLC) in the development of the virtual inertia control strategy. The proposed type-II FLC method gives a better performance than the type-I FLC and derivative-based control methods with adaptive inertia gain, faster response time for active power injection/discharge, and damped frequency oscillations. Lastly, a novel hybrid LFC scheme is developed to further improve the dynamic response and stability of the system. The hybrid LFC scheme consists of a robust unknown input observer (UIO) for state estimation of the system in the presence of unknown inputs/disturbances, and the interval type-II FLC for the LFC loop. The robust UIO relays the true state of the system frequency to the LFC block in each control area to maintain its frequency and net tie line power flow at scheduled values. The proposed methods are designed and implemented using the MATLAB/Simulink Software.

Keywords: Artificial intelligence, dynamic state estimation, frequency control, fuzzy logic control, heuristic optimization, power system deregulation, power system stability, renewable energy, virtual inertia

PUBLICATIONS ARISING

Frequency Stability Study of Interconnected Power Systems with High Penetration of Renewable Energy in the Restructured Environment: Emulation and Control of Virtual Inertia Using Intelligent Techniques

Anuoluwapo Oluwatobiloba Aluko
School of Engineering
Doctor of Philosophy

Journal Papers

1. Anuoluwapo O. Aluko, David G. Dorrell, Rudiren Pillay Carpanen, and Evans E. Ojo. Heuristic optimization of virtual inertia control in grid-connected wind energy conversion systems for frequency support in a restructured environment. *Energies*, 13(3):564, 2020

2. Anuoluwapo O. Aluko, David G. Dorrell, Rudiren Pillay Carpanen, and Evans E. Ojo. A virtual inertia control method for high renewable energy-integrated interconnected power systems. *Energy Science and Engineering*, Submitted

3. Anuoluwapo O. Aluko, David G. Dorrell, Rudiren Pillay Carpanen, and Evans E. Ojo. Robust state estimation method for adaptive load frequency control of interconnected power system in a restructured environment. *IEEE Systems Journal*, Early Access:1–11, 2020

4. Anuoluwapo O. Aluko, Rudiren Pillay Carpanen, David G. Dorrell, and Evans E. Ojo. Real-time cyber attack detection scheme for stand-alone microgrids. *IEEE Transactions on Smart Grid*, Submitted

Conference Papers

1. Anuoluwapo O. Aluko, David G. Dorrell, Rudiren Pillay Carpanen, and Evans E. Ojo. Frequency control of modern multi-area power systems using fuzzy logic controller. In *IEEE PES/IAS PowerAfrica*, pages 645–649. IEEE, 2019

2. Anuoluwapo O. Aluko, David G. Dorrell, Rudiren Pillay Carpanen, and Evans E. Ojo. Heuristic secondary frequency control of AC/DC interconnected power system in a deregulated environment. In *International SAUPEC/RobMech/PRASA Conference*, pages 1–6. IEEE, 2020

3. Anuoluwapo O. Aluko, David G. Dorrell, Rudiren Pillay Carpanen, and Evans E. Ojo. Impact assessment and mitigation of cyber attacks on frequency stability of isolated microgrid using virtual inertia control. In *2020 IEEE PES/IAS PowerAfrica*, pages 1–5, 2020

4. Anuoluwapo O. Aluko, David G. Dorrell, Rudiren Pillay Carpanen, and Evans E. Ojo. Vulnerability analysis of false data injection attacks on the frequency stability of isolated microgrids. In *2021 Southern African Universities Power Engineering Conference/Robotics and Mechatronics/Pattern Recognition Association of South Africa (SAUPEC/RobMech/PRASA)*, pages 1–6, 2021

5. Anuoluwapo O. Aluko, David G. Dorrell, Rudiren Pillay Carpanen, and Evans E. Ojo. Real-time dynamic disturbance estimation of stand-alone microgrids based on unknown input observer for frequency regulation. In *IEEE PES/IAS PowerAfrica*, pages 1–5, Submitted 2021

ACKNOWLEDGMENTS

Firstly, I am thankful to **God** for his graciousness upon my life and for giving me the mental capacity and health to accomplish such a feat.

I would want to express my deepest gratitude to my supervisors; **Dr. R. Pillay Carpanen** for his guidance and constructive criticism that has been of tremendous advantages in my Ph.D. study; **Prof. David G. Dorrell** for his tutelage, patience, and great support throughout my Ph.D. study, it is a golden opportunity to work with him; and **Dr. Evans E. Ojo** for his immeasurable support and valuable comments that shaped my skills during the doctoral journey. I have garnered research finesse from their wealth of experience and professionalism.

It is my pleasure to acknowledge the bursary awards and travel grants received from the **UK Newton fund**, the **Eskom Power Plant Engineering Institute (EPPEI)**, and the **Council for Scientific and Industrial Research**.

My special thanks to my colleagues and postgraduate students **Adeniyi Onaolapo**, **Abayomi Adebiyi**, **Elutunji Buraimoh**, and **Oluwasegun Oladoyinbo** for their innumerable contributions and timely provision of solutions during the challenging times of my Ph.D. program.

My sincere gratitude goes to my family; parents–**Mr. and Mrs. Adebayowa Aluko**, siblings–**Titilayo, Oluwapelumi**, and **Peter Aluko**; cousins–**Amuda Akeem, Amuda Adeniyi** and **Olugbenle Oluwatoyin**; whose words of encouragement and prayers kept me going throughout my Ph.D. journey.

Finally, I would like to extend my appreciation to my friends; **Tade Ayodeji**, **Akinwoye Tosin**, and **Olushola Elijah**; who have been supportive during the period of my Ph.D. study.

ACRONYMS

ABC	Artificial bee colony
ACE	Area control error
ACO	Ant colony optimization
AGC	Automatic generation control
ANN	Artificial neural network
CGU	Conventional generating unit
CPM	Contract participation matrix
DISCO	Distribution company
DE	Differential Evolution
DFIG	Doubly fed induction generator
DU	Distribution utility
ESS	Energy storage system
FLC	Fuzzy logic control
FOU	Footprint of uncertainty
FS	Fuzzy set
GA	Genetic algorithm
GENCO	Generation company

GSC	Grid side converter
HVAC	High voltage alternating current
HVDC	High voltage direct current
ISO	Independent system operator
IPP	Independent power producer
IT2/II FLC	Interval type-2/II fuzzy logic control
LMF	Lower membership function
LFC	Load frequency control
MF	Membership function
MPPT	Maximum power point tracking
MSC	Machine side converter
NP	Nectar position
PI	Proportional integral
PMSG	Permanent magnet synchronous generator
PSO	Particle swarm optimization
RE	Renewable energy
REP	Renewable energy plant
SFC	Secondary frequency control

SMC	Sliding mode control
T1FLC	Type-1 fuzzy logic control
TRANSCO	Transmission company
UIO	Unknown input observer
UMF	Upper membership function
VIU	Vertically integrated utility
VSC	Voltage source converter
VSG	Virtual synchronous generator
WECS	Wind energy conversion system

Contents

References **i**

Table of Contents **xi**

List of Figures **xvi**

List of Tables **xx**

1 Introduction **1**

1.1 Background 1

1.2 Problem Statement 3

1.3 Aim and objectives 4

1.4 Contributions of Thesis 5

1.5 Thesis structure 7

2 Frequency Response Modeling of an Interconnected Power System **8**

2.1 Chapter Introduction 9

2.2 Traditional power system 10

2.2.1 Frequency control 11

2.2.2 Primary frequency control 12

2.2.3 Secondary frequency control 13

2.3 Conventional generation system 14

2.3.1 Speed governor model 14

2.3.2 Turbine model 16

2.3.3 Power grid model 17

2.4 Multi-area interconnected power system 17

2.4.1 Frequency response modeling of HVAC transmission line 18

2.4.2 Frequency response model of the HVDC transmission line 20

2.5 Load frequency control 24

2.6 Modern power system 26

2.6.1 Power system deregulation 26

2.6.2 Integration of renewable energy 28

2.6.3 Impact of inertia on frequency response 30

2.6.4 Frequency response of wind energy conversion systems 32

3 Heuristic Optimization of Virtual Inertia Control in Grid-Connected Wind Energy Conversion Systems for Frequency Support in a Restructured Environment 35

3.1 Chapter Overview 36

3.2 Chapter Introduction 36

3.3 Small-Signal Model of Interconnected Power System in a Restructured Environment 43

3.4 Derivative Control Strategy in Grid-connected Wind Energy Systems for Frequency Support . . . 48

3.5 Artificial Bee Colony Optimization Algorithm . . . 52

3.6 Results and Discussions . . . 56

3.6.1 Eigenvalue Analysis . . . 57

3.6.2 Load–Frequency Analysis . . . 59

3.7 Summary . . . 71

4 A Virtual Inertia Control Method for High Renewable Energy-Integrated Interconnected Power Systems 72

4.1 Chapter Overview . . . 73

4.2 Chapter Introduction . . . 73

4.3 System Modelling . . . 78

4.3.1 Dynamics of Power System Deregulation . . . 78

4.3.2 Small-Signal Modelling of Modern Power System . . . 79

4.4 Inertia Control . . . 83

4.4.1 Concept of Inertia . . . 83

4.4.2 Virtual Inertial Control . . . 84

4.4.3 Type-II Fuzzy Logic System . . . 86

4.4.4 Artificial Bee Colony Algorithm . . . 89

4.5 Adaptive Virtual Inertia Based on Type-II Fuzzy Logic Control . . . 91

4.6 Simulation and Discussion . . . 94

4.6.1 Stability Analysis . . . 95

4.6.2 Load variation . . . 97

4.6.3 High renewable energy fluctuation . . . 99

4.6.4 Parameter variation . . . 101

4.7 Summary . . . 104

5 Robust State Estimation Method for Adaptive Load Frequency Control of Interconnected Power System in a Restructured Environment 105

5.1 Chapter Overview . . . 106

5.2 Chapter Introduction . . . 106

5.3 System Modelling . . . 110

5.3.1 Dynamics of power system restructuring . . . 110

5.3.2 LFC modelling in a restructured environment . . . 111

5.4 Proposed Methodology . . . 115

5.4.1 Unknown Input Observer . . . 115

5.4.2 Design Procedure of Robust UIO . . . 118

5.4.3 Interval Type-2 Fuzzy Logic Control . . . 119

5.5 Interval Type-2 Fuzzy-UIO in LFC problem . . . 122

5.6 Simulation . . . 124

5.6.1 Eigenvalue analysis . . . 125

5.6.2 Demonstration of the Robust UIO Model . . . 125

5.6.3 Estimation and Control of Unknown load variation . . . 129

5.6.4 Performance during parametric variations . . . 134

5.6.5 Comparison with other control methods 135
5.7 Summary 136

6 Conclusion and Future Work 138

6.1 Main findings and conclusion 138
6.2 Future work 141

References 142

A Simulation Parameters for Chapter 3 170

B State Matrix for system in Chapter 3 171

List of Figures

2.1 A typical conventional power system [10]. 11

2.2 Frequency control classification. 12

2.3 Primary frequency control (Droop control). 13

2.4 Comparison of primary and secondary frequency control. 14

2.5 Schematic diagram of a speed governor system. 15

2.6 Small-signal model of a speed governor. 15

2.7 Schematic diagram of a steam turbine. 16

2.8 Small-signal model of turbine. 16

2.9 Small-signal model of a power system [11]. 18

2.10 Representation of HVAC interconnected power system. 19

2.11 Frequency response model of an interconnected power system via the AC transmission line. 21

2.12 Two-area HVDC interconnected power system. 22

2.13 Block diagram of first-order HVDC system. 23

2.14 Small-signal model of HVDC system [12]. 23

2.15 A hybrid AC/DC frequency response model. 25

2.16 PMSG-based wind energy conversion system [13]. 33
2.17 Small-signal model of WECS 34

3.1 Classification of frequency control techniques in wind energy systems. 40
3.2 System model. 44
3.3 Frequency response model of a two area power system in a deregulated environment. 45
3.4 Dynamics of deregulation contract. 46
3.5 Frequency deviation comparison of AC and AC/DC systems. 48
3.6 Grid-connected PMSG WECS. 49
3.7 Modified control scheme of MSC. 50
3.8 Derivative control loop for WECS. 51
3.9 Flowchart of ABC optimization algorithm. 55
3.10 Eigenvalue plot of two systems. 59
3.11 Frequency deviation in a Poolco transaction. 61
3.12 Change in power generation of GENCOs in a Poolco transaction. 62
3.13 Tie line power flow in a Poolco transaction. 63
3.14 Frequency deviation in bilateral transaction. 64
3.15 Change in power generation of GENCOs in bilateral transaction. 65
3.16 Tie line power flow in a bilateral transaction. 66
3.17 Frequency deviation in contract violation. 67
3.18 Active power generation of GENCOs in contract violation. 68
3.19 Tie line power flow in contract violation. 69

3.20 Wind power fluctuation. 70

3.21 Frequency deviation during wind power fluctuation. 70

4.1 Frequency response model of a power system in the restructured environment. . . . 80

4.2 Small signal model of virtual inertia strategy. 85

4.3 Block diagram of type-II fuzzy logic system. 86

4.4 Symmetrical triangular type-II fuzzy set. 88

4.5 Flowchart of ABC optimization algorithm. 90

4.6 Proposed virtual inertia control strategy. 91

4.7 Type-II Fuzzy membership functions. 92

4.8 Two-area test system model. 95

4.9 (a) Frequency deviation in Area 2 (b) rate of change of frequency deviation in Area 2 under step load variation. 98

4.10 Frequency deviation in Area 1 under step load variation in Area 2. 98

4.11 Output power of ESS under step load variation. 99

4.12 Net fluctuation in RE power in Area 2. 99

4.13 (a) Frequency deviation in Area 2 (b) rate of change of frequency deviation in Area 2 under RE fluctuation. 100

4.14 (a) Output power of ESS (b) Virtual inertia gain under RE fluctuation. 101

4.15 (a) Frequency deviation in Area 2 (b) rate of change of frequency deviation in Area 2 under parametric variation. 102

4.16 (a) Output power of ESS (b) Virtual inertia gain under parametric variation. 103

5.1 Block diagram of LFC model in a restructured environment 112

5.2 Block diagram of unknown input observer 116

5.3 Fuzzy logic system (a) Type-1 (b) Type-2 120

5.4 Proposed Fuzzy-based LFC for Robust UIO model 122

5.5 Fuzzy logic membership function (a) Type-1 (b) Type-2 124

5.6 Area 1 plot (a) frequency deviation (b) active power deviation in GENCO 1 (c) active power deviation in GENCO 2 128

5.7 Area 2 plot (a) frequency deviation (b) active power deviation in GENCO 3 (c) active power deviation in GENCO 4 129

5.8 Frequency estimation error in Areas 1 and 2 130

5.9 Plots of frequency deviation 130

5.10 Plot of GENCOs response to unknown input 131

5.11 Plot of frequency response in Area 1 133

5.12 Plot of frequency response in Area 2 134

5.13 Plot of frequency response during parametric variations 135

List of Tables

3.1 ABC Algorithm Parameters. 56

3.2 Comparison of Eigenvalues. 58

3.3 Comparison of Total Damping. 59

4.1 Fuzzy Rule Table 93

4.2 Optimal weights of the proposed strategy 94

4.3 Eigenvalues of System Model 96

5.1 Fuzzy rules 123

5.2 Eigenvalues 126

5.3 Comparison of proposed method with other control methods 136

A.1 System model parameters. 170

Chapter 1

Introduction

1.1 Background

Power system stability as defined in [14] is "the ability of an electric power system, for a given initial operating condition, to regain a state of operating equilibrium after being subjected to a physical disturbance, with most system variables bounded so that practically the entire system remains intact". The primary objective of power system operation and control is to supply quality and reliable power to consumers while maintaining the system's stability. Traditionally, the major operations and controls of generation, transmission, and distribution are monitored by a central utility. Under this regulated environment, conventional plants (power producers) such as coal, steam, and gas-powered plants use synchronous generators that are resilient during and after significant transient faults, the power flow is scheduled and the uncertainties in load fluctuations are minimal. Therefore, classical controllers are efficient in maintaining the stability of the system.

The increasing demand for electrical power, depletion of fossil fuels, need to reduce environmental pollution from greenhouse gases emission, and changing government policies, has led to the exploitation of renewable energy sources such as wind, solar, and hydro, for the generation of electricity and rapid development of renewable energy industry [15]. Globally, renewable energy sources make up about 26% of electricity generation as of 2019, this is expected to rise to 30% in 2024, with wind and solar projects playing a significant part [16]. This presents new technical challenges in the operation and control of the power system because their dynamic behavior is different from the convention generating system. Also, the changing market framework (deregulation) of the power system brought about by the decentralized ownership of generation, transmission, and distribution utilities have introduced new challenges to the operation and control of the power system. This has been characterized with several blackouts that have occurred in different parts of the world in recent years [17–20]; Iran (Spring 2001 and 2002), USA/Canada (August 2003), Sweden/Denmark (September 2003), Italy (September 2003), Russia (May 2005), India (July 2012), Thailand (May 2013) and UK (August 2019); these blackouts reiterated the need to redesign and improve the existing control systems to guarantee a more secure and reliable power system.

From the frequency control viewpoint, frequency instability is the failure of the power system to restore the system's frequency to its nominal operating limits after a mismatch between power generated and load demanded [21]. In today's power system, the problem of frequency control is becoming more complex and prevalent because of the active power fluctuation associated with renewable energy sources, reduction of inertia caused by increased grid-interfaced power electronic devices, demand stochasticity, and improper coordination of the deregulated power system environment. Traditionally, frequency control is classified as primary, secondary, tertiary, and emergency control, depending on the amplitudes and duration of the deviation [22]. The primary frequency control is deployed locally in the speed governing mechanism of the individual generating unit, the secondary frequency control is utilized as a central control technique for generating units within a control area to restore the system to its nominal frequency (e.g 50Hz for South Africa) and maintain tie line power flow between interconnected control areas, the tertiary and emergency frequency control are the slowest levels of control usually triggered for economic dispatch and unit commitment [23]. It is imperative to mention that the phrase 'frequency control' used in this thesis is focused on the secondary frequency control level whose boundary of operation can be studied using small-signal models. The classical frequency control schemes may be difficult to use in the modern power system, which includes separate power producers, renewable energy sources, distribution utilities, and in a deregulated environment, as compared to the vertically integrated utility of the traditional power system environment. Laden with these new tasks, novel control schemes is needed to provide virtual or synthetic inertia, carry out frequency control tasks, maintain efficiency and robustness, and assert reliability.

This thesis analyses the impacts of adopting intelligent control techniques for virtual inertia and frequency controls, and the combined effect of both on the frequency response of a multi-area power system with high penetration of renewable energy systems in the restructured power system environment.

1.2 Problem Statement

The technical issues, specifically active power and frequency control, associated with the increasing penetration level of renewable energy and power system deregulation in the modern power system sector are the underlying factors that motivated this research work.

The ongoing restructuring or deregulation in the power system sector has changed the mode of planning, operation, and control of the electrical power system. It has provided the freedom for market participants to transact without involving the grid operators, thereby increasing the number of inter-area power contracts. This has led to a rise in the unpredictability of load changes/fluctuations, poor coordination between control areas, and other disturbances that create large frequency deviations affecting the steady-state operation of the power system.

Furthermore, the reduction of traditional synchronous generators and increasing penetration of renewable energy is contributing to the frequency control problem in today's power system. The renewable energy sources, mainly wind and solar, are intermittent, thus, their contribution to electricity needs cannot be accurately predicted. Also, the absence of rotating parts in solar plants and the application of power electronics for interfacing in wind energy conversion systems electronically decouple the renewable energy systems from the grid. Hence, the inertia per unit of active(online) generation in the power system is reducing. It is therefore acknowledged that, in the area of frequency control, the non-despatchable nature of renewable sources and shortage of inertia are regarded among the most technical issues that introduce serious problems of instability in a power system with high renewable energy penetration.

These technical challenges created by power system deregulation, as well as the increasing penetration of renewable energy system, therefore pose great challenges to the safe, stable and reliable operation of the grid, and become difficult for classical controllers to perform optimally outside the operating conditions for which they are designed. Consequently, there is a need to develop novel frequency control techniques and new methods to add virtual inertia, that are robust to handle uncertainties and improve the dynamic performance of the power system in the new environment.

1.3 Aim and objectives

This thesis aims to investigate the application of intelligent control schemes in the frequency control problem to improve the stability of interconnected multi-area power systems with high penetration of renewable energy in the new(restructured) power system environment. The proposed control schemes are adopted in the design of virtual inertia controllers to increase the nadir of the system frequency deviations and improve the response of the load frequency controller during contingencies that trigger frequency events. Based on the aforementioned concepts, the objectives of this thesis are:

1. To model and simulate the small-signal model of a two-area network interconnected via HVAC and HVDC transmission lines in the restructured power system environment.
2. To design a virtual inertia control strategies that improve the frequency response of the system during contingencies such as load variations and renewable energy fluctuations by developing advanced and intelligent control strategies for inertia emulation in renewable energy systems and energy storage systems.
3. To design a dynamic state estimation method to provide real-time information on system states, and detect the presence of unknown inputs.
4. To evaluate the robustness of the proposed control strategies under varying operating conditions by investigating the response time, settling time, damping oscillation characteristics and reduction in frequency deviation amplitude.

1.4 Contributions of Thesis

- Developing a derivative-based virtual inertial controller for a grid-connected wind energy conversion system to provide short-term active power during frequency events. The parameters of the proposed virtual inertia controller are heuristically determined using the artificial bee colony optimization algorithm. This contribution has been published in [1].

- Adopting an energy storage system for the inertia emulation due to the variable nature of renewable energy sources. The interval type-2 fuzzy logic control is used to design the virtual inertia control loop, to improve the frequency response of a power system with a high penetration of renewable energy sources. The scaling factors of the interval type-2 fuzzy logic control are tuned using the artificial bee colony algorithm. The proposed virtual inertia control strategy can handle uncertainties in model parameters, renewable energy fluctuation, and demand variation that pose challenges to the power industry. This contribution has been presented in [2].

- Developing a novel robust state estimation method based on an unknown input observer for online state estimation of the power system without prior knowledge of a disturbance to generate an appropriate input control signal to the load frequency controller. The interval type-2 fuzzy logic control strategy is used to design the load frequency control loop. The virtual inertia control is considered in the system modeling, the proposed hybrid control scheme is robust to handle unknown inputs that pose a threat to the frequency stability of the system and provide real-time information on the system state. This contribution has been published in [3].

- The proposed intelligent control strategies are independent of the system parameters and easy to implement; therefore, they can be effectively used in different system configurations. The proposed framework is beneficial to large and complex power systems because of the increasing renewable energy penetration where traditional load frequency control frameworks and control schemes cannot provide efficient performance over a wide range of unknown operating conditions.

1.5 Thesis structure

The remainder of this thesis comprises of five chapters that are structured as:

- Chapter 2 provides the theoretical background of the thesis. It covers the mathematical modeling of power system elements for small-signal analysis in the traditional and restructured power system environment, presents the issues affecting frequency stability in modern power systems considering inertia and renewable energy integration.
- Chapter 3, which has appeared in [1], deals with the design of a heuristically-tuned virtual inertia controller for grid-connected wind energy systems in the restructured environment. It presents the mathematical model of the artificial bee colony optimization algorithm as a tool to tune the design parameters of the virtual inertia controller.
- Chapter 4, which has appeared in [2], provides the details in the design of a novel virtual inertia controller using an intelligent control strategy–interval type-2 fuzzy logic control– and heuristically tuning the design parameters of the controller as above. It presents the mathematical modeling of the fuzzy logic control and its application to frequency control problem in the restructured power system environment with high penetration of renewable energy.
- Chapter 5, which has appeared in [3], presents the design of a dynamic state estimation scheme using the unknown input observer method. It also presents the modeling of a type-2 fuzzy logic load frequency controller. The hybrid control scheme is implemented and validated under various operating conditions in a restructured power system environment.
- Chapter 6 is the concluding chapter. It gives the conclusion from the work carried out in this thesis and highlights recommendations for future works.

Chapter 2

Frequency Response Modeling of an Interconnected Power System

2.1 Chapter Introduction

The electrical power system consists of a diverse range of parts systematically interconnected together to form a large-scale, intricate, nonlinear, and high-order multivariate system capable of generating, transmitting, and distributing electricity across a wide area [24]. Load variability and other types of disruption in power system operations lead to a variety of complex anomalies that manifest themselves at various time frames due to the differences in the dynamics of the elements that make up the power system. In real-world power systems, there is usually an interlink between these time frames since one disturbance may lead to another. However, distinguishing between these time frames is relevant in understanding disturbance and developing appropriate control and safety procedures.

Power system analyses have revealed that an instantaneous variance between the combined mechanical input power and the combined electrical output power of grid-synchronized generators causes their rotors to accelerate or decelerate and thus deviating from the system nominal frequency. That is, the reduction in their angular speed (excess electrical output power) or increment (deficiency in the electrical output power) that results in a decrease or increase in frequency is due to the direct proportionality between angular speed and frequency. Conventionally, in a generating unit, the input power (mechanical) is synonymous with active power production, and the output power (electrical) is basically what system loads absorb. Therefore, the frequency control problem is traditionally interpreted as the speed control problem of the generating units. To ensure stable and reliable operation of the power system, and supply quality power, the power generated must accurately meet the load demand at every instant of time. Depending on the duration of the frequency deviation, more than one control loop may be required to restore the system frequency of the power system to its nominal value [25].

Real-time frequency control systems should be simple, robust, and reliable, however, the empirical method to determine the control parameters is by software simulation. The magnitude of the disturbance involved is a cardinal factor in the design of control systems (to improve system stability and reliability), particularly with regard to modeling details. In general, disturbances affecting power systems are categorized into small-signal disturbance and large-signal disturbance. The severity of system disturbances studied in the small-signal analysis is one in which the phenomena of interest can be investigated through linearization of the system's mathematical models, whilst in the large-signal analysis (mainly extreme disturbance whose impact may prompt protections), the system's nonlinear properties must be taken into consideration in the system equations [26]. The work in this thesis, frequency response, and control is based on the small-signal analysis in which linearized models are applicable and the nonlinear dynamics/coupling effects are neglected.

2.2 Traditional power system

In the traditional power system, the operations of the utilities are specifically supervised by the government. It is a regulated environment that maintains a vertical structure, taking into account the generating units, transmission systems, and distribution utilities. The vertical utility sells power to customers at regulated prices. The generating units mostly use conventional sources (fossil fuel, coal, nuclear, etc.) as a primary source for base power generation. The generated power is usually transmitted to the load centers via high voltage overhead(underground) transmission lines [27]. The Figure 2.1 represents the typical example of a thermal-powered conventional power system.

In the traditional power system environment, ancillary services, which are defined as individual elements of electrical services that are needed to provide adequate support for optimal power supply, reliable distribution of high-quality power, satisfactory and secure operation of the system, are supervised by the state-owned utility [28]. The major elements of the ancillary services are voltage

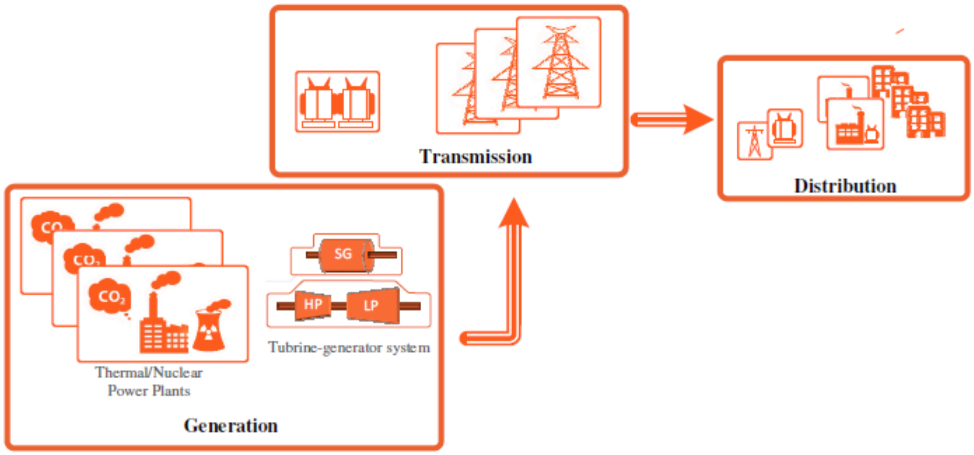

Figure 2.1 A typical conventional power system [10].

control, frequency control, active and reactive power control, and reserve capacities [29]. In this thesis, the main focus is the active power and frequency control.

2.2.1 Frequency control

A mismatch between the aggregated electrical loads and the total power supplied by the generating units causes the electrical power system to deviate from the nominal operating frequency. Continuous frequency deviations affect the power system stability, security, reliability, and efficiency [30]. In a generating unit, since the frequency is directly proportional to the rotational speed of the generator, the task of frequency control can be directly linked to the speed control of the generator. This is traditionally achieved by using a speed governing mechanism that modifies the position of the valve to change the mechanical power to track the load offset and return the frequency to nominal value [31]. There are various classifications of frequency control that are dependent on the frequency deviation range and duration of frequency deviation as shown in Figure 2.2. During steady-state or normal operation, the primary frequency control can attenuate small frequency deviations but cannot restore the system frequency to the nominal value, rather, a new steady-state operating point is reached. For larger and prolonged deviations, the secondary frequency control can restore the system to nominal operating conditions depending on the available power reserve. However, for much more large deviations, the tertiary and emergency frequency controls are activated to protect the system from cascaded faults, loss of synchronization, and blackouts through under-frequency load shedding (UFLS) and reserve power from large scale energy storage systems. In power system operations, demand fluctuations occur mostly throughout the day due to demand prediction errors, and because electricity cannot be easily stored in large quantities, therefore, an active and continuous frequency regulatory scheme is needed to maintain system balance on an ongoing basis.

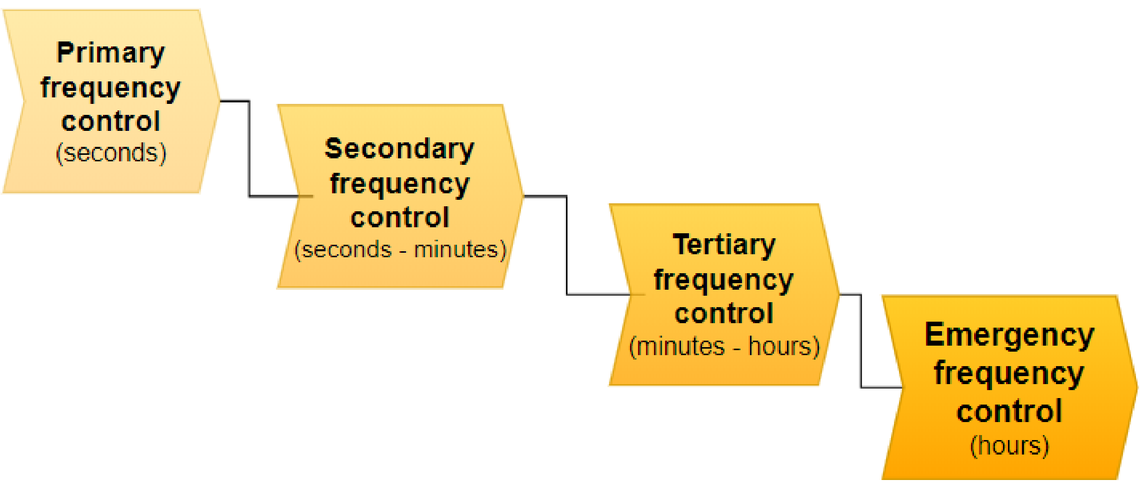

Figure 2.2 Frequency control classification.

2.2.2 Primary frequency control

The primary frequency control is the first response of the conventional generators to a frequency deviation. It also known as a droop control mechanism, usually working within seconds to tens of seconds, it is the local operation of turbine control systems in power generating plants and its role is to rapidly reject unwanted load disturbances and maintain the frequency close to the nominal value by changing the set-point of the speed governor as shown in Figure 2.3. This droop method enables the active generators to automatically change their outputs (increase/decrease) and to share the load deviation collectively at a common frequency [32]. Since the primary frequency control is a proportional control technique, it leaves some frequency offset. Therefore, supplementary control action is necessary to return the frequency to its nominal value which is the purpose of the secondary control of frequency as shown in Figure 2.4.

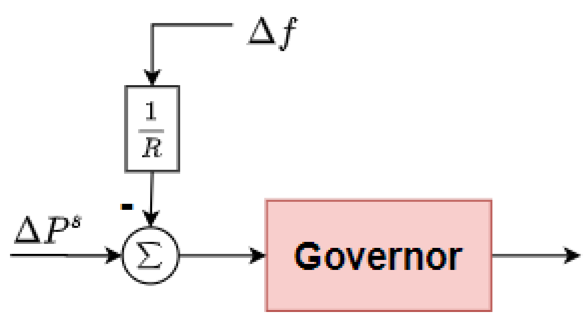

Figure 2.3 Primary frequency control (Droop control).

2.2.3 Secondary frequency control

The primary frequency control cannot restore the system frequency to its nominal value, therefore a secondary control is employed to complement the droop control by providing additional feedback [33]. The control strategy is mostly an integral-type control strategy, it is usually sufficient to generate the appropriate signal that tracks the load change/power imbalance and drives the system to nominal frequency or zero steady-state frequency error [34]. For multi-area power systems interconnected together, the secondary frequency control must regulate the tie line power at scheduled values, this would be formulated in the later section of this chapter.

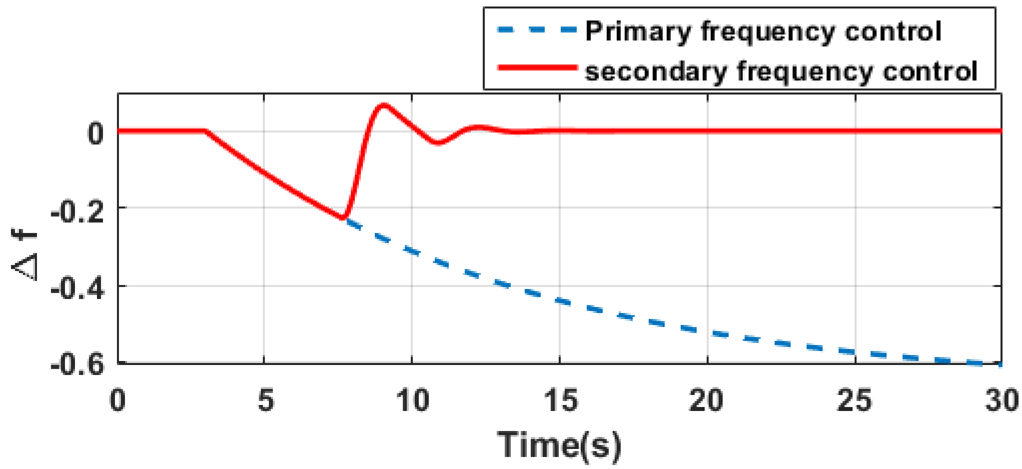

Figure 2.4 Comparison of primary and secondary frequency control.

2.3 Conventional generation system

The conventional generation system is an arrangement of various subsystems working together to generate electric power at specified frequency and voltage from conventional energy sources such as coal, oil, gas, etc. The subsystems usually consist of a generator, turbine, governing unit, cooling units, transformers, and protective devices. However, for frequency response analysis, only the small-signal model of the speed governor and turbine subsystems are necessary [35].

2.3.1 Speed governor model

For frequency response analysis, the slow boiler dynamics are neglected when representing the speed governor model of a steam-based power generation system. The block diagram in Figure 2.5

shows the schematic of the speed governing system of a steam turbine generating unit. Based on the speed deviation, the valve position is adjusted to allow steam flow into the steam turbine.

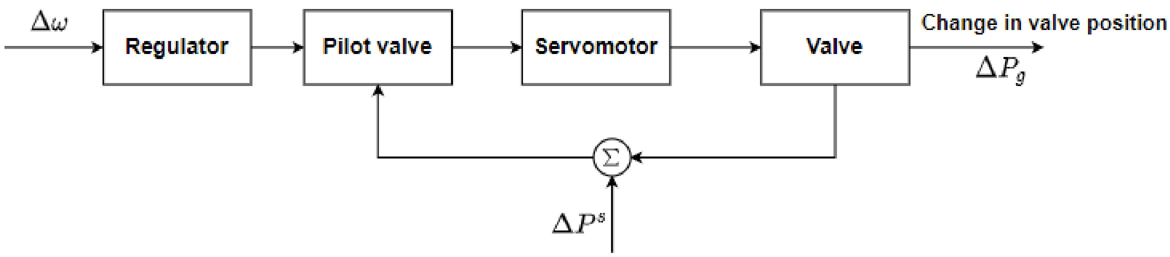

Figure 2.5 Schematic diagram of a speed governor system.

The small-signal model of the speed governor of can be represented with a first-order transfer function as shown in Figure 2.6 based on the dynamic equation which can be given by

$$\Delta P_g = \frac{1}{sTg+1}\left(\frac{-1}{R}\Delta f + \Delta P^s\right) \tag{2.1}$$

where T_g is the time constant of the governor, R is the droop parameter of the primary frequency controller, and ΔP^s is the control set point from the secondary frequency control mechanism.

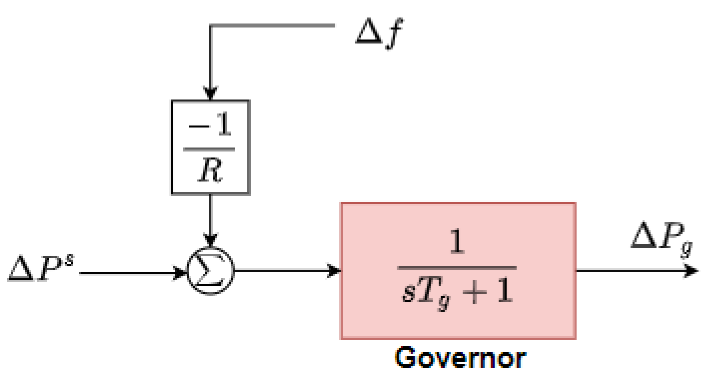

Figure 2.6 Small-signal model of a speed governor.

2.3.2 Turbine model

When there is a change in valve position of the speed governor system, the turbine translates the changes in steam flow (for a steam turbine generating unit) to a mechanical power that drives the generating units (synchronous generators) and changes their output (electrical power) as shown in Figure 2.7. In the small-signal analysis, the rapid generator dynamics can be neglected when representing the turbine model of a generating unit. The block diagram of the non-reheat steam turbine model is shown in Figure 2.8, the different kinds of turbines and their models can be found in [36] as recommended by the IEEE committee. The dynamic equation for small-signal analysis can be written as [37]

$$\Delta P_m = \frac{1}{sT_t + 1} \Delta P_g \tag{2.2}$$

where ΔP_m is the change in mechanical output power of the turbine and T_t is the time constant of the turbine. It is worth noting that the primary interest is the corresponding change in the electrical power output of the synchronous generator.

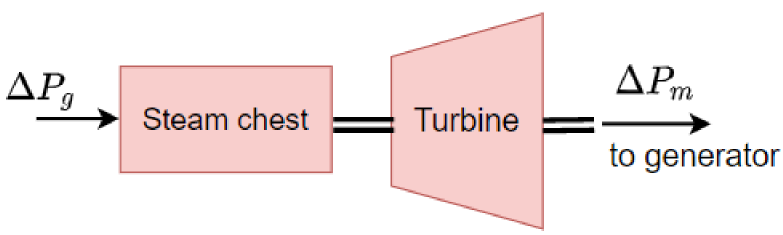

Figure 2.7 Schematic diagram of a steam turbine.

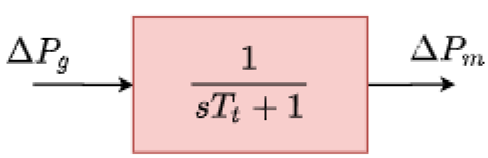

Figure 2.8 Small-signal model of turbine.

2.3.3 Power grid model

For the frequency response study, a linearized small-signal model is sufficient to analyze the behavior of the system with a slower response when compared to voltage control dynamics. Furthermore, it is presumed that the various generating units synchronized to the network within a control area form a homogeneous group, that is, in response to any mismatch, the generators will swing in simultaneously; this presumption is typical in frequency control analysis [38]. Therefore, a common frequency can be specified for a control area. Using the swing equation, the dynamic relationship between the change in frequency and the power imbalance can be expressed by [11]

$$2H\frac{d\Delta f(t)}{dt} + D\Delta f(t) = \Delta P_m(t) - \Delta P_L(t) \tag{2.3}$$

where H is the combined inertia of the system, Δf is the frequency deviation, D is the damping coefficient or load sensitivity, ΔP_m is the total change in mechanical power (output of the turbine), and ΔP_L is the total change in load/demand (electrical power output). Taking the Laplace transform of (2.3):

$$2Hs\Delta f(s) + D\Delta f(s) = \Delta P_m(s) - \Delta P_L(s) \tag{2.4}$$

$$\Delta f(s) = \frac{1}{2Hs + D}\left(\Delta P_m(s) - \Delta P_L(s)\right) \tag{2.5}$$

Representing (2.5) in a block diagram as shown in Figure 2.9. This simplified power system model is sufficient to represent the closed loop response of a generating unit, as will be present later in this chapter.

2.4 Multi-area interconnected power system

For an isolated or single power system, the control of power flow in other parts is not a control objective, the secondary frequency control is limited to regulate the frequency to its nominal value.

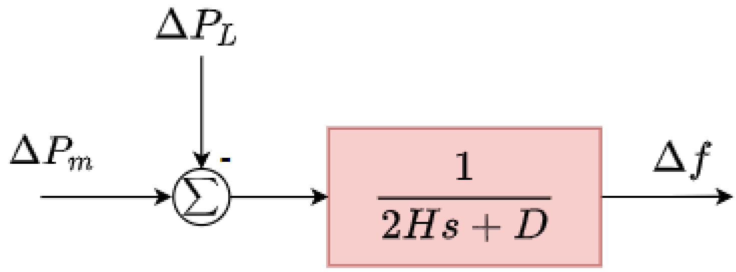

Figure 2.9 Small-signal model of a power system [11].

For frequency response studies, an isolated power system can be represented with its overall performance by an identical generating unit model. This equivalent model ignores the inter-machine oscillations with the assumption that individual generators are in synchronization with common frequency, this is the concept of a 'control area'. A control area essentially describes a territory where the strength of electrical interconnections within that area is greater than the tie-lines connecting it to neighboring control areas, and thus that area is distinguished by a single frequency; a control area may be a whole country or region within a country. The frequency deviation in a control area is a result of a power imbalance in the interconnected control areas and not in a particular area. It is also worth to note that the secondary frequency control in each interconnected control area must consider the inter-area power exchange. To develop the small-signal model of an interconnected power system, it is important to study the dynamics of the transmission lines, a hybrid transmission network comprising of the HVAC and HVDC transmission lines is considered in this thesis.

2.4.1 Frequency response modeling of HVAC transmission line

To determine the flow of power through HVAC transmission lines from one control area to another, the following assumptions are made which are peculiar to frequency response modeling [39]:

1. The power flow on the tie line is lossless, that is, the tie line between any two control area is strictly inductive.
2. The voltage control loops are considered to be faster than the frequency control loop and can keep the nodal voltages at unity for a per-unit system.
3. Lastly, to consider linearization, a small-signal disturbance is considered.

We consider a two-area power system interconnected by an HVAC transmission line as shown in Figure 2.10. The power flow from Area 1 to Area 2 can be calculated from [11]

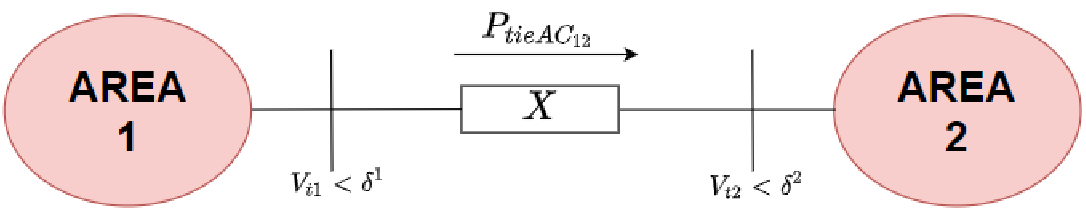

Figure 2.10 Representation of HVAC interconnected power system.

$$\Delta P_{ac_{12}} = \frac{V_{t1}V_{t2}}{X} sin\left(\delta^1 - \delta^2\right) \tag{2.6}$$

where V_{t1} and V_{t2} are the terminal voltages in area 1 and 2 respectively, δ^1 and δ^2 are the power angles of the equivalent machines in area 1 and 2 respectively, and X is the line reactance between areas 1 and 2.

Using Taylor's series to linearize (2.6) about an initial operating point $\left(\delta^{01} - \delta^{02}\right)$, then

$$\Delta P_{ac_{12}} = T_{12}\left(\Delta\delta^1 - \Delta\delta^2\right) \tag{2.7}$$

where T_{12} is the synchronising torque coefficient between control areas 1 and 2 which is expressed as

$$T_{12} = \frac{V_{t1}V_{t2}}{X} cos\left(\delta^{01} - \delta^{02}\right) \tag{2.8}$$

From the relationship between power angle and frequency, 2.7 can be rewritten as

$$\Delta P_{ac_{12}} = 2\pi T_{12} \int (\Delta f_1(t) - \Delta f_2(t))\, dt \tag{2.9}$$

Taking the Laplace transform of (2.9) yields

$$\Delta P_{ac_{12}}(s) = \frac{2\pi T_{12}}{s} (\Delta f_1(s) - \Delta f_2(s)) \tag{2.10}$$

For N interconnected areas, the tie line power flow can be deduced by

$$\Delta P_{ac_i} = \sum_{\substack{j=1 \\ j \neq i}}^{N} \Delta P_{ac_{ij}} = \frac{2\pi}{s} \left[\sum_{\substack{j=1 \\ j \neq i}}^{N} \Delta T_{ij} \Delta f_i - \sum_{\substack{j=1 \\ j \neq i}}^{N} \Delta T_{ji} \Delta f_j \right] \tag{2.11}$$

The block diagram representation of (2.11) is shown in Figure 2.11.

2.4.2 Frequency response model of the HVDC transmission line

The power system industry also incorporates high voltage DC (HVDC) transmission lines for long-distance power transfer because of the need for lower losses, damping of large oscillations associated with HVAC lines, and improved stability [40]. Furthermore, the technological improvements in power electronics have enabled the efficient use of HVDC lines. To develop the model of an HVDC transmission line based on a back-to-back voltage source converter (VSC) topology as shown in Figure 2.12 for frequency response analysis, a dynamic canonical steady-state model can be used with the following assumptions [12]:

1. The DC line is lossless.
2. The two AC sides operate at unity voltage in per unit representation.
3. There is a bi-directional flow of power between the interconnected areas based on the active power reference command.

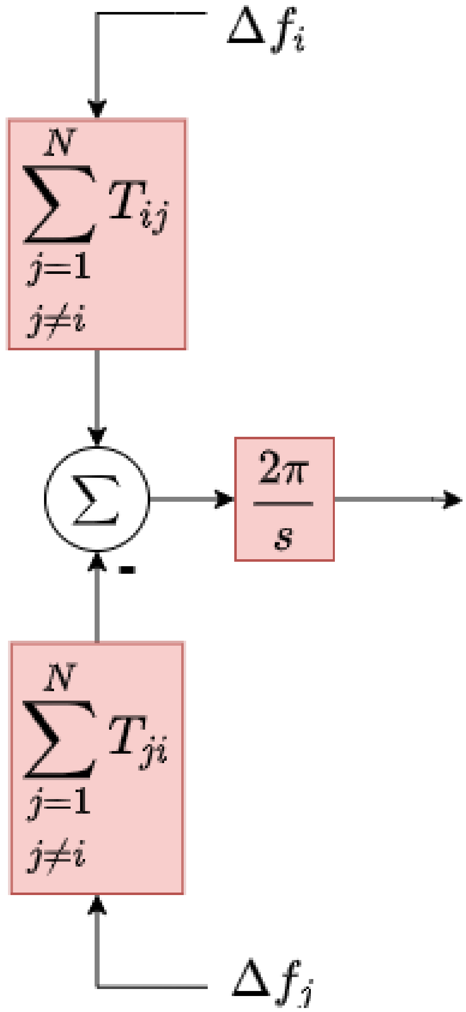

Figure 2.11 Frequency response model of an interconnected power system via the AC transmission line.

4. The reactive power is assumed constant at a pre-specified value during operation.

5. The DC bus voltage is usually regulated at the pre-specified values.

The model of the HVDC transmission system includes faster dynamics than those associated with AC systems because of the control of the power electronics converter; however, these dynamics are neglected because they are insignificant when compared to the time frame of the frequency

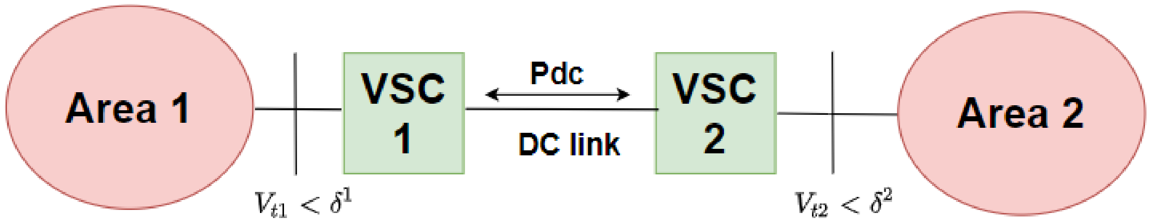

Figure 2.12 Two-area HVDC interconnected power system.

response analysis as considered in this thesis. In the HVDC transmission system, there are two essential control loops; the first loop is dedicated to the control of active power/DC voltage, while the second loop is dedicated to the control of reactive power/AC voltage. For the frequency control problem, the active power loop is of utmost importance, thus, it is of interest in this thesis. The VSC-based HVDC systems can rapidly regulate the power flow from one end to another with bi-directional capability, the active power controller is implemented using the current-mode control strategy, this control strategy is used for controlling the active power that the AC side of a VSC exchange with the AC side of the other VSC.

For frequency response analysis, the HVDC system could be modeled as a first-order system as shown in Figure 2.13. The active power tracks its reference based on a first-order transfer function $G(s)$ with a time constant T_{dc} which is usually determined according to the design specification [41, 42]. This controller modifies the active power by processing the frequency signal obtained from the AC side of the converters. The objective is to flatten/dampen the critical low-frequency inter-area oscillations that can affect the stability during load deviations. The frequency deviation in each area is used as an input signal to the control system to generate the references for the HVDC link between interconnected control areas [43].

$$\Delta P_{dc_{ref}} - \Delta P_{dc} = T_{dc}\frac{d\Delta P_{dc}}{dt} \tag{2.12}$$

Considering the relationship between change in active power and frequency deviation, the active power reference for the HVDC link during frequency deviation between control areas i and j as

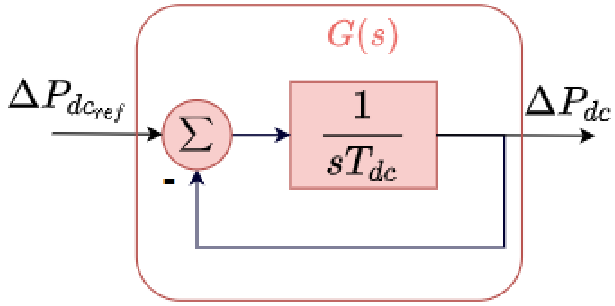

Figure 2.13 Block diagram of first-order HVDC system.

shown in Figure 2.14 can be written as [44]

$$\Delta P_{dc,i} = \frac{1}{sT_{dc}+1}\left(\Delta f_i - \Delta f_j\right) \tag{2.13}$$

where T_{dc} is the time constant of the HVDC converter.

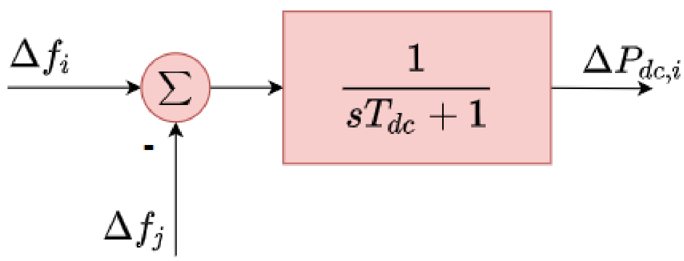

Figure 2.14 Small-signal model of HVDC system [12].

As earlier mentioned, in this thesis, a hybrid interconnection using HVAC and HVDC transmission lines will be considered. The net tie line power flow deviation resulting from the HVAC and HVDC interconnection can be written as

$$\Delta P_{tie,i} = \Delta P_{ac,i} + \Delta P_{dc,i} \tag{2.14}$$

For a two-area interconnected power system, a positive $\Delta P_{tie_{12}}$ means an increase in power transfer from area 1 to area 2, that is, an increased ΔP_L load change in area 1 would result in a decrease in frequency in both areas and tie line power flow of $\Delta P_{tie_{12}}$. The next important thing to consider is the secondary frequency control loop in the presence of transmission lines.

2.5 Load frequency control

Since the primary frequency control cannot restore the system frequency to its nominal value after a load deviation, the secondary frequency control, commonly known as load frequency control (LFC), is deployed to offset the frequency deviation of a control area. For an interconnected power system consisting of two or more control areas, while preserving the system frequency in its control area, the LFC is also tasked to maintain the tie line power flow between the control areas at scheduled values [45]. In practical terms, the load demand fluctuates perpetually, even without forecast anomalies, so that continuous secondary frequency control is required in real-time. Contrary to an isolated control area, the LFC signal for an interconnected system is computed using a new control signal, known as area control error (ACE), the *ACE* is a linear summation of the weighted frequency deviation and the tie line power flow measurements. The *ACE* estimation provides the amount of active power mismatch (shortage or excess), and in response, the LFC sends signal to the speed governor of the generating units in its control area for appropriate action [46]. For the i^{th} control area in a multi-area interconnected power system, the *ACE* can be mathematically expressed as [37]

$$ACE, i = \beta_i \Delta f_i + \Delta P_{tie,i} \tag{2.15}$$

and

$$\beta_i = \frac{1}{R_i} + D_i \tag{2.16}$$

where β_i is a weighting factor known as the frequency bias factor of the i^{th} control area. The LFC control signal for the i^{th} control area can expressed as

$$\Delta P_i^s = h_i(ACE) \tag{2.17}$$

where $h_i(\cdot)$ is the load(secondary) frequency controller, which is conventionally based on the integral control strategy.

When more than one generating unit in a control area participate in frequency control, the LFC signal ΔP^s is distributed among the generating units using a participation index known as "area participation factor (apf)", it is usually determined using an economic dispatch method. The sum of participation factors in a control area must be equal to 1. For example, in the i^{th} control area, the control signal sent to the speed governor of the n^{th} generating unit by the LFC system can be expressed as [11]

$$\Delta P^s_{i,n} = apf_{i,n} \Delta P^s_i \tag{2.18}$$

Given that

$$\sum_{j=1}^{n} apf_{ij} = 1 \quad | \in \{0,1\} \tag{2.19}$$

The tertiary frequency control and other higher level frequency controls are not considered in this thesis; this is because they are usually not automated and require offline economic dispatch decisions outside the time-frame for digital control action. The complete frequency control block diagram of a the i^{th} control area in a large power system in shown in Figure 2.15.

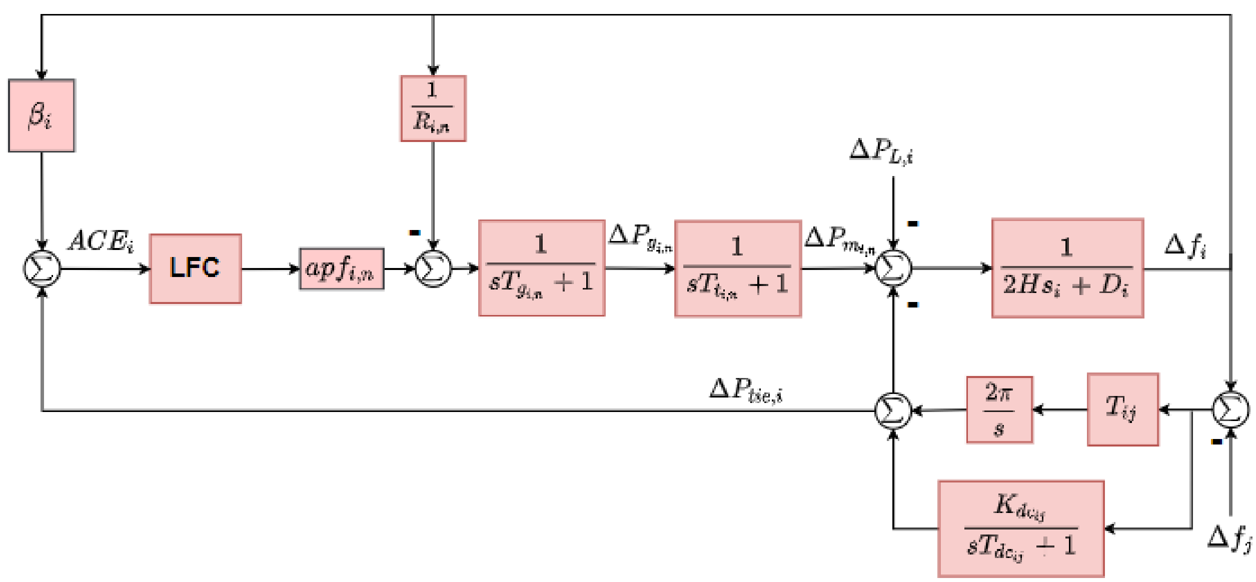

Figure 2.15 A hybrid AC/DC frequency response model.

2.6 Modern power system

With the tremendous advancement in technology, more specifically with power electronics, changing government regulations, and growing environmental concerns, the power system industry is experiencing a paradigm shift with increasing exploitation of renewable sources for power generation. Power system deregulation and renewable-based generation such as wind and solar, are the major participants in modern power systems. They affect the dynamic operation the power system differently from the traditional power system, therefore, the modern power system presents new technical issues in terms of frequency control, voltage control, power quality, and economic dispatch; therefore, the conventional controls are inefficient to provide consistent power system stability and reliability.

2.6.1 Power system deregulation

In the early stages of the electric power system industry, its operation is based on a vertically integrated utility (VIU) framework. Here, the utility holds a government-issued monopolistic franchise, granting it the protected right to perform principal power system operations of generation, transmission, and distribution within its control area. Due to the absence of competition, the utility has to supply electricity to all customers within its control area, rather than to those it might consider as fiscally rewarding. In this regulated environment, electricity tariffs are usually regulated by the government. The utility also provides the frequency regulation within a control area, and also other ancillary services, because it owns and supervises all the system facilities within its region.

Many countries have begun to restructure and deregulate their power system sectors to reduce government participation with the aim of providing affordable and reliable electricity to consumers.

The main steps in the transition are the disintegration and transfer of the operations performed by the vertical utility in the traditional/regulated environment to private entities or independent companies; this allows for transparent and open-access operation. The major players within a control area in the restructured environment are the power producers (generating companies), transmission company, and the distribution companies [47]. The power producers in a control area can compete or make an offer to sell power to distribution companies within and outside its control area borders, and each distribution company has the discretion to negotiate with power producers within and outside their control areas to meet their demands; competition is a driving force in the deregulated environment. Also, an unbiased entity known as an independent system operator (ISO) has emerged in each control area, whose functions include ensuring non-discriminatory access by all power producers to the grid, ensuring the reliability and security of its control area, managing transmission overloading, and coordinating power contractual agreements between power producers and consumers. The ISO oversees the operation of the grid and provides all ancillary services in the newly deregulated environment.

Unlike the vertical utility in the traditional environment that owns and supervises the generation utility, and provides frequency regulation service from its unloaded reserve capacity, the ISO that offers frequency regulation does not own any generation utility in the new power system environment. Therefore, ISOs providing frequency regulation services must buy reserve capacity from power producer(s); however, the power producer is not legally bound to sell to the ISO. This new development modifies the frequency response framework of the traditional power system environment.

Globally, there are several market scenarios for electricity transactions, and thus frequency regulation [48]. However, three main market scenarios will be addressed in this thesis:

1. Poolco scenario: In this scenario, the power producers have the autonomy to change their power outputs, submit bids to ISO, and indicate ancillary service information. This scenario is similar to the traditional environment since the ISO controls the operation of the utilities in its control area [49].

2. Bilateral scenario: In this scenario, the distribution utilities can choose to enter a contract with power producers within or outside their control areas depending on the predicted demand variation. However, this contractual agreement must be submitted to the ISO for real-time coordination [50].

3. Contract violation scenario: In this scenario, it is assumed that the distribution utilities demand more power than contractually agreed upon. The ISO secures reserves from the power producers for LFC purposes, this usually from the power producers within its control area to preserve the net tie line power flow at scheduled values [51].

2.6.2 Integration of renewable energy

The exponential increase in demand for electrical power, depletion of fossil fuels, rise in environmental and global policies for the reduction of greenhouse gases emission, has led to the rapid development of renewable energy (RE) technology. Amongst the natural renewable energy sources available, wind and solar have found the most application in the power system industry [52]. As the growth of RE continues, there is an increasing interest in its effect on the operation, control, and stability of the power system. Several studies have shown that the impacts of the integration of renewable energy sources (RESs) into the power system are non-negligible and cannot be considered insignificant because of the increasing penetration level and size [53]. While the aggregation of RES units reduces the effects of random power outputs, the RES needs to meet some technical requirements specified by the grid code. However, with the increasing penetration of RES into large power systems, there is a need to update the grid codes to mitigate the effect of high RES penetration [54]. The framework of the modern power system that integrates RES is different from the traditional power system framework.

The RESs have a different impact on the transient behavior and response of power systems, different from typical synchronous generators used in conventional power plants. The major technical issues that affect RES penetration relates to their inability to perform efficiently as conventional power plants [55]. When a considerable amount of RE generation is tripped or reduced due to fault, the operation of the system, including frequency, may be affected. High penetration of RES increases the uncertainties during off-normal operations and presents various technical complications. The integration of RESs has impacts on power flow, frequency control, voltage control, transmission line congestion, network augmentation, economic load dispatch, power quality, and reactive power requirement. Despite the considerable advancement in RE technology, there is still the challenge of frequency regulation and this contributes to the limitation of increasing RES penetration in large interconnected power systems [56]. For example, When a substantial amount of power generation from wind during off-peak periods in a power system with high wind power penetration may cause some units of the conventional power plants to be shut down to preserve the generation-demand balance, this decreases the overall system inertia and has a negative effect on the performance of the system during frequency events. The power variation resulting from the renewable energy plants in a control area consists of fast components (from independent renewable energy unit) and slow components (from composite renewable energy unit) within the control area. Unlike the fast components, studies have shown that the slow components contribute adversely to power imbalance and consequentially unacceptable frequency fluctuations, this must be taken into account in the frequency response model of the system.

2.6.3 Impact of inertia on frequency response

Traditionally, the frequency stability of the power system is dependent on the conventional synchronous generators connected to the grid. In a control area, when there is an instantaneous increase in load, there should be a corresponding increase in the output of mechanical power from the turbine to balance the load. This does not automatically increase the electrical power output of the generator, however, there is a rapid extraction of kinetic energy stored in the rotating part of the generating unit to augment the power imbalance. The kinetic energy is a function of the inertia present in the rotating masses directly coupled together in the power system [57]. The inertia is considered as an important system upon which governs the instantaneous frequency response of the power system to the power imbalance. Conventionally, the two major sources of inertia in power system generation are turbines and synchronous generators whose kinetic energy is rapidly extracted counteract power imbalance. Also, some industrial loads, motor-driven compressors, and pumps that are directly coupled to the grid can contribute to the inertia response of the system because their rotational speed is a function of the system frequency [58].

In modern power systems, the fleet of power system generation is briskly shifting from conventional generation to RE generation. Besides the intermittence of RE generation, they are decoupled from the grid through the power electronics converters. Consequently, as the conventional generation is displaced by RE generation, the overall inertia of the grid is decreased, impacting the power system reliability and stability [59]. This consequence has been considered a major downside to the integration of a high share of RE generation into the grid. Additionally, it is projected that future power systems will experience an increase in the use of HVDC technology to transport bulk power from RE plants to load centers and inherently improve the existing HVAC network. Since the HVDC links electrically decouple the interconnected control areas, the inertia of a control area is not directly accessible to the other control areas. In the actual sense, a system with low inertia is characterized by the following [60, 61]:

1. Increased frequency deviation (deeper nadirs) within a short timespan
2. Faster rate of change of frequency

It is straightforward that any technique of incorporating virtual inertia to the grid can greatly enhance the dynamic response and reliability of the system [62]. Virtual inertia can be emulated by dedicated control of power electronics converter in RE systems. Also, the rotating devices present in wind energy conversion systems (WECSs) have led to the enactment of wind farms participation in frequency regulation and provision inertia response; this is mainly achieved by operating the WECS below maximum power and devising a control strategy for the reserve active power with respect to frequency. The paper [63] investigates the capability of WECS to provide inertia support and primary frequency control in the Rhode Island power system. A supplementary controller is included in the control system of directly-driven WECS to render frequency control as an ancillary service [64]. Reference [65] introduced a dynamic droop-inertia control to improve the frequency nadir and ascertain the reliable operation of a doubly-fed induction generator WECS. In [66], a coordinated control strategy to enable grid-connected wind farms to participate in LFC is implemented. For future power systems with high penetration of RE and absence of rotating masses, dedicated ESSs can be used to emulate spinning reserves and virtual inertia to maintain the reliability and stability of the power system [67]. Due to the considerable technological advancement in the wind energy industry, the impacts of wind power on frequency regulation is considered in this thesis.

2.6.4 Frequency response of wind energy conversion systems

The wind energy conversion system is a collection of mechanical and electrical subsystems operated and controlled together to harness the power from wind and convert it to useful electrical power within specified voltage and frequency. Depending on the type of wind turbine (fixed-speed or variable-speed), the generator converts the mechanical power harvested by the blades of the turbine and converts it to electrical power and transfers it to the grid through a back-to-back power electronics converter and a power transformer. Recently, the variable speed wind turbine (VSWT) based on permanent magnet synchronous generator (PMSG) as shown in Figure 2.16, has gained tremendous attention due to their high efficiency, absence of gearbox, etc, compared to VSWT based on doubly fed induction generator (DFIG) [68, 69]. The back-to-back converters, consisting of the machine side converter (MSC) and grid side converter (GSC), are used to decouple the generator from the grid, therefore, its inertia cannot be immediately extracted during frequency events. The control scheme of the MSC is used to regulate active and reactive powers from the PMSG; the active power control loop is used to obtain maximum power from the wind turbine through maximum power point tracking (MPPT) and the reactive power control loop is used to keep the net reactive power at zero. The GSC control scheme keeps the dc-link voltage at a constant value to enable maximum power transfer from the MSC to the grid at specified voltage and frequency, it can also be used to provide independent protection during abnormal voltage conditions.

To develop a simplified small-signal model of the PMSG-based WECS for frequency response analysis, the switching of the MSC is considered; the voltage equations in the $d-q$ reference frame used for pulse width modulation (PWM) switching of the MSC is given by [13]

$$v_d(t) = R_d i_d(t) + L\frac{di_d}{dt} \tag{2.20}$$

$$v_q(t) = R_q i_q(t) + L\frac{di_q}{dt} \tag{2.21}$$

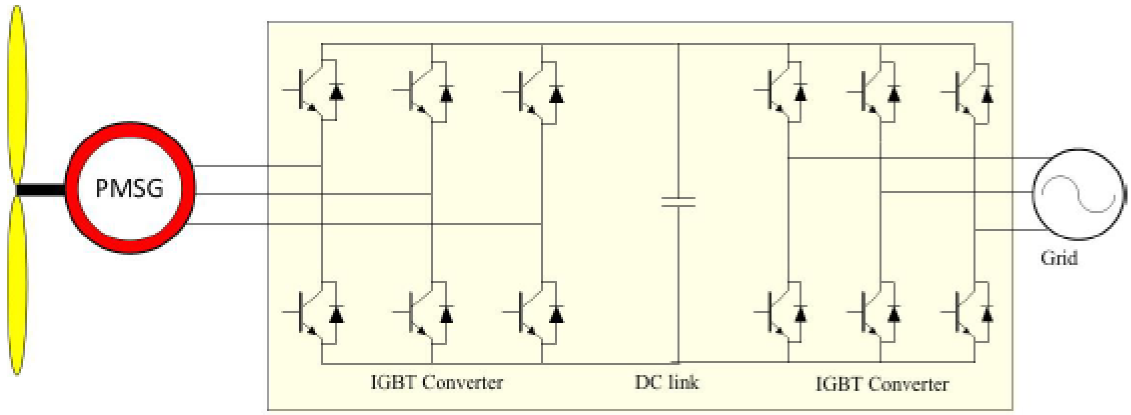

Figure 2.16 PMSG-based wind energy conversion system [13].

where v, i, R and L are the output voltage, output current, resistance and inductance of the PMSG respectively. Taking the Laplace transform of (2.20) and (2.21) gives

$$v_d(s) = R_d i_d(s) + sLi_d(s) \tag{2.22}$$

$$v_q(t) = R_q i_q(s) + sLi_q(s) \tag{2.23}$$

The open loop transfer functions of (2.22) and (2.23) can be deduced as

$$G_d(s) = \frac{i_d(s)}{v_d} = \frac{1}{R_d + sL_d} \tag{2.24}$$

$$G_q(s) = \frac{i_q(s)}{v_q} = \frac{1}{R_q + sL_q} \tag{2.25}$$

For a surface-mounted PMSG, $i_d(s) = 0$, therefore $G_d(s) = 0$, rewriting (2.25) in standard form gives

$$\frac{i_q(s)}{v_q(s)} = \frac{K_w}{sT_w + 1} \tag{2.26}$$

where $K_w = \frac{1}{R_q}$ and $T_w = \frac{L_q}{R_q}$ are the gain and time constant of the MSC respectively. It can be interpreted that a change in v_q would cause a change in i_q, and by convention, a change in wind speed Δv_w would cause a change in wind power output ΔP_w. Therefore, the small-signal model shown in Figure 2.17 is used for frequency response analysis.

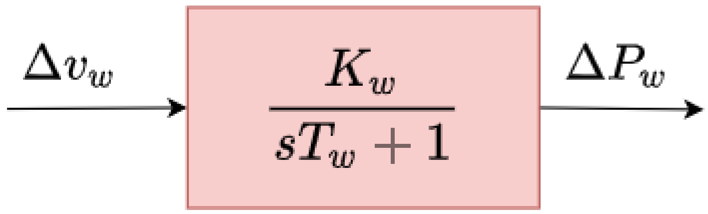

Figure 2.17 Small-signal model of WECS

To update the frequency response model of the traditional environment with the additional dynamics of the power system and wind power penetration, the following parameters will be modified: change in speed governor setting ΔP_g, ACE computation, and change in net tie lie deviation ΔP_{tie}, while the change in wind power ΔP_w will be added to the updated model. To circumvent repetition, these modifications will be presented in the models of the subsequent chapters of this thesis.

Chapter 3

Heuristic Optimization of Virtual Inertia Control in Grid-Connected Wind Energy Conversion Systems for Frequency Support in a Restructured Environment

This chapter is based on the work reported in [1].

3.1 Chapter Overview

In the work reported in this chapter, a novel application of the artificial bee colony (ABC) algorithm is used to implement a virtual inertia control strategy for grid-connected wind energy conversion systems. The proposed control strategy introduces a new heuristic optimization technique that uses the ABC optimization algorithm to calculate the optimal gain value of an additional derivative control loop added to the control scheme of the machine side converter (MSC) in a wind energy system to enable wind farms to participate in frequency control as specified by recent grid codes. This helps to minimize the frequency deviations, reduce active power deviation in the system, and increase the penetration level of wind energy in power systems. The study was performed in a restructured power system environment. The robustness of the proposed control scheme is first validated with eigenvalue analysis and then evaluated using load–frequency analysis by considering three real-life transaction scenarios that can occur in an interconnected open-energy market. The results in this study show that the optimal gain of the proposed controller reduces the frequency deviations and improves stability and overall performance of the system.

3.2 Chapter Introduction

To meet increasing load demand and reduce environmental pollution caused by fossil-fuelled power plants, power generation from renewable sources has become a viable solution in many instances. Modern power systems consist of many control areas with different sources of generation [70]. Any variance between the generated power and required load demand results in the deviation of the system frequency from its nominal value. This also creates an inadvertent exchange of power between interconnected control areas. The intrinsic characteristic of conventional generators that make them applicable for frequency control is “inertia”. The large moment of inertia present in synchronous generators allows conventional/traditional power systems to maintain stability during disturbance as a result of frequency regulation action. In the past, the impacts of renewable energy plants (REPs) in large power systems were considered negligible because of low-level penetration. With the increasing penetration of REPs, most countries have developed renewable energy grid codes that REPs seeking connection to the grid must comply with [71–73]. In a similar manner to codes for conventional plants, REPs grid codes specifies that some ancillary services must be provided during transient conditions [74]. One of these ancillary services is frequency control. Depending on the amplitude and duration of the frequency deviation, frequency control can be classified into primary, secondary, tertiary, and emergency frequency control [11]. This study is concerned with the impacts of inertia on primary and secondary frequency control because the efficiency of these controls can mitigate against the need for a higher level of frequency control. Primary frequency control is able to attenuate small frequency deviation but is not able to restore the system to the nominal frequency; thus, secondary frequency control is activated by harnessing the available power reserve to restore the system to the nominal operating frequency. Secondary frequency control is also known as automatic generation control (AGC) or load frequency control (LFC). This is now becoming a complex control problem in power system design, operation, and control because of the emerging complexities such as renewable energy penetration, deregulation, new standards, environmental constraints, and various uncertainties [75]. Early studies on LFC problems focused on a single-area power systems with conventional power plant generation [76–78]; LFC models for hydropower plants were introduced in [79–81]. By interconnecting power systems, reliability and resilience are improved because there is inter-area support during deviating conditions. High voltage AC (HVAC) tie lines are used for interconnection in traditional power systems; the effects of HVAC tie line models were investigated in [82, 83]. Studies for a two-area power system considering conventional multi-source plants were presented in [84–88] and higher-order interconnected areas were studied in [89–94]. The application of HVAC lines for long-distance transmission is associated with several drawbacks such as effect of capacitance for underground transmission [95], line inductance [96], Ferranti effect [97], asynchronous interconnection [98], and reduce active power transmission-to-length ratio [99]. Modern power systems have adopted the application of high voltage DC (HVDC) transmission link for long-distance transmission to provide solutions to inherent HVAC transmission problems. This leads to economic and technical advantages [98, 100, 101].

In the traditional power system environment, the vertically integrated utility (VIU) solely owns the generation companies (GENCOs), transmission companies (TRANSCOs), and distribution companies (DISCOs), which supply power to clients at regulated prices [102, 103]. The physical boundaries of a VIU define the control areas which are interconnected via tie lines. In a restructured or deregulated environment, GENCOs may choose to participate in frequency regulation, and independent power producers (IPPs) or REPs seeking connection to the grid must meet the grid code requirements by providing frequency support to the system during disturbances. DISCOs have the freedom to individually contract power from GENCOs and IPPs in different areas. The transactions among the GENCOs, IPPs, and DISCOs are supervised by an independent system operator (ISO) or any other transparent organization [11]. Provision of ancillary services such as frequency control is optional and usually based on competitive pricing, thus it is regarded as an open energy market [104]. Frequency response models for power systems in a deregulated environment must consider the contracts between DISCOs and GENCOs; Reference [105] investigated LFC models for hydro plants. Thermal plants were considered in [106] and multi-sources were studied in [107].

In modern power systems, the impacts of REPs can no longer be considered negligible because of the increased level of penetration. The increasing integration of renewable energy plants (almost zero-inertia) reduces the overall inertia of the system, which makes the system more susceptible to high transient frequency deviations, thus making LFC problems more complex [108]. The reduction in inertia causes some problems in the deregulated environment for the ISO, such as a reduction in frequency and system oscillation. Due to the rotational parts present in wind energy conversion systems, recent grid codes require that they participate in frequency regulation within a specified range [109]. Authors in [110] investigated the capability of doubly-fed induction generators for providing short term frequency regulation through rotor flux manipulation. The kinetic energy in a WECS turbine and dc-link capacitor energy were extracted to provide extra inertia in [111]. A comparative evaluation of short term frequency response between fixed-speed and doubly-fed induction generators (FSIG and DFIG) was done in [112]. The results show that the DFIG can provide more kinetic energy than the FSIG. Several studies have proposed primary and secondary frequency control strategies for grid-connected WECS from the generator point of view; however, they failed to address the limitations of the power electronics devices that connect the generator to the grid [113]. For the power electronics-based devices, the emulation of inertia for frequency response can be achieved by the control of the power that is proportional to the first-order derivative of the system frequency [5, 10]. This control scheme is termed "virtual inertia control" because it imitates the inertia characteristics of a conventional synchronous generator. The concept of a virtual synchronous generator (VSG) or a virtual synchronous machine (VSM) was originally proposed by Project VSYNC [114]. The VSG consists of an energy storage device interfaced with a power electronics device (mostly VSCs) and a control algorithm to make it behave as a synchronous generator for intermediate energy requirements. This mimics the damping and inertia characteristics of a synchronous generator by injecting active power when the frequency deviation is negative and vice versa. In this work, a virtual inertia control strategy is proposed. A grid-connected PMSG is considered as an intermediate frequency controller for short-term inertia response, which is highlighted in the red box in Figure 3.1, given that the time constant of the power electronics devices is smaller when compared to conventional devices. However, for long-term frequency regulation, the use of ESS can be adopted.

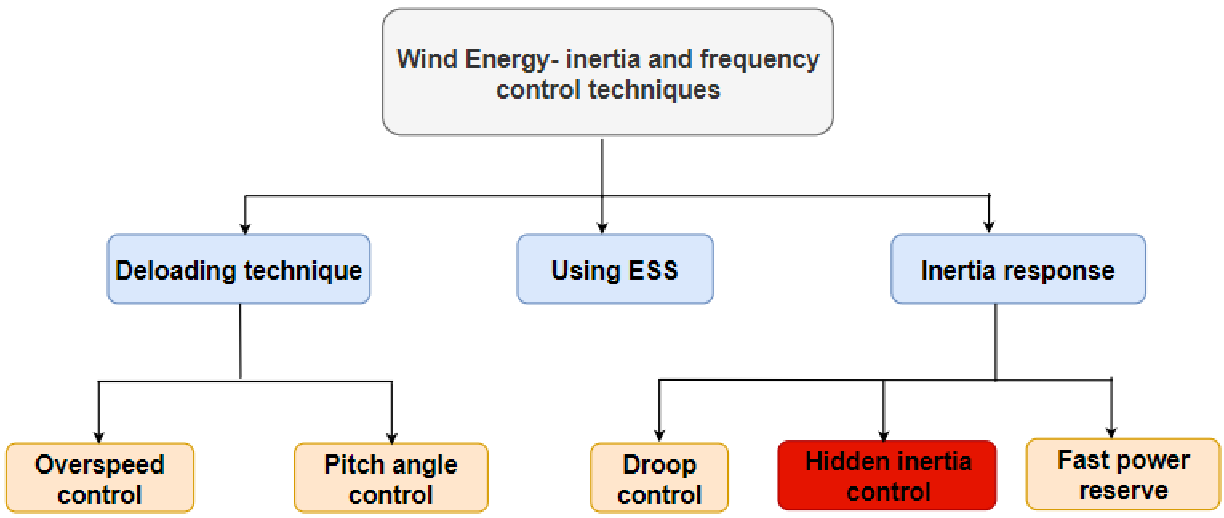

Figure 3.1 Classification of frequency control techniques in wind energy systems.

In frequency control studies, the control strategies that are applied in traditional power systems cannot be extended to modern power systems with renewable energy penetration and power system deregulation. This makes it necessary to search for new and efficient control strategies [115]. Early designs of load frequency controllers used classical PI, PID, robust and optimal control theory, a dual-mode PI control [116], and decentralized PI control [117]. These were proposed for LFC studies. The hydro-powered plant was investigated in [118]; the PI control strategy was used to design the LFC scheme. By analyzing the small-signal stability of a hybrid power system—diesel engine generator, wind turbine, PV, and ESSs in [119]—a PI-based scheme was proposed to mitigate frequency deviations during load and RES variations. In [120, 121], optimal linear control theory was used to model linear regulators for AGC studies. To improve the robustness of the frequency control, the authors of [122, 123] used linear matrix inequalities. The Ricatti equation was used in [124] and the authors of [107, 125–127] adopted optimal feedback theory in traditional and deregulated power system environments. The drawbacks of these approaches such as non-robustness to parametric variations, fault intolerance, and inaccurate estimation of state variables have led to the research in intelligent control approaches [128]. Recently, modern intelligent control methods such as artificial neural networks (ANNs), fuzzy logic, evolutionary algorithms (genetic algorithms (GAs) and differential evolution (DE) algorithms), and heuristic algorithms (ant colony optimization (ACO) algorithms, particle swarm algorithms (PSOs), and artificial bee colony (ABC) algorithms) have been utilized as efficient tools for solving complex and nonlinear engineering problems. In [129], a combination of fuzzy logic, genetic algorithm, and neural network was used to design a load frequency control for a single area power system. The flatness-based approach was applied to a three-area power system with a high penetration of wind energy to reduce frequency deviations [130]. With the penetration of electric vehicles, a PSO-based ANN technique [131] and model-free control, based on the sliding mode technique [132], were used for the secondary frequency control. An adaptive-VSG was used in [133] to improve the frequency response of a permanent magnet synchronous generator-based WECS. AGC of a DFIG-based WECS using the least square support vector machine approach was proposed in [134]. Authors in [103] used the gradient newton algorithm (GNA) for trajectory sensitivity analysis to determine the optimal parameters of the system for LFC studies. A differential evolution algorithm was applied to a fuzzy-PID controller to optimize the control parameter for ACE signals in a deregulated environment [135].

From the literature survey, the following omissions were observed: no study considered the combination of integration of renewable energy and deregulation; most reported research studies have focused on the demerits and limitations of increasing renewable energy penetration in terms of intermittent operation and variability [136]. However, since deregulation and grid codes require IPPs to participate in electricity pricing [11] and frequency support [137], respectively, this study investigated how renewable energy plants can perform frequency support operation in a deregulated environment given that modern wind energy conversion systems (WECS) are equipped with synchronous generators and power electronic converters that can produce virtual inertia control in a restructured power system environment.

Because the power system industry is conservative and reluctant to replace well-known classical controllers with modern control technologies, heuristic optimization techniques have been used to optimally tune the controller to adapt to the revolving power system environment. The artificial bee colony (ABC) algorithm is a relatively new member of the heuristic optimization techniques. It is based on the foraging behavior, learning, memorizing, and information sharing characteristics of honeybees. Several research papers have already evaluated and established the performance of the ABC algorithm against other algorithms such as PSO, ACO, and other optimization techniques [138–141]. Based on these investigations, it was established that the ABC algorithm has less computational complexity, high solution accuracy, simplicity, and independent convergence. The authors of [142–144] used the ABC algorithm in the maximum power point tracking (MPPT) control of a PV farm. The proposed controller provides a better tracking reference than the PSO-based MPPT. For optimal allocation and sizing of DGs in a distributed system, the ABC algorithm was employed in [145]. Due to its advantages, the ABC algorithm has found application in this work. To the best of the authors' knowledge, the ABC optimization algorithm has not been applied to frequency control problems in a deregulated environment. The major contributions of this chapter are development of a small-signal frequency response model for HVAC/DC interconnected power systems with high integration of renewable energy in a restructured power system environment; development of a short-term virtual inertia control strategy for wind energy conversion systems in the restructured power system environment; and novel application of the ABC algorithm to determine the optimal gain value of the virtual inertia controller.

3.3 Small-Signal Model of Interconnected Power System in a Restructured Environment

The modern power system is a multi-area, highly complex, nonlinear, and the time-variant environment because there exist various dynamics with varying response times that need complex numerical computations to simultaneously handle various time steps. For the frequency response study, a linearized first-order model is sufficient to analyze the dynamic behavior of the system. The model used in this study is presented in Figure 3.2; it represents a two-area power system that is interconnected by HVAC and HVDC lines (modified Kundur model) [37, 146]. Each area has two conventional power plants and a wind farm; there are industrial and domestic loads in both areas. Each area has to operate at the same frequency within the area. In the frequency response, primary frequency control is provided locally by each generating plant (pink label), secondary frequency control is achieved by each area (blue label), and the wind farms are equipped with the proposed virtual inertia control for frequency support (red label).

The power–frequency response of the system has to be demonstrated as being suitable for modeling the system in the frequency domain (Laplace domain). In this section, the small-signal model of the two-area power system in a deregulated environment is developed, as shown in Figure 3.3 [147]. There are four GENCOs, two IPPs, and four DISCOs in the model. The DISCOs in Areas 1 and 2 have an aggregated load of PL1 and PL2, respectively, and all GENCOs participate in secondary frequency control.

In the open energy market, DISCOs can purchase power from GENCOs and IPPs at competitive prices. DISCOs have the autonomy to choose which GENCOs to negotiate prices with; i.e., they may or may not have contracts with GENCOs in the same area. To allow for different types of

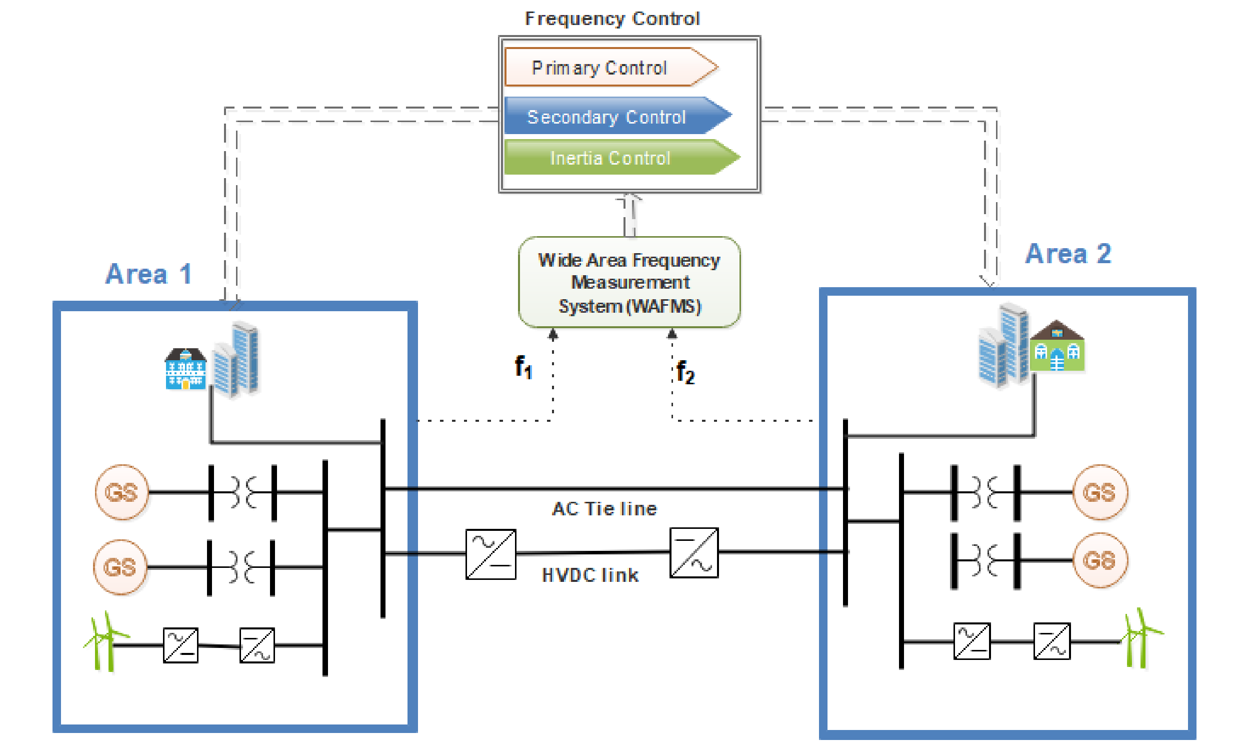

Figure 3.2 System model.

contracts such as Poolco (Power pool company), bilateral, and combinations of both, the concept of the contract participation matrix (CPM) is introduced [148]. The CPM is a matrix with m rows and n columns, where m corresponds to the number of GENCOs and n corresponds to the number of DISCOs in the system. The ijth element of the CPM is a fraction of the total load contracted by the jth DISCO to the ith GENCO. The sum of all the elements in a column of the CPM must be equal to 1 as given by [102]:

$$\sum_{i}^{n} cpf_{ij} = 1 \tag{3.1}$$

In this study, there are four GENCOs and four DISCOs that participate in the deregulation contract. The two wind farms participate in the frequency response control to reduce the power deviation caused by the load demand variations from the DISCOs. Hence,

$$CPM = \begin{bmatrix} cpf_{11} & cpf_{12} & cpf_{13} & cpf_{14} \\ cpf_{21} & cpf_{22} & cpf_{23} & cpf_{24} \\ cpf_{31} & cpf_{32} & cpf_{33} & cpf_{34} \\ cpf_{41} & cpf_{42} & cpf_{43} & cpf_{44} \end{bmatrix} \tag{3.2}$$

Since the load demand variations from the DISCOs must be reflected in the dynamics of the GENCO model, the GENCOs must follow the information signals sent by the DISCOs in contract with them. Figure 3.4 shows the typical schematic representation of a four GENCO–DISCO contract.

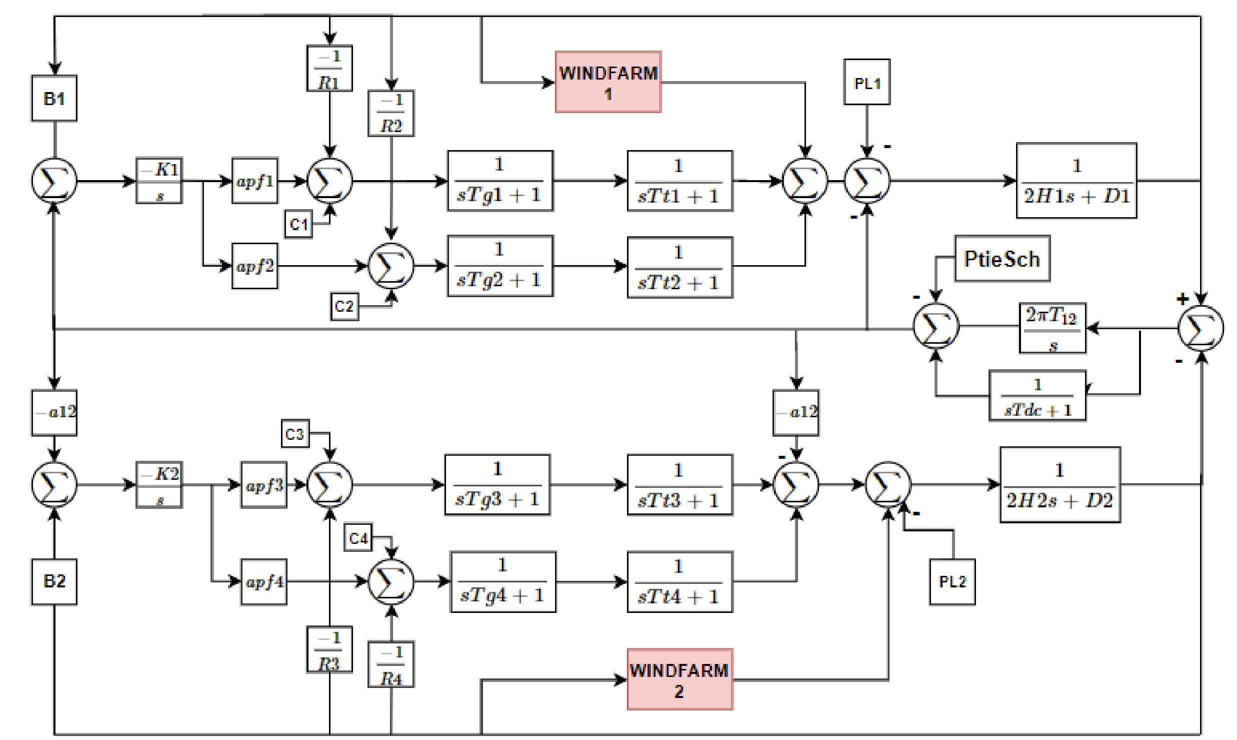

Figure 3.3 Frequency response model of a two area power system in a deregulated environment.

The change in frequency as result of mismatch between the generated power and load de-

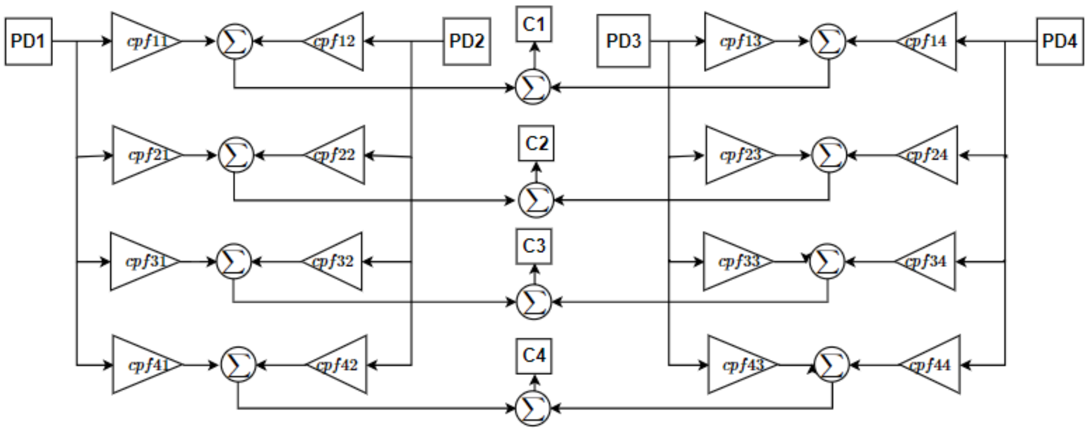

Figure 3.4 Dynamics of deregulation contract.

manded in the interconnected system can be defined by:

$$\Delta f_1 = \frac{1}{2H_1 s + D_1} \left(\Delta P_{m1} + \Delta P_{m2} + \Delta P_{w1} - \Delta P_{Tie12} - \Delta P_{L1} \right) \tag{3.3}$$

$$\Delta f_2 = \frac{1}{2H_2 s + D_2} \left(\Delta P_{m3} + \Delta P_{m4} + \Delta P_{w2} - \alpha_{12} \Delta P_{Tie12} - \Delta P_{L2} \right) \tag{3.4}$$

where H_i and D_i are the inertia and damping constant in area i, respectively; ΔPmi is the change in mechanical power of GENCO i; ΔPwi is the change in wind power output; α_{12} is the area capacity ratio ΔP_{Tie12} is the tie line power deviation between Areas 1 and 2; and ΔP_{Li} is the lumped demand in area i.

To formulate the frequency response in a deregulated environment, the absent information from the traditional environment is introduced [149]. Firstly, the area control error (ACE) signals sent to the speed governor of the GENCOs are modified to include the scheduled demand from the DISCOs. For the model considered in this chapter, the equations for the governor dynamics can be expressed as:

$$\Delta P_{g1} = \frac{1}{sT_{g1} + 1} \left(C_1 - \frac{1}{R_1} \Delta f_1 - apf_1 K_1 \int ACE_1 \right) \tag{3.5}$$

$$\Delta P_{g2} = \frac{1}{sT_{g2} + 1} \left(C_2 - \frac{1}{R_2} \Delta f_1 - apf_2 K_1 \int ACE_1 \right) \tag{3.6}$$

$$\Delta P_{g3} = \frac{1}{sT_{g3}+1}\left(C_3 - \frac{1}{R_3}\Delta f_2 - apf_3 K_2 \int ACE_2\right) \tag{3.7}$$

$$\Delta P_{g4} = \frac{1}{sT_{g4}+1}\left(C_4 - \frac{1}{R_4}\Delta f_2 - apf_4 K_2 \int ACE_2\right) \tag{3.8}$$

and

$$C_i = \sum_{j=1}^{4} cpf_{ij}\Delta P_{Li} \tag{3.9}$$

The scheduled steady-state power flow in the tie line can be defined as ΔP_{tiesch} = (load demand variation of DISCOs in Area 1 to GENCOs in Area 2) − (load demand variation of DISCOs in Area 2 to GENCOs in Area 1). It can be mathematically expressed using

$$\Delta P_{\text{tiesch}} = \sum_{i=1}^{2}\sum_{j=3}^{4} cpf_{ij}\Delta P_{Lj} - \sum_{i=3}^{4}\sum_{j=1}^{2} cpf_{ij}\Delta P_{Lj} \tag{3.10}$$

The net tie line power flow can be expressed as:

$$\Delta P_{Tie12} = \Delta P_{\text{tieact}} - \Delta P_{\text{tiesch}} \tag{3.11}$$

Where ΔP_{tieact} is the total power flow of the ac tie line and the HVDC link which is

$$\Delta P_{\text{tieact}} = \Delta P_{\text{TieAc}} + \Delta P_{dc} \tag{3.12}$$

Following on from this:

$$\Delta P_{\text{TieAc}} = \frac{2\pi T_{12}}{s}\left(\Delta f_1 - \Delta f_2\right) \tag{3.13}$$

$$\Delta P_{dc} = \frac{1}{(sT_{dc}+1)}\left(\Delta f_1 - \Delta f_2\right) \tag{3.14}$$

The impact of adding an HVDC link in parallel with the HVAC line is shown in the frequency deviation plot in Figure 3.5. It can be observed that the parallel AC/DC system suppresses the oscillations associated with the AC system and settles more quickly with zero steady-state error.

To generate the ACE signal by the secondary controller for each area of the interconnected systems, the net tie line power deviation must be included, which can be by deduced using:

$$ACE_1 = \beta_1\Delta f_1 + \Delta P_{Tie12} \tag{3.15}$$

$$ACE_2 = \beta_2 \Delta f_2 + \alpha_{12} \Delta P_{Tie12} \tag{3.16}$$

In the steady-state, the power generated by the GENCOs must match the demand of DISCOs in contract with them. This can be expressed as:

$$\Delta P_{mi} = \sum_{j=1}^{4} cpf_{ij} \Delta P_{Lj} \tag{3.17}$$

The load demand variation for the DISCOs in each area is given by:

$$\Delta P_{L1} = \Delta P_{D1} + \Delta P_{D2} \tag{3.18}$$

$$\Delta P_{L2} = \Delta P_{D3} + \Delta P_{D4} \tag{3.19}$$

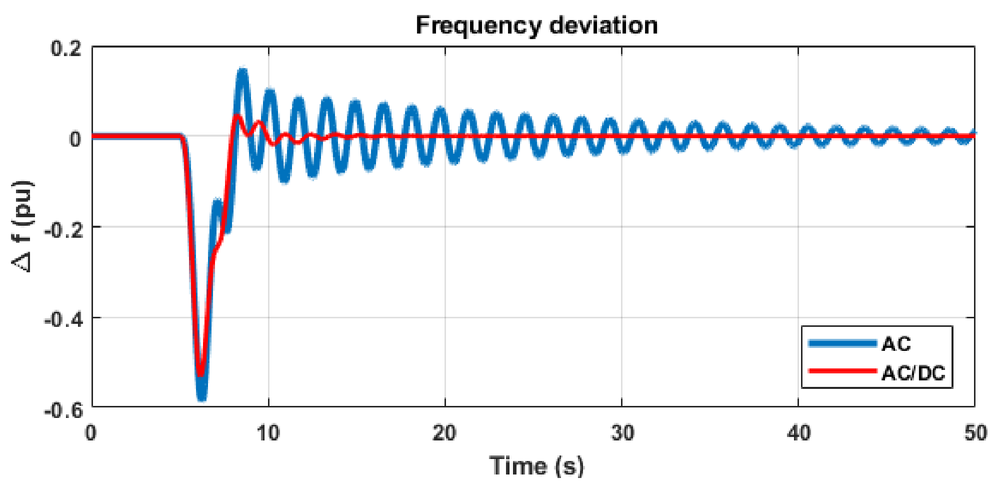

Figure 3.5 Frequency deviation comparison of AC and AC/DC systems.

3.4 Derivative Control Strategy in Grid-connected Wind Energy Systems for Frequency Support

The main configuration of a grid-connected WECS is depicted in Figure 3.6. It consists of a wind turbine directly coupled to the generator (PMSG); the generator is connected to the grid through the bidirectional converter topology and a transformer. Traditionally, WECS are not considered in frequency regulation and therefore do not alter their power production during frequency deviations. More recently, due to the increasing penetration of the full power converter-based wind energy systems to the grid, most wind farms are expected to respond to frequency changes in the system by changing their active power set-points. For example, the South Africa renewable energy grid codes specify that grid-connected wind farms of category C (20 MVA and above) are required to regulate active power at 50 Hz and respond to frequency changes by regulating active power generation within its limits [150]. An active power reserve margin known as P_{delta}, usually 3% above the available wind power, is used for primary control. For grid-connected wind energy systems to

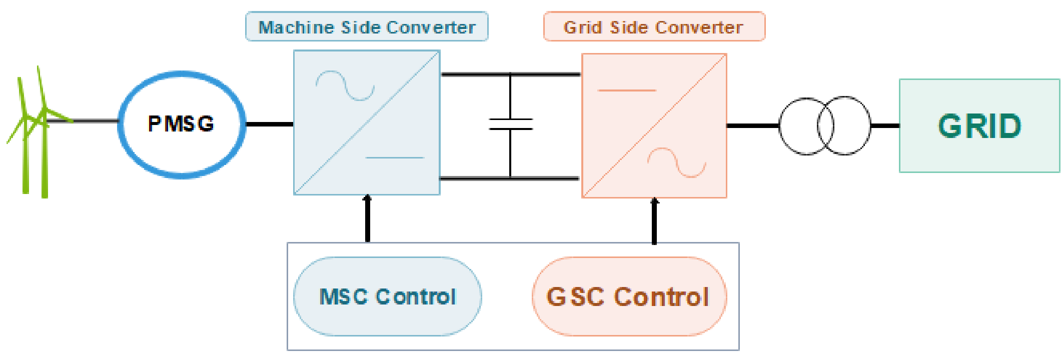

Figure 3.6 Grid-connected PMSG WECS.

suppress the frequency perturbations during load demand variations, the machine side converters (MSCs) should be able to imitate the characteristics of the prime mover used in conventional synchronous generators [151]. To achieve this aim, an extra control loop is added to the MSC control scheme, as shown in Figure 3.7. The modified control scheme of the MSC includes the conventional active and reactive power control loops, and a virtual inertia control loop. The control scheme has d-q voltage controllers, in which the output powers (active and reactive) of the PMSG are controlled using the d and q components of the voltage references. The voltage references are obtained from the PI controllers used to regulate the d and q reference currents. The grid side converter (GSC) control scheme is usually used to regulate the dc-link voltage by considering the power balance between the grid and the generator; the GSC control architecture is described in reference [13]. The additional control loop in the MSC control scheme forms the basis for virtual

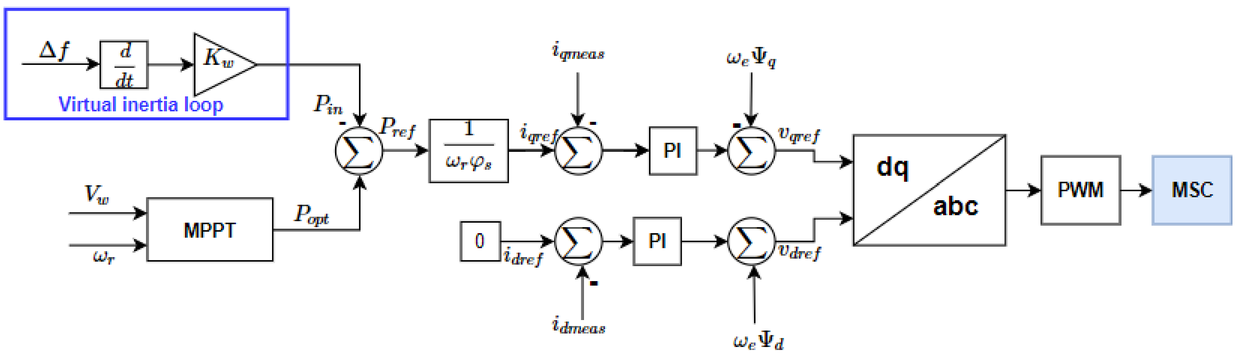

Figure 3.7 Modified control scheme of MSC.

inertia power that can contribute to the increase of the overall inertia response of the system by injecting/absorbing active power during frequency dips/spikes. This work proposes a derivative control strategy to implement the control loop for virtual inertia emulation. The proposed control strategy is capable of reducing the transient frequency deviation by injecting short-term active power into the system. In this work, the wind farms in both areas are equipped with the proposed control scheme to mitigate frequency deviation in both areas. It is assumed that the wind farms are operating at a de-loading point, i.e., below the maximum power that can be extracted at the current wind speed.

To represent the proposed derivative control strategy in the frequency domain, the control law can be evaluated from [5]

$$\Delta P_{wi} = \frac{Kw_i}{(sT_{wi}+1)} \frac{d\Delta f_i}{dt} \tag{3.20}$$

where T_{wi} is the time constant for imitating the dynamic response of the MSC in area i and K_{wi} is the derivative virtual inertia control gain in area i. From (3.20), it is clear that the gain of the controller will modify the active power set point of the MSC based on the rate of change of the frequency and this can be illustrated by the control diagram in Figure 3.8. To effectively support the

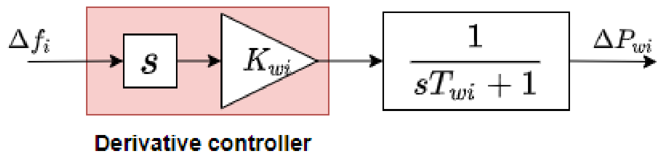

Figure 3.8 Derivative control loop for WECS.

system during disturbances, the control gain parameter must be tuned properly. As stated above, the ABC optimization algorithm is used to tune the control gain. To ascertain the robustness of this optimized control strategy, a comparative evaluation with the conventional tuning method (interior-point algorithm), as presented in [10], is designed.

Using the generalized state-space equation, (3.3)–(3.20) can be written as

$$\begin{aligned} \Delta\dot{x} &= A\Delta x + B\Delta u \\ \Delta\dot{y} &= C\Delta x \end{aligned} \tag{3.21}$$

where Δx is the state vector, A is the state or plant matrix, B is the input matrix, Δu is the input vector, Δy is the output vector, and C is the output matrix. The elements of the state, input, and output vectors are given by

$$\Delta x = \begin{bmatrix} \Delta f_1 & \Delta f_2 & \Delta P_{m1} & \Delta P_{m2} & \Delta P_{m3} & \Delta P_{m4} & \Delta P_{g1} & \Delta P_{g2} \\ \Delta P_{g3} & \Delta P_{g4} & \Delta P_{ACE1} & \Delta P_{ACE2} & \Delta P_{TieAc} & \Delta P_{DC} & \Delta P_{w1} & \Delta P_{w2} \end{bmatrix}^T$$

$$\Delta u = \begin{bmatrix} \Delta P_{D1} & \Delta P_{D2} & \Delta P_{D3} & \Delta P_{D4} \end{bmatrix} \tag{3.22}$$

$$\Delta y = \begin{bmatrix} \Delta f_1 \\ \Delta f_2 \end{bmatrix}$$

3.5 Artificial Bee Colony Optimization Algorithm

The ABC optimization algorithm is a nature-inspired optimization approach proposed by Karaboga in 2005 [152]. It is a computational intelligence method that mathematically mimics the behavior of bees in search of food. The bee colony consists of three classes of bees. The first class is known as the employed bees (B_{em}); they randomly explore the search area for nectar positions (possible solutions). After finding a nectar position (NP), they memorize the details of this position (nectar amount) and share the information of the NP with the colony by dancing to the other bees in the hive. The duration of the dance denotes the quality of nectar (fitness value). The second class of bees is known as the onlooker bees (B_{on}); this set of bees watch the dance of the employed bees before choosing an NP. A rich NP attracts more onlooker bees than a poor NP. The third class of bees is called the scout bees; these are employed bees whose NP are abandoned because of poor quality after a certain number of trials. Onlooker bees can become employed bees if they discover a new NP. In this search process, exploration, and exploitation are simultaneous processes [153].

In the ABC optimization algorithm, the number of employed bees is equal to the number of onlooker bees. The number of possible NPs is equal to the number of employed bees. The initialization of the scouting process is done by scout bees and each iteration involves three major steps:

1. Search for various NPs and information on the quality of each NPs.
2. Selection of NP by the onlooker bees through the information shared by the employed bees.
3. Employed bees with poor NPs become scout bees and are then sent to new NPs.

For the initialization stage, a random distribution of initial population of solutions $x_i \, (i = 1, 2, \ldots, B_{em})$

is generated, where i is the size of the population and B_{em} is the number of employed bees. For each solution, dimension D_n is the number of parameters to be optimized. After initialization, the population of the solutions is subjected to repeated cycles $(C = 1, 2, \ldots, MCN)$ of the search process for the three classes of bees, where MCN is the maximum number of cycles of the search process. For each cycle, the employed bees modify the NP based on the local information (visible content) and the amount of nectar. If the amount of nectar in the new position is greater than the previous one, the bee memorizes it and discards the previous solution; otherwise, it retains the previous position. When all the employed bees have finished the exploration process, they share the information with the onlooker bees in the hive. The onlooker bees select an NP by evaluating the nectar information shared. The probability of selecting an NP is related to the nectar amount. For this study, the roulette wheel selection method is adopted. Thus, the probability of selecting an NP can be evaluated using

$$P_i = \frac{\text{fitness}_i}{\sum_{i=1}^{B_{em}} \text{fitness}_i} \tag{3.23}$$

where $fitness_i$ is the fitness value of the solution i.

It can be deduced from (3.23) that a rich NP will attract more onlooker bees than a poor NP. Before the onlooker bees select another NP, they compare the fitness value of position i to $i+1$. This cycle is repeated until all onlooker bees are dispersed. If the fitness of the solution does not improve for a predetermined limit, the employed bees abandon this solution and become scout bees. When a new position is selected, the cycle starts again until the final conditions are met. To determine the surrounding NP relative to the current NP, the ABC algorithm uses:

$$x_{ij_{new}} = x_{ij_{old}} + \text{rand}\,[0,1]\left(x_{ij_{old}} - x_{kj}\right) \tag{3.24}$$

where $k \neq i, j \in (1, 2, \ldots, D_n)$ and $k \in (1, 2, \ldots, B_{em})$. For each cycle, the scout bees produce a new solution, which is given by

$$x^j_{i_{new}} = x^j_{i_{min}} + \text{rand}\,[0,1]\left(x^j_{i_{\max}} - x^j_{i_{min}}\right) \tag{3.25}$$

In summary, the ABC algorithm has three control parameters: the size of the colony, the limit value, and the maximum cycle number [154]. To apply the ABC optimization algorithm to the frequency response problem of the model described in Section 3.3, an objective function needs to be defined. The objective of this study is to minimize the frequency deviations in both areas. The integral of the squared error (ISE) function is used to define our objective function J, which is obtained from

$$\min\ J = \int_0^t \left(|\Delta f_1|^2 + |\Delta f_2|^2\right) dt \tag{3.26}$$

subject to

$$K_{wi_{min}} \leq K_{w1}, K_{w2} \leq K_{wi_{max}}$$

After the definition of the objective function, the following sequence must be followed to apply the ABC algorithm to the model. The flowchart for the algorithm is shown in Figure 3.9.

Step 1: Generate initial population of solution $x_i\,(i = 1, 2, \ldots, B_{em})$ from (3.19)

Step 2: Evaluate the fitness of the population using $fitness_i = \dfrac{1}{1 + J^2}$

Step 3: Using (3.24), generate new NPs for the employed bees and evaluate the fitness

Step 4: Apply the roulette wheel selection process to choose an NP

Step 5: For the onlooker bees, calculate the probability P_i for the solutions

Step 6: If all onlooker bees are dispersed, go to Step 9; else, go to the next step

Step 7: Generate new NP for the onlooker bees and evaluate their fitness

Step 8: Apply the roulette wheel selection process

Step 9: If there is an abandoned solution for the scout bees, replace it with a new solution and evaluate its fitness

Step 10: Memorize the best solution reached so far

Step 11: Repeat Steps 1–10 for another cycle until $C = MCN$

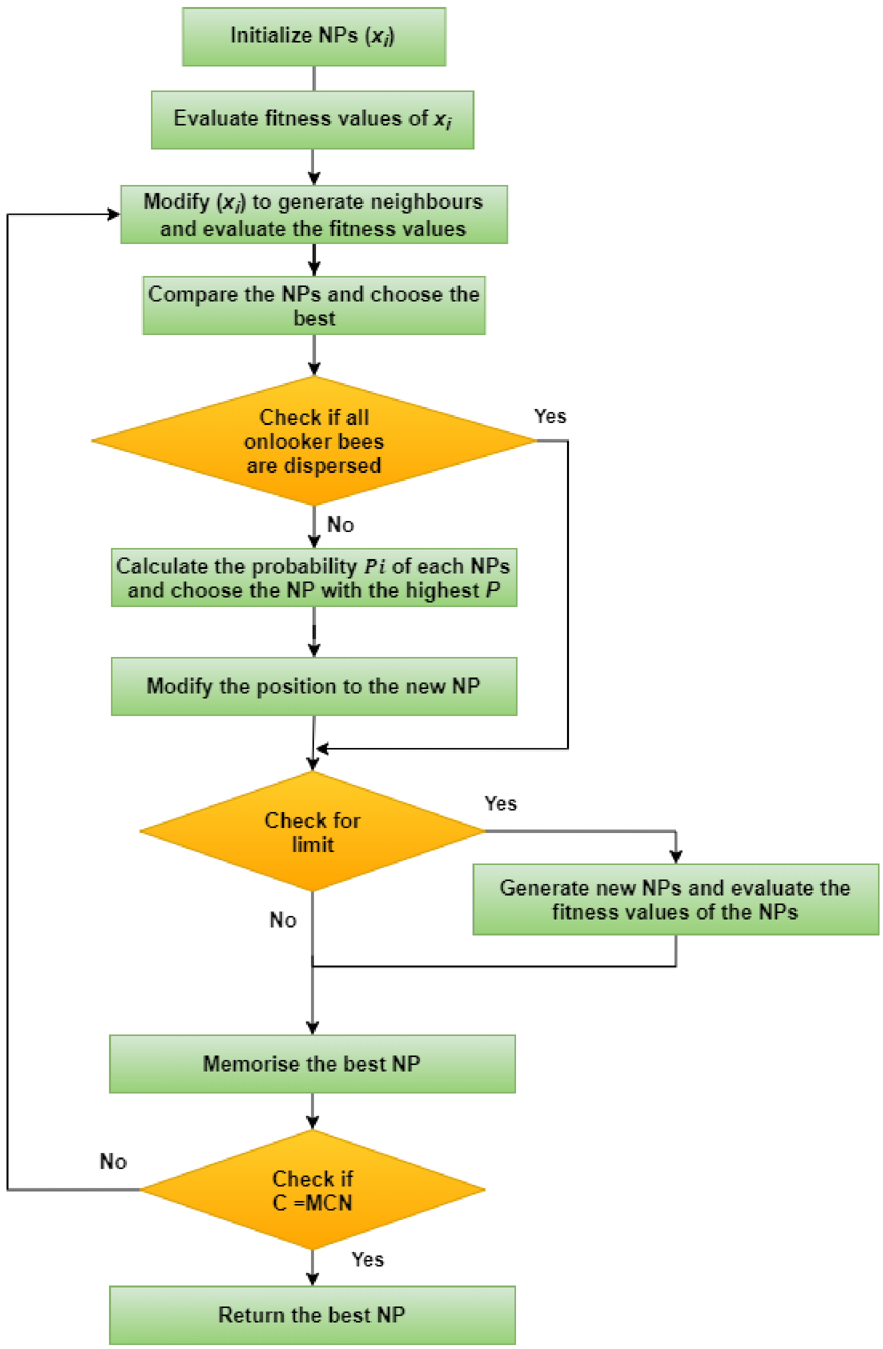

Figure 3.9 Flowchart of ABC optimization algorithm.

The initialization parameters of the ABC algorithm are provided in Table 3.1:

Table 3.1 ABC Algorithm Parameters.

Parameter	Value
Maximum cycle number (MCN)	300
Colony size (CS)	200
Number of employed bees	100
Number of design variables (V)	2
Limit	$0.6^{*}CS^{*}V$

3.6 Results and Discussions

Two analyses are performed with the system model and the results are presented with discussion in this section. The first analysis is the eigenvalue analysis, which is used evaluate and validate the stability of the system model and proposed control strategy. The second analysis is the load–frequency study, which is used to analyze the frequency response of the system in order to demonstrate the robustness of the proposed strategy with respect to different realistic market transaction scenarios. The performance is compared without wind farm support and with the wind farm providing conventional frequency support (classical interior-point algorithm), as described in [10]. The simulations are done in the MATLAB/Simulink environment. The system is modeled in Simulink and the ABC algorithm is written as a script file in the MATLAB environment. The parameters used for the simulation are documented in Table A.1 of Appendix A.

3.6.1 Eigenvalue Analysis

The state-space model described in Section 3.3 is used to analyze the stability of the study system by considering the location of the eigenvalues. To obtain the eigenvalues of the system, the characteristic equation is defined from the state matrix A as:

$$\det(A - \lambda I) = 0 \tag{3.27}$$

where λ is the eigenvalues which can be real or complex and I is an identity matrix. The elements of state matrix A are given in Appendix B. The locations of λ in the s-plane determine the stability of the system. From Lyapunov's first method of stability [155], the following stability criteria apply:

1. If all of the eigenvalues have a negative real part, the system is asymptotically stable.

2. If one or more of the eigenvalues have a positive real part, the system is unstable.

The complex conjugates of eigenvalues can be defined by:

$$\lambda = \sigma \pm j\omega \tag{3.28}$$

where σ is the damping and ω is the frequency of oscillation. A positive σ corresponds to an increasing oscillation while a negative σ corresponds to a damped oscillation.

The location of the eigenvalues of the study system used are shown in Table 3.2. The Table 3.3 shows the total amount of system oscillation damping. It can be deduced that the addition of the wind farm adds two extra modes to the system. The total damping increased and a significant improvement is noticed using the proposed optimization method. In Figure 3.10, the positive effect of the proposed strategy is observed by the shifting of the eigenvalues to the left side of the s-plane.

Table 3.2 Comparison of Eigenvalues.

Mode	No WF Support	Conventional WF Support	Optimized WF Support
λ_1	-17.1457	-17.1558	-17.2131
λ_2	-17.0903	-17.0886	-17.1309
λ_3	-13.0917	-13.0257	-13.0843
λ_4	-14.6662	-14.6012	-14.6278
λ_5	$-0.1780 + j4.7456$	$-0.7186 + j5.2526$	$-1.6315 + j5.2273$
λ_6	$-0.1780 - j4.7456$	$-0.7186 - j5.2526$	$-1.6315 - j5.2273$
λ_7	$-0.9682 + j3.0929$	$-1.3347 + j3.0070$	$-2.2055 + j3.2540$
λ_8	$-0.9682 - j3.0929$	$-1.3347 - j3.0070$	$-2.2055 - j3.2540$
λ_9	-0.4172	$-0.9282 + j0.6974$	$-0.8046 + j0.8489$
λ_{10}	$-1.2326 + j0.4645$	$-0.9282 - j0.6974$	$-0.8046 - j0.8489$
λ_{11}	$-1.2326 - j0.4645$	$-0.4723 + j0.1527$	$-0.3370 + j0.2541$
λ_{12}	-2.9151	$-0.4723 - j0.1527$	$-0.3370 - j0.2541$
λ_{13}	-3.2156	-0.6382	-0.5834
λ_{14}	-3.2314	-3.0310	-3.0355
λ_{15}	———-	$-3.2264 + j0.0034$	$-3.2258 + j0.0033$
λ_{16}	———-	$-3.2264 - j0.0034$	$-3.2258 - j0.0033$

From the presented results, it can be concluded that the participation of renewable energy sources in frequency control can improve system performance through proper control. The improvement in the dampening of oscillation is largely reflected when the control parameters are obtained using the ABC algorithm.

Table 3.3 Comparison of Total Damping.

Parameter	No WF support	conventional WF support	Optimized WF support
Total Damping	76.4590	78. 9008	82.0837

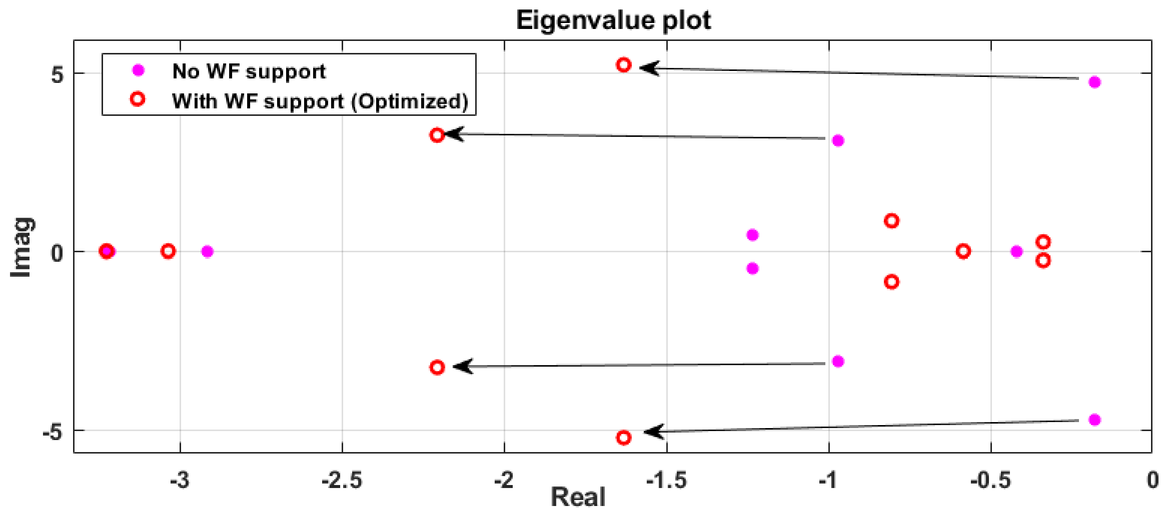

Figure 3.10 Eigenvalue plot of two systems.

3.6.2 Load–Frequency Analysis

In this subsection, the robustness of the proposed control strategy is investigated using LFC analysis, the active power and frequency responses of the system in Figure 3.2 over varying operating conditions are simulated and the results are discussed. For the initial execution of the ABC algorithm, a wide search space is allotted to observe the convergence of the solution, this is reduced afterward. In a restructured environment, the proposed control strategy should be efficient for all possible power system transactions. Three market/transaction scenarios are considered for this analysis.

Scenario 1: Poolco Transaction

In a Poolco based transaction, the GENCOs participate in the frequency response control of their control area only. In this scenario, the load demand variations of DISCO1 and DISCO2 are provided by GENCO1 and GENCO2, while the load demand variations of DISCO3 and DISCO4 are provided by GENCO3 and GENCO4. For a total load demand variation of 0.2 pu in each area, DISCO1 and DISCO2 demands are equal from GENCO1 and GENCO2, while DISCO3 and DISCO4 demands are equal from GENCO3 and GENCO4. The CPM for a Poolco based contract between the GENCOs and DISCOs used in this study is given by:

$$CPM = \begin{bmatrix} 0.5 & 0.5 & 0 & 0 \\ 0.5 & 0.5 & 0 & 0 \\ 0 & 0 & 0.5 & 0.5 \\ 0 & 0 & 0.5 & 0.5 \end{bmatrix}$$

The Figures 3.11–3.13 show the response of the system following a Poolco transaction. Figure 3.11 represents the plot of frequency deviations in both areas. It can be observed that the amplitudes of the first undershoot and overshoot are highest when there is no frequency support provided by the wind farm. With the wind farm providing support using a conventional strategy, the undershoots and overshoots are reduced by 15% and 24%, respectively, for Area 1. Using the proposed control strategy, the deviations are quickly reduced to zero steady-state with minimal oscillations in both areas.

In the steady-state operation, the power generated by the GENCOs must match the demand of the DISCOs in contract with them. From (3.17), the power generated by each GENCO for the respective DISCOs in contract with it can be calculated from

$$\Delta P_{m1} = \Delta P_{m2} = \Delta P_{m3} = \Delta P_{m4} = 0.5 \times 0.1 + 0.5 \times 0.1 + 0 + 0 = 0.1 \text{ pu}$$

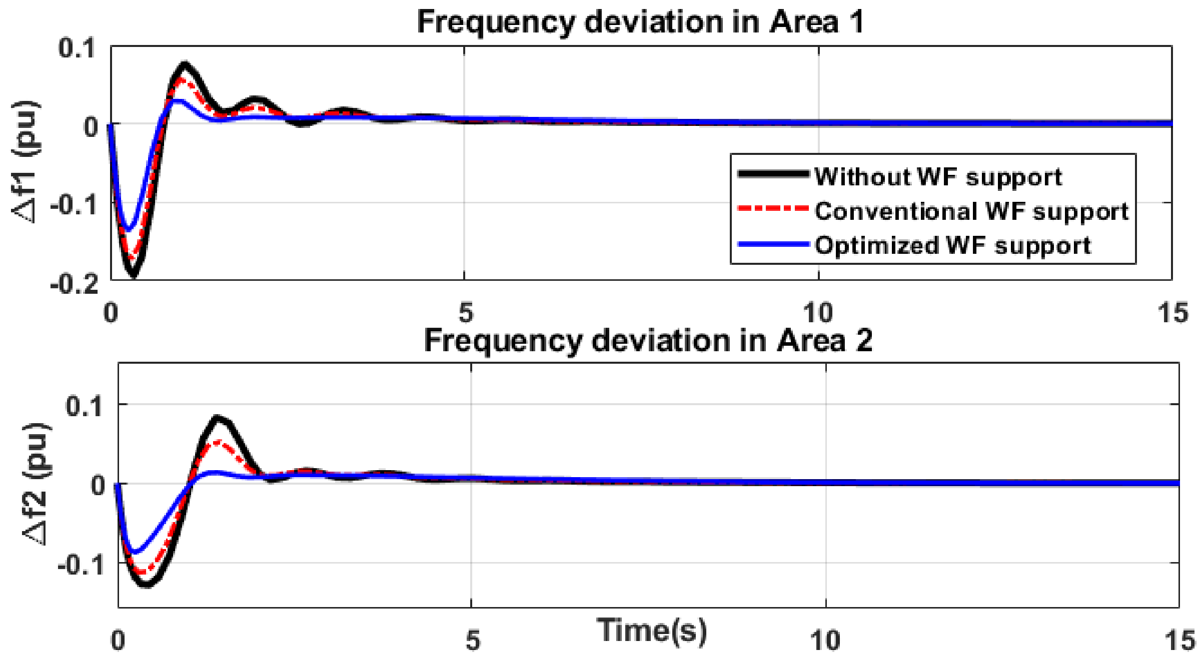

Figure 3.11 Frequency deviation in a Poolco transaction.

Figure 3.12 shows the changes in active power generated by the GENCOs due to the load demand variations. The new steady-state value of each GENCO is the amount of contracted demand from the DISCOs in its area. It can be observed that the participation of wind farms in frequency control can reduce the amount of transient power needed by the GENCOs to reach the new steady-state values. By using the ABC algorithm for optimal control, the wind farm is capable of providing active power, thereby reducing the amplitude of the transient power provided by the GENCOs. It can be observed that overshoots were reduced by 16%, 14.3%, 16%, and 13.3% in the GENCOs when compared to the conventional control strategy. Since there is no exchange of power between the areas, the scheduled tie line power flow will be zero as defined by (3.10), so that

$$\Delta P_{tiesch} = 0 \text{ pu}$$

However, tie line perturbations will occur when there is load demand variation due to interconnection, as shown in Figure 3.13. It is generally observed that the proposed optimized controller helps the system to reach a faster settling time, with the system experiencing damping, which suppresses

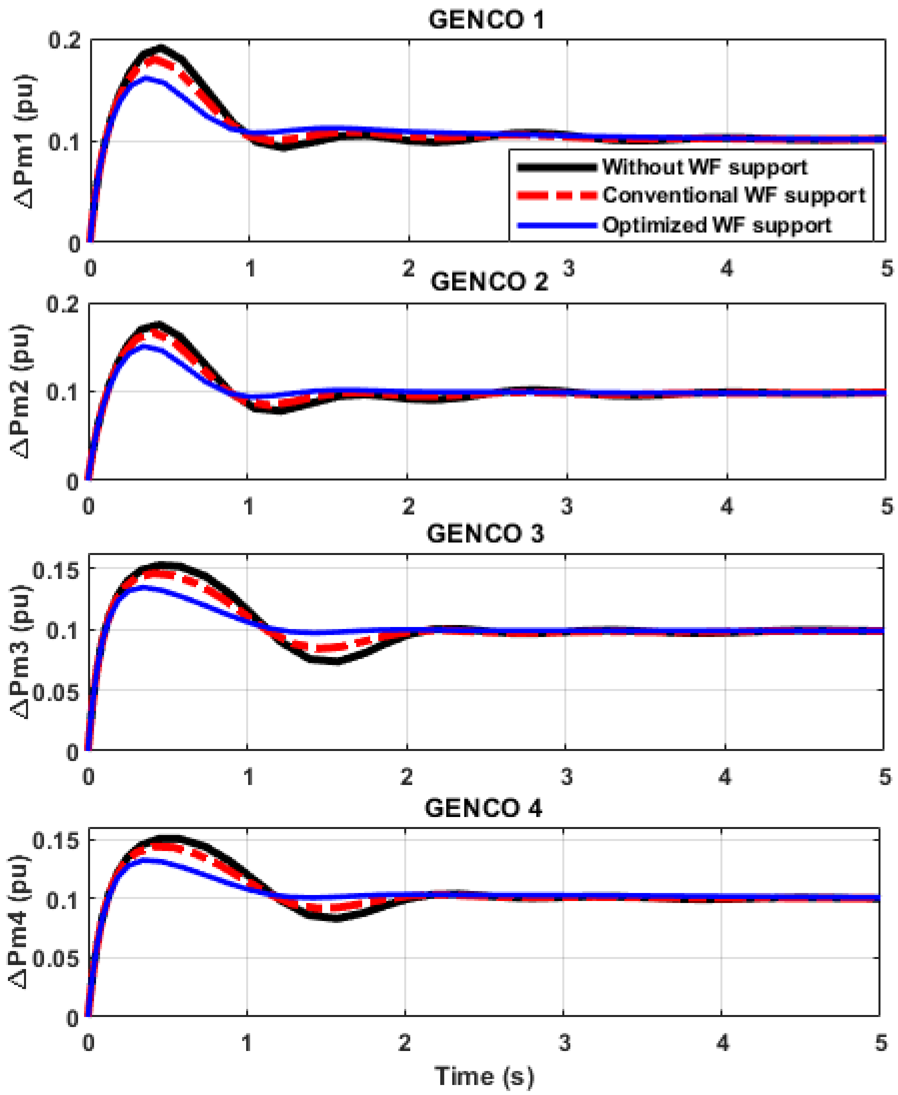

Figure 3.12 Change in power generation of GENCOs in a Poolco transaction.

the oscillation, thereby providing a better dynamic response.

Scenario 2: Bilateral Transaction

In the bilateral transaction, DISCOs can be in contract with any GENCO within or outside their own areas; i.e., GENCOs in Area 1 can transfer power to DISCOs in Area 2 and vice versa.

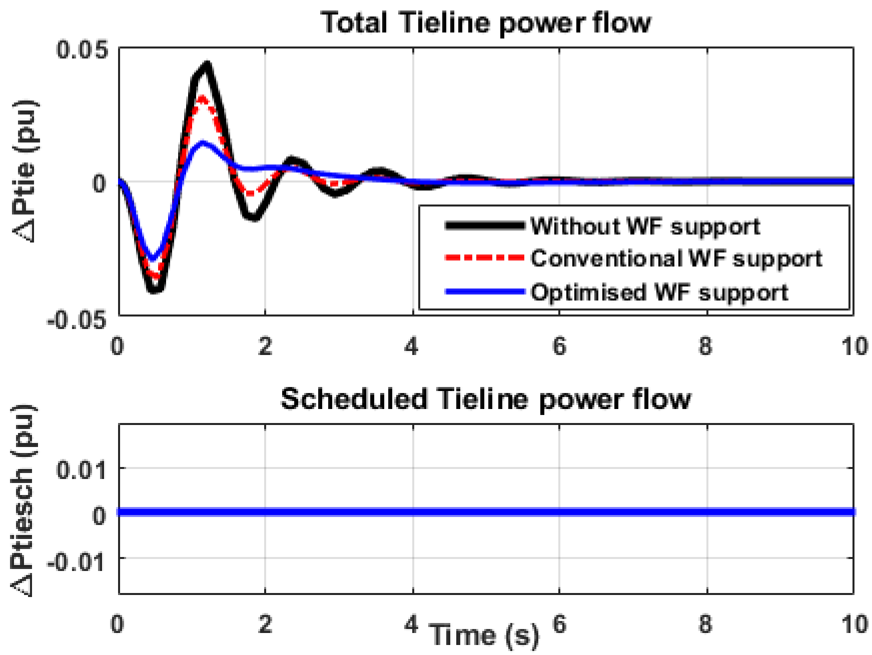

Figure 3.13 Tie line power flow in a Poolco transaction.

Therefore, inter-area exchange of power via the tie lines is scheduled at a non-zero steady-state value. In this study, each DISCO demands 0.1 pu power from the GENCOs in both areas, as defined by the CPM below

$$CPM = \begin{bmatrix} 0.5 & 0.4 & 0.5 & 0 \\ 0.2 & 0.1 & 0 & 0.5 \\ 0.15 & 0.3 & 0.4 & 0 \\ 0.15 & 0.2 & 0.1 & 0.5 \end{bmatrix}$$

The non-diagonal elements of the CPM correspond to the contract of a DISCO in one area with a GENCO in another area. The Figures 3.14–3.16 show the response of the system as a result of the bilateral transaction. Figure 3.14 shows the frequency deviation in Areas 1 and 2. It can be seen that the peak undershoot and overshoot are the highest when there is no support from the wind farms. When the wind farms participate in frequency control using conventional control, the undershoot and overshoot are reduced by 15% and 18% in Area 1 and 13% and 50% in Area 2, respectively. A further reduction is noticed when the gain of the controller is optimized using the ABC algorithm. The oscillations are suppressed and the system frequency deviation settles faster to zero in the steady-state condition.

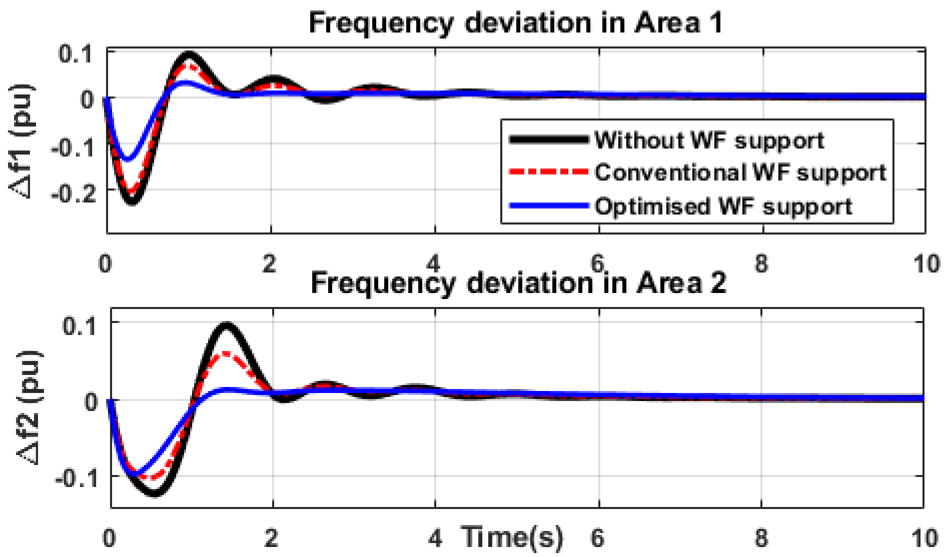

Figure 3.14 Frequency deviation in bilateral transaction.

From (3.17), the change power generated by each GENCO in the bilateral transaction scenario can be calculated from

$$\Delta P_{m1} = 0.5 \times 0.1 + 0.4 \times 0.1 + 0.5 \times 0.1 + 0 = 0.14 \text{ pu}$$

$$\Delta P_{m2} = 0.2 \times 0.1 + 0.1 \times 0.1 + 0 + 0.5 \times 0.1 = 0.08 \text{ pu}$$

$$\Delta P_{m3} = 0.15 \times 0.1 + 0.3 \times 0.1 + 0.4 \times 0.1 + 0 = 0.085 \text{ pu}$$

$$\Delta P_{m4} = 0.15 \times 0.1 + 0.2 \times 0.1 + 0.1 \times 0.1 + 0.5 \times 0.1 = 0.095 \text{ pu}$$

The change in power generated by each GENCO is presented in Figure 3.15. It can be observed that, without the wind farm support, there is increased transient power generation by the GENCOs;, this deviation is reduced when there is support from the wind farm by providing active power for a short time. The effect of wind farm participation is largely noticed when the optimized derivative control is applied. This results in over 20% reduction in transient power from the GENCOs when the proposed strategy is implemented. The scheduled tie line power flow is shown in Fig-

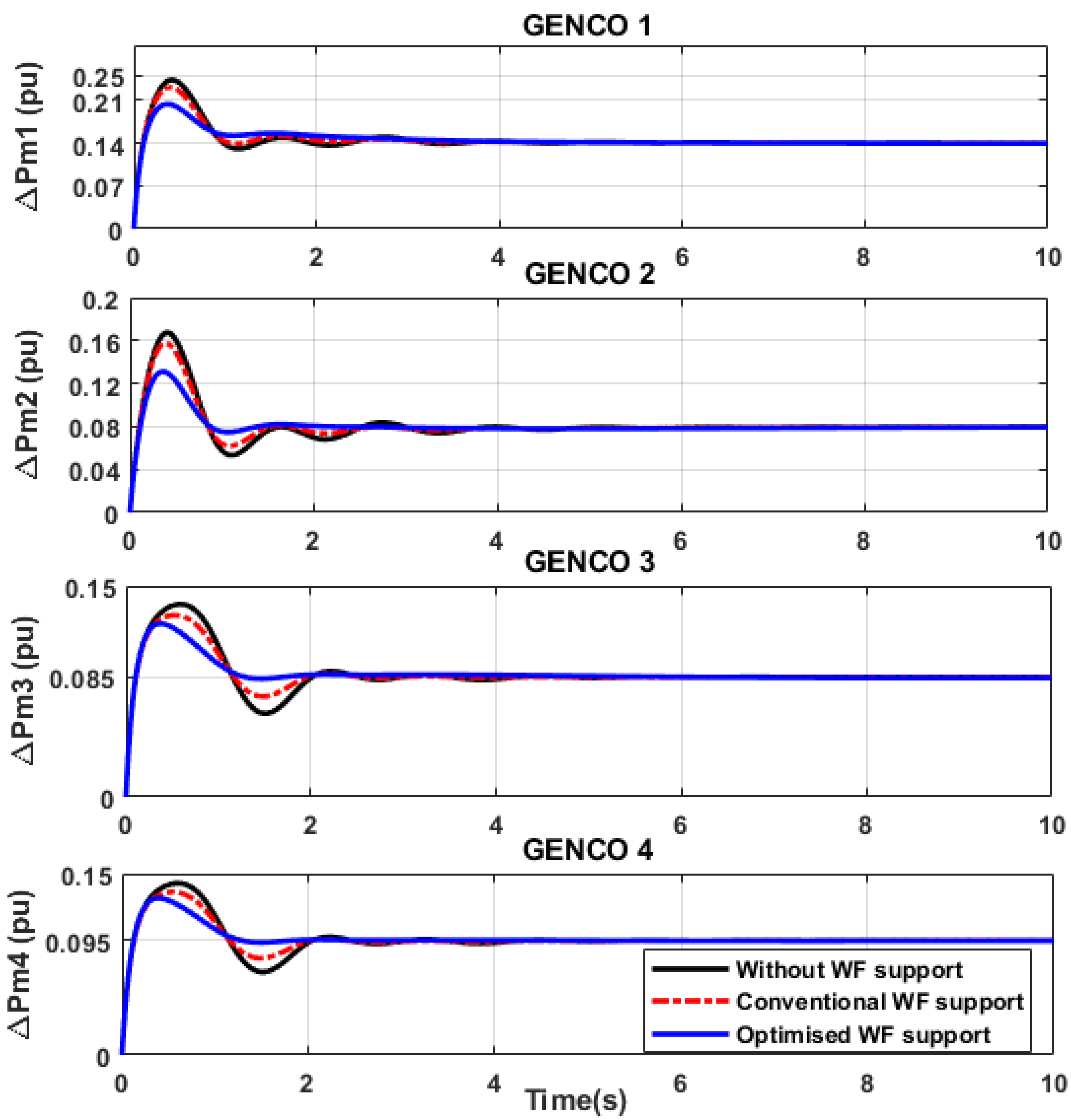

Figure 3.15 Change in power generation of GENCOs in bilateral transaction.

ure 3.16. This illustrates the exchange of power between both areas at steady-state operation, it can be calculated as

$$\begin{aligned}\Delta P_{\text{tiesch}} =&[0.5\times 0.1+0+0+0.5\times 0.1]\\&-[0.15\times 0.1+0.3\times 0.1+0.15\times 0.1+0.2\times 0.1]\\=&0.1-0.08\\=&0.02\text{ pu}\end{aligned}$$

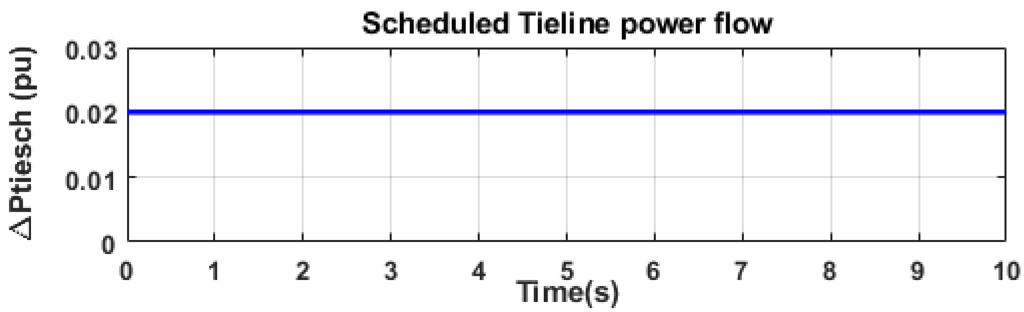

Figure 3.16 Tie line power flow in a bilateral transaction.

Scenario 3: Contract Violation

At times, DISCOs may demand more power than that specified in the contract. This extra variation is usually not contracted to any GENCO. When this happens, only GENCOs in the affected area can respond to the excess demand variations from the DISCO. The excess demand variation is always regarded as a local load demand variation. Modifying Scenario 2 (bilateral transaction) with an extra demand variation of 0.1 pu from DISCOs in Area 2 at 15s, the CPM in Scenario 2 remains the same.

Starting the analysis from 15s in Figures 3.17–3.19, the effect of the uncontracted load demand variation in Area 2 can be observed. From the frequency deviation plots shown in Figure 3.17, it can be seen that the extra load demand variation in Area 2 causes frequency dips in Areas 1 and 2 due to interconnection. The oscillations associated with the system without wind farm support are damped when the wind farms participate in frequency control; however, the proposed optimized controller has a better damping response than the conventional control strategy.

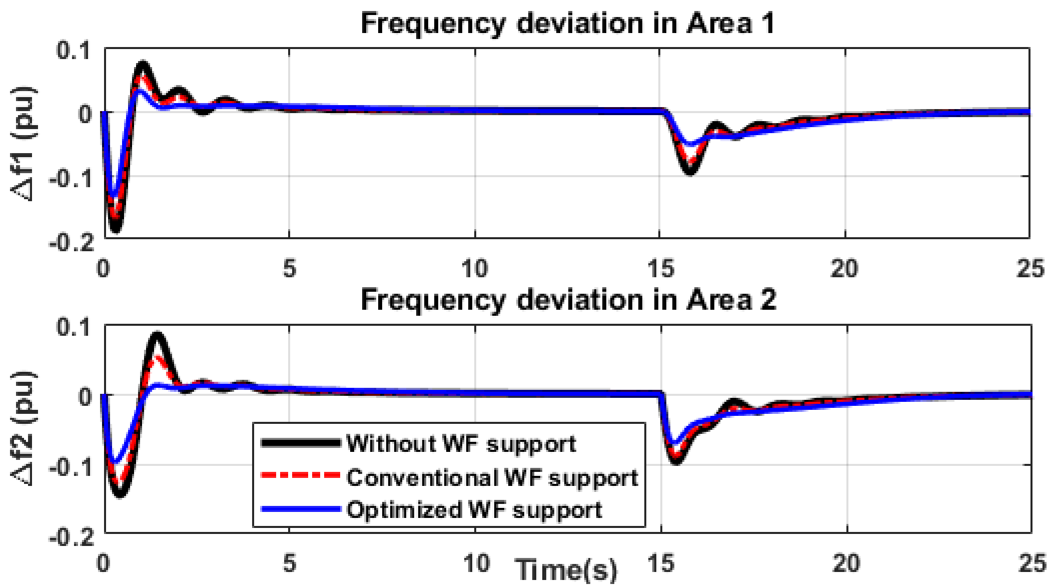

Figure 3.17 Frequency deviation in contract violation.

In this transaction, the change in power generation due to un-contracted variation is the responsibility of the GENCOs in that area; that is, the GENCOs in other areas return to the initial steady-state values after participating in the frequency control. In Figure 3.18, the change in power generated by GENCO1 and GENCO2 remains the same; i.e., $\Delta P_{m1} = 0.14$ pu and $\Delta P_{m2} = 0.08$ pu. However, there are new steady-state values for GENCO3 and GENCO4. The changes after 15s can be calculated using:

$$\Delta P_{m3} = 0.085 + 0.5 * 0.1 = 0.135 \text{ pu}$$

$$\Delta P_{m4} = 0.095 + 0.5 * 0.1 = 0.145 \text{ pu}$$

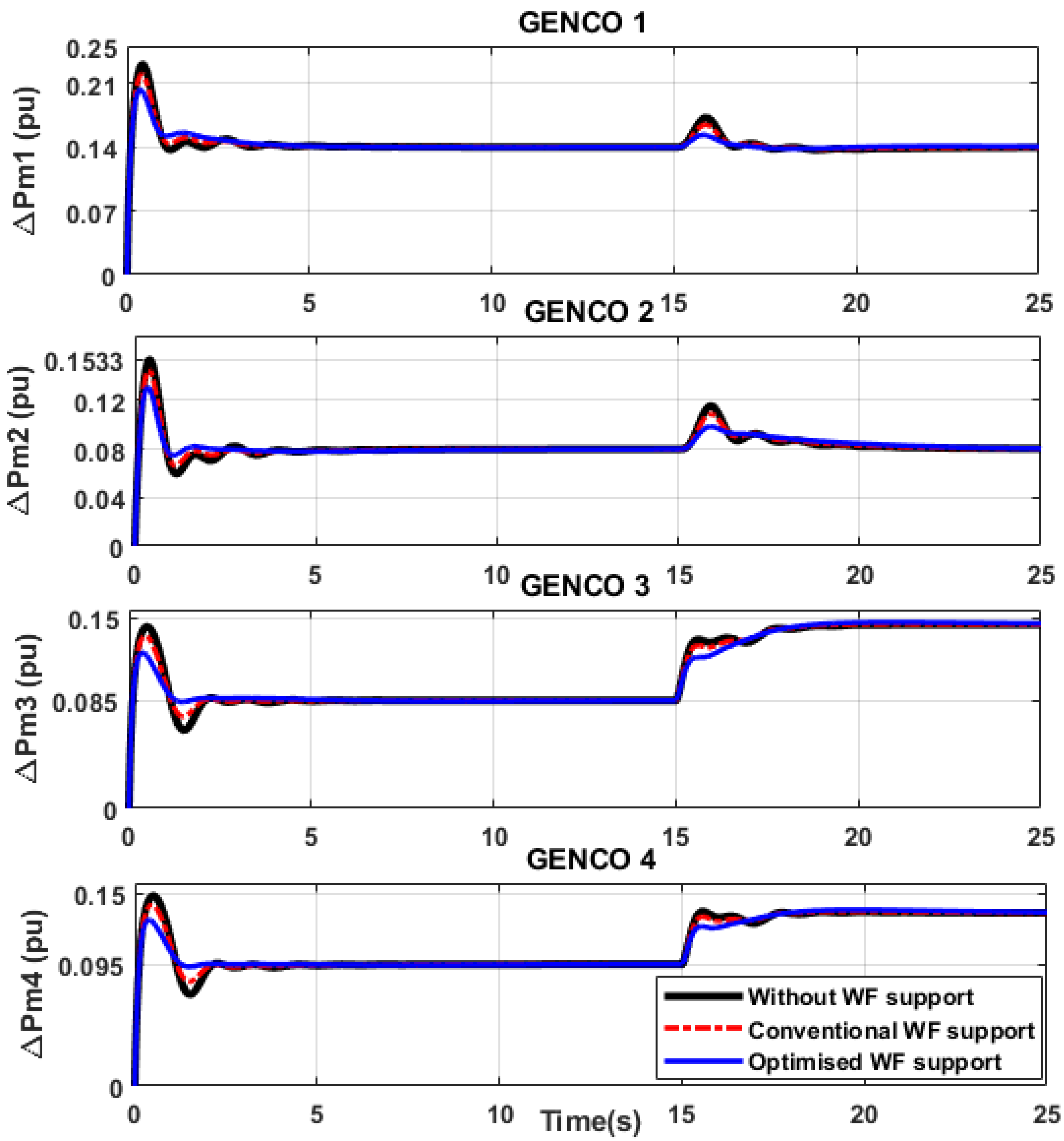

Figure 3.18 Active power generation of GENCOs in contract violation.

The scheduled tie-line power flow remains unchanged because only the GENCOs in Area 2 supply the extra demand, as shown in Figure 3.19.

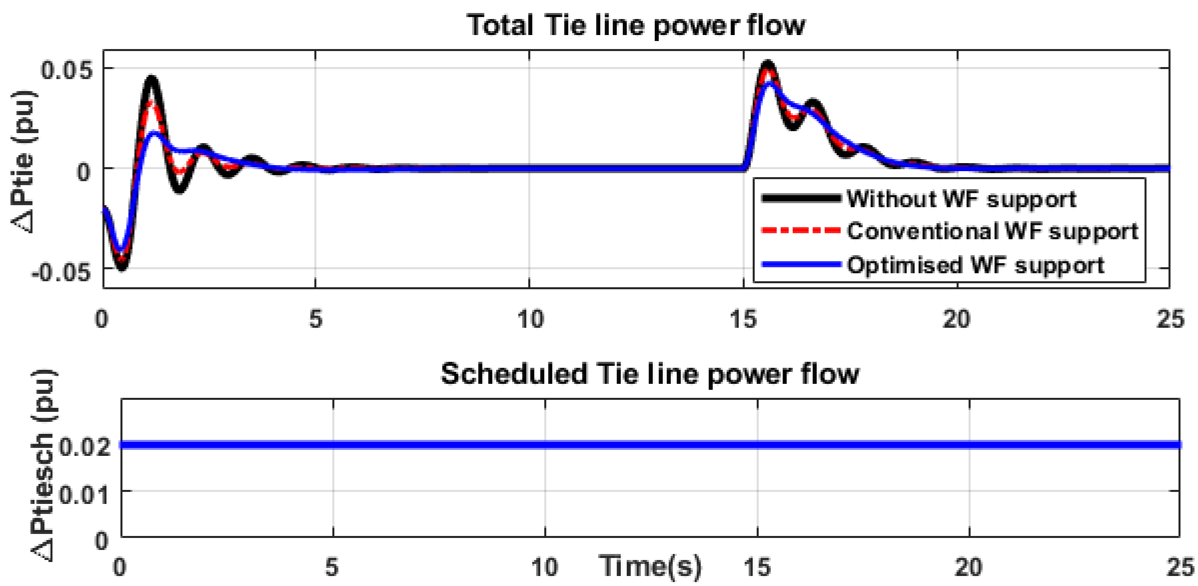

Figure 3.19 Tie line power flow in contract violation.

Scenario 4: Wind Power Fluctuation

Since wind power is largely dependent on wind speed, which is usually intermittent, it is expected that the contribution of wind farms in frequency response control will be limited. In this work, it is assumed that the de-loading margin is available in all range of wind speeds and the short-term support lasts for a fraction of second to a few seconds. To test the robustness of the proposed control strategy, during wind power fluctuation, as shown in Figure 3.20, a change in load demand of 0.15 pu in Area 1 is simulated at 5s.

In Figure 3.21, the frequency deviations in both areas of the system are presented for cases where the wind farms support in frequency stability using the conventional tuning method (dashed blue) and ABC tuning method (red). It is observed that the proposed tuning method provides better damping characteristics and reduced frequency excursions. It is pertinent to point out that the control approach proposed in this work can be extended to energy storage systems to provide mid-

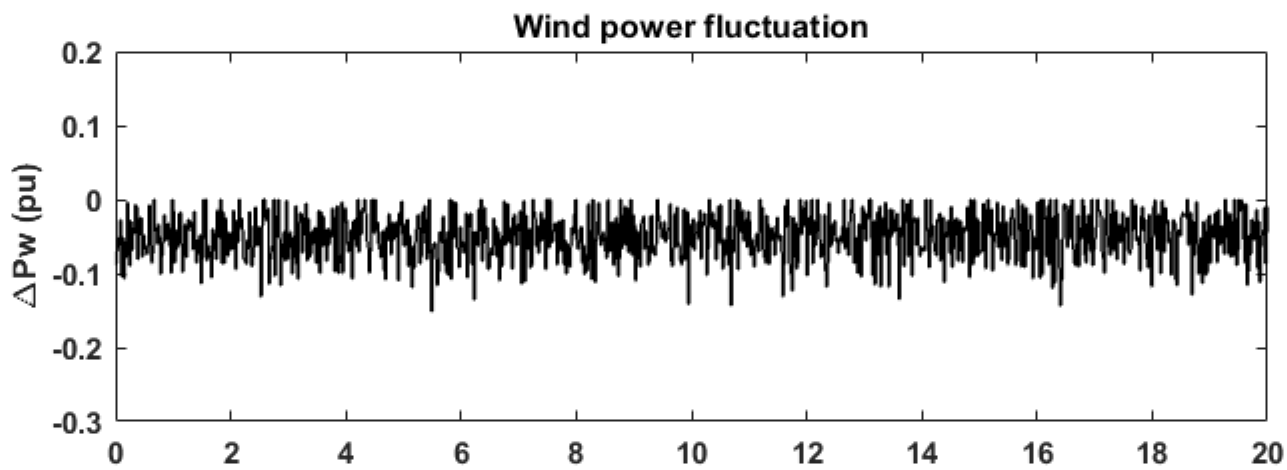

Figure 3.20 Wind power fluctuation.

and long-term frequency support to power systems.

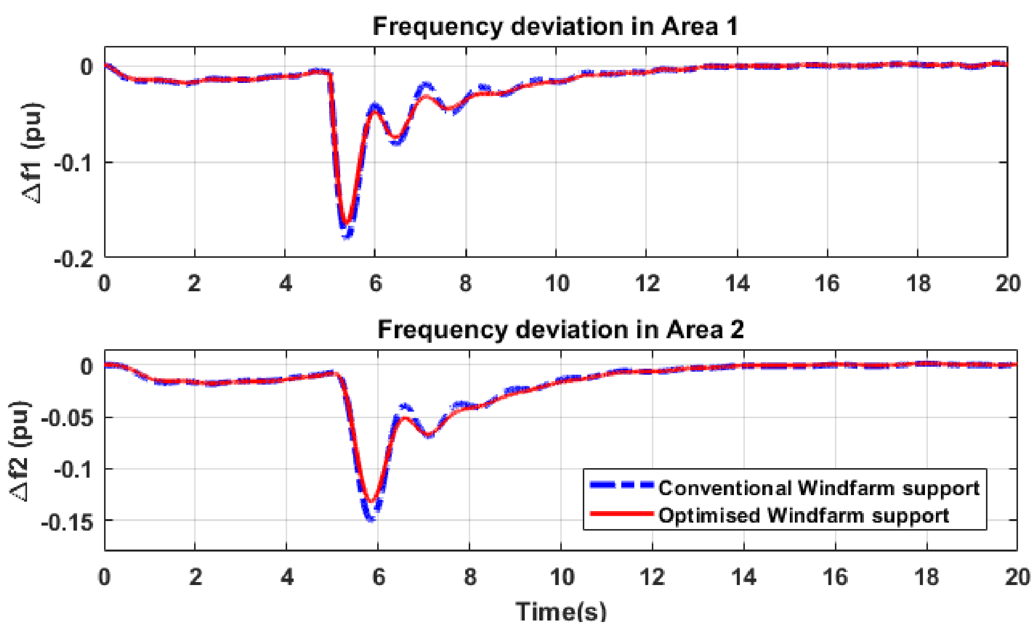

Figure 3.21 Frequency deviation during wind power fluctuation.

3.7 Summary

In this study, the artificial bee colony algorithm was used in the implementation of a virtual inertia control strategy. This involves the formulation, development, and simulation of a system model that can be used in traditional power systems and can be extended to modern power systems with renewable energy penetration and power system deregulation. This optimization algorithm was used to investigate the positive impact that renewable energy has on the network with respect to frequency control. The heuristic method is used to optimally tune the gain of the virtual inertia control scheme that is proposed to reduce the frequency transient deviations in a restructured power system environment. The control strategy was tested in a two-area system having conventional generation, wind power plants, and parallel ac/dc links to model a simple modern power system. Three transaction scenarios (Poolco, bilateral, and contract violation) were implemented to show the robustness of the proposed control strategy. It is generally observed that peak overshoots and undershoots, settling time, and oscillations of the system were greatly reduced. In addition, the overall dynamic performance and stability of the system are improved. The proposed strategy can be applied to expanded power systems that include more interconnected areas with additional generating plants such as solar, geothermal, ocean, and tidal power plants.

Chapter 4

A Virtual Inertia Control Method for High Renewable Energy-Integrated Interconnected Power Systems

This chapter is based on the work reported in [2].

4.1 Chapter Overview

With the growing penetration level of renewable energy (RE) systems, the overall inertia of the power system is expected to reduce to values that expose the system to inadvertent frequency eventuality that can threaten the stability, security, and resilience of the system. To tackle this issue, this paper proposes a new intelligent virtual inertia control strategy in an interconnected power system which considers high renewable energy penetration and power system deregulation. The virtual inertia control is capable of providing dynamic inertia support by adjusting the active power reference of the power electronic converter of an energy storage system (ESS). This improves the response and stability of the system during frequency events. The proposed virtual inertia control strategy is based on the type-II fuzzy logic control scheme. This is because of the extra degree of freedom it gives which can handle uncertainty. To improve the accuracy and performance of the proposed controller, the artificial bee colony algorithm is used for optimal tuning of the input and output weights of the type-II fuzzy-based virtual inertia control. The proposed control strategy is designed to competently perform during load variation, RE fluctuations, and other power system dynamic disturbances. The simulation results show its robustness in minimizing the frequency deviation and maintaining system frequency within specified operating limits. This is while efficiently operating over a wide range of operating conditions in the new restructured power system environment.

4.2 Chapter Introduction

Major changes have been introduced in the structure of electric power utilities around the world to improve the efficiency and reliability of power systems. These new developments require innovations in various parts of the system and reliability plays a critical role in the newly restructured environment [156]. Power system deregulation and increased renewable energy (RE) integration and penetration are the major factors in the restructured power system environment. In this environment, control is greatly decentralized and Independent System Operators (ISOs) are responsible for maintaining the system frequency and tie-line power flow amongst other ancillary services [?]. The load demand from distribution utilities requires a different control procedure from the traditional environment; however, this procedure must be coordinated to retain the nominal system frequency and scheduled tie line power flow. Generation utilities may or may not take part in automatic generation control (AGC) or load frequency control (LFC); these make the task of frequency control more complicated to achieve. Several works have reported various approaches for LFC design when considering power system deregulation to improve the frequency response of the system [103, 107, 135, 136, 157].

In a similar way to power system deregulation, the structure of the emerging power system that incorporates RE systems, such as wind and solar plants, is different from the conventional power system structure. The key technical concern that affects the increasing penetration level of RE systems is associated with their capability in performing as efficiently and consistently as conventional generation systems. This is because they affect the dynamic behavior and response of large power systems differently from their conventional counterparts [158]. While the aggregation of RE systems can dampen the effects of fluctuating power outputs from individual RE units, there is a need for RE systems to meet some technical requirements known as "grid code" to achieve reliable operation of the grid. However, with the growing penetration of RE systems, there is a need to update the grid codes to continuously mitigate the impacts of RE system integration.

Despite the rapid technological advancements in the RE industry, the task of frequency regulation remains a challenge, and this constitutes the limitation of increasing RE share in modern power systems. Grid codes such as the South Africa Renewable Energy Grid Code (SAREGC) require that wind farms seeking connection to the grid must participate in active power-frequency response to support the grid during short-term frequency events [159]. A dynamic demand control scheme was proposed in the control loop of a doubly-fed induction generator-based wind farm for fast frequency support [160]. A rapid active power control was designed for photovoltaic (PV) systems to mitigate frequency contingency scenarios [161]. However, this study predicted that with the current growth rate of RE penetration, the total system inertia would reduce significantly to values that threaten system frequency recovery and stability during power imbalance and other power system contingencies [162]. Therefore, technical methods for providing or emulating inertia need to be developed.

The virtual inertia control strategy is a promising solution in emulating the inertia characteristics of a prime mover by deploying an appropriate control algorithm in the power electronics converter of a dedicated energy storage system (ESS) [115]. Several control strategies have been adopted in the design of a virtual inertia control: the authors in proposed a coefficient diagram method [163]; a dynamic equation and adaptive fuzzy technique were proposed [164]; a linear-quadratic regulator approach was adopted [165]; the H-robust control method was used [166]; a derivative-controlled solar and ESS was proposed [167], and a model predictive control (MPC) approach was designed to improve the frequency regulation capability of low-inertia microgrid systems [168]. Small-signal modelling and analysis of a virtual inertia system was presented in [169].

While the classical control strategies used for inertia emulation provide good frequency response, they perform poorly outside the operating range for which they are designed. This is because they have a fixed inertia gain for a wide range of operating points. The optimization of conventional control techniques using heuristic optimization algorithms can improve the performance of the virtual inertia control. The artificial bee colony (ABC) algorithm was used to tune the derivative-virtual inertia control for wind energy systems [1]. The chicken swarm optimization algorithm was adopted in tuning the parameters of an adaptive virtual inertia controller [170], and the particle swarm optimization (PSO) was used in [171]. The performance of the optimized controller is usually trapped within the operating points for which the controller is tuned, therefore cannot efficiently handle a wide range of operating conditions. Some artificial intelligence techniques have found application in the design of virtual inertia systems [172–174]. A reinforcement learning-based approach [172, 173] to design a virtual inertia controller for low-inertia power systems. A radial basis function neural network [174] was trained to implement a virtual synchronous generator. A virtual inertia controller using the wavelet fuzzy neural network [175]. These control methods that apply artificial neural networks are largely dependent on the availability of data to sufficiently train the model, therefore, such control methods might result in over-fitting if the training data is insufficient, thereby compromising the performance of the control system. The fuzzy logic control is an intelligent control technique that has been used to improve performance in terms of virtual inertia control because of its high computational efficiency in handling nonlinear complexities that are characterized with modern power systems [176]. The type-I fuzzy logic [5] was proposed for virtual inertia control of an interconnected microgrid with high RE penetration. The low-inertia wind farm was augmented with a type-I fuzzy-based ESS to improve the primary frequency response of the system [177]. A type-I fuzzy and particle swarm algorithm was combined to design a frequency controller for an AC microgrid [178]. A dynamic virtual inertia using type-I fuzzy logic was proposed for interconnected microgrids [179]. While the type-I fuzzy system has been successfully implemented, it is less efficient in handling different power quality threshold requirements and uncertainties. Uncertainty is a property of information that can be vague, contain prediction errors, obtained from inaccurate system models, and time-variant system models, some of which can be attributed to RE systems [180]. Based on this limitation, the type-II fuzzy system was introduced. It uses a three-dimensional membership function (MF) to represent its fuzzy sets. This offers an extra degree of freedom to model the uncertainties that cannot be quantified by two-dimensional MFs of the type-I fuzzy system [181]. A type-II fuzzy control was used to design the converter control of a DFIG system to reduce power overshoots and increase voltage recovery during parameter variation [182]. The type-II fuzzy logic system to mitigate LFC problems in RE-integrated power systems [183–186].

Based on the literature, the authors have focused on the design of several virtual inertia control methods for microgrid systems. No previous work has been reported on the development of type-II fuzzy logic control strategies for virtual inertia emulation; there has been no report on the investigation of inertia emulation for large power systems with high penetration of RE systems in the deregulated environment. These gaps form the basis of the major contributions of this paper which can be highlighted as:

- Design of a new type-II fuzzy-based virtual inertia control strategy to improve the frequency response and stability of power systems.
- The performance of the proposed type-II fuzzy-based virtual inertia controller is improved by tuning its weights with the ABC optimization algorithm. The choice of ABC is due to its less computational complexity, high solution accuracy, simplicity, and independent convergence when compared to other heuristic algorithms [187]. The cost function used in the optimization process is formulated to be model-dependent such that the proposed virtual inertia system does not behave as a continuous infinite energy source.
- The proposed optimal type-II fuzzy-based virtual inertia control strategy is implemented in the emerging power system environment which considers high RE penetration, deregulation, hybrid transmission between interconnected control areas, and unequal control areas.
- The robustness of the proposed control strategy is validated with practical power systems

scenarios such as load variation, high RE fluctuation, and parameter variation.

- The proposed control strategy can be adapted to different system models by simply re-tuning the weights of the type-II fuzzy control and proper selection of cost function used in the optimization/tuning process.

The remainder of this chapter is structured as follows: Section 4.3 presents the small-signal modelling of power system for frequency response analysis in the restructured environment, Section 4.4 presents the concept of inertia and introduces the virtual inertia control strategy, Section 4.5 presents the proposed optimized type-II fuzzy logic for inertia emulation, Section 4.6 discusses the simulation results of the proposed control strategy and Section 4.7 presents the conclusion.

4.3 System Modelling

In this section, the small-signal model of the interconnected power system is presented. The system model takes into account the emerging complexities such as power system deregulation, high renewable energy integration, and hybrid power transmission that exist in the modern power system environment.

4.3.1 Dynamics of Power System Deregulation

In the formulation of the frequency response model of the interconnected power system in the restructured environment, it is important to include the dynamics of the open-energy market scenarios that occur between power vendors–generating companies (GENCOs) and vendees–distribution companies (DISCOs). For an interconnected power system with N control areas, the contract participation matrix (CPM) between GENCOs and DISCOs can be defined as

$$\text{CPM} = \begin{bmatrix} cpf_{11} & cpf_{12} & \cdots & cpf_{1N} \\ cpf_{21} & cpf_{22} & \cdots & cpf_{2N} \\ \vdots & \vdots & \ddots & \vdots \\ cpf_{n1} & cpf_{n2} & \cdots & cpf_{nN} \end{bmatrix} \tag{4.1}$$

where cpf_{nN} is the contract participation factor of the n^{th} GENCO of the N^{th} area. The sum of the elements in each column of the CPM must be equal to 1. Furthermore, there could exist a scenario where there is exchange of power between interconnected areas via tie lines at scheduled values during steady-state operation. In this scenario, the GENCOs in Area i are in a power purchase contract with the DISCOs is Area j; therefore, the non-diagonal elements of the CPM are non-zero. The scheduled tie line power flow to Area i for N interconnected control areas can be written as

$$\begin{aligned} \Delta P_{tie,i}^{sch} = & \sum_{\substack{j=1 \\ j\neq i}}^{N} \left(\sum_{k=1}^{n} cpf_{kj} \right) \Delta P_{D_{c,j}} \\ & - \sum_{k=1}^{n} \left(\sum_{\substack{j=1 \\ j\neq i}}^{N} cpf_{jk} \right) \Delta P_{D_{c,i}} \end{aligned} \tag{4.2}$$

where $\Delta P_{D_{c,i}}$ and $\Delta P_{D_{c,j}}$ are the total power demand (contracted) of DISCOs in Areas i and j respectively, given that $\{i,\, j \in N\}$.

4.3.2 Small-Signal Modelling of Modern Power System

In this subsection, the canonical frequency response model of a modern power system is presented using small-signal derivations. The system model takes into account the deductions from the previous subsection, frequency response of RE systems as specified by different grid codes. The frequency response model shown in Figure 4.1 represents the small signal derivation of the i^{th} control area of an interconnected power system in the restructured power system environment. The frequency response of Area i resulting from the net active power generation and demand is

$$\Delta f_i = \frac{1}{2H_i s + D_i}(\Delta P_{m_i} + \Delta P_{res_i} - \Delta P_{tie,i} - \Delta P_{D_i}) \tag{4.3}$$

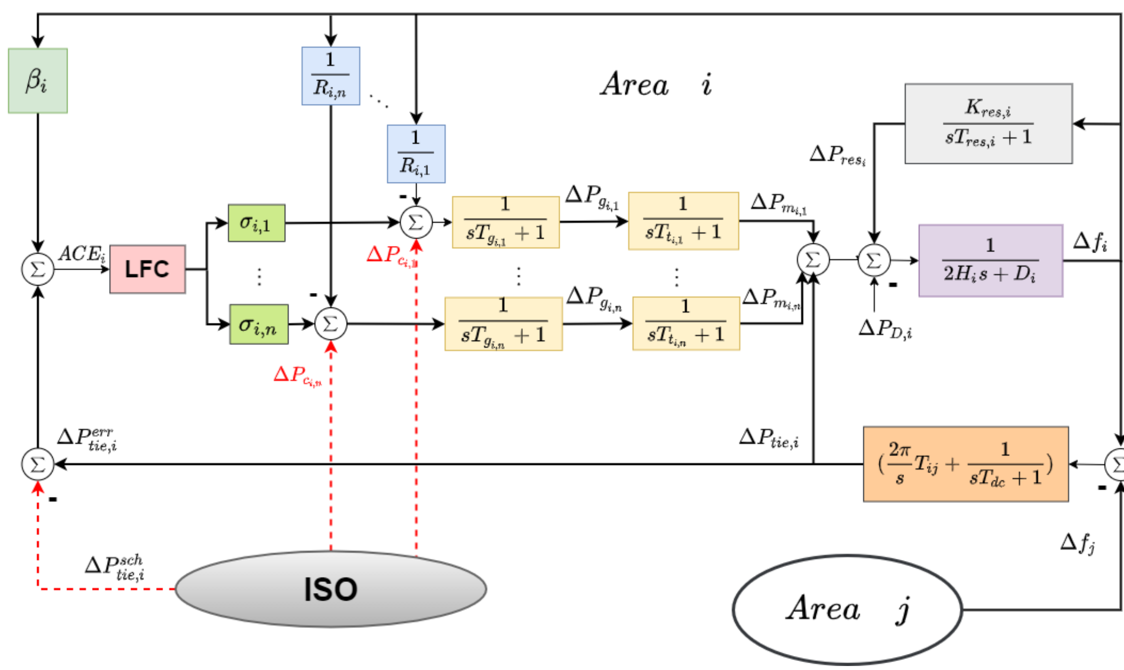

Figure 4.1 Frequency response model of a power system in the restructured environment.

where H is the total inertia constant of the synchronized rotating masses, D is the damping parameter, ΔP_m is the total change in mechanical power of the GENCOs, ΔP_{res} is the total change in power of the RE systems, ΔP_{tie} is the change in tie line power flow, and ΔP_D is the total load change in Area i.

The change in output mechanical power of the GENCOs in the i^{th} area is given by

$$\Delta P_{m_i} = \sum_{j=1}^{n} \Delta P_{m_j} = \sum_{j=1}^{n} \frac{1}{sT_{t_j} + 1} \Delta P_{g_j} \tag{4.4}$$

where T_t is the time constant of the turbine and ΔP_g is the change in input set point to the turbine, i.e., adjustment of speed governor set point. It is important to note that unlike the traditional power system environment, the dynamics of the speed governor must include a set point resulting from power system deregulation (contracted power). [6] Therefore, the response of the speed governor of the GENCO in the restructured system can be obtained from

$$\Delta P_g = \frac{1}{sT_g + 1}\left(\frac{-1}{R}\Delta f + \sigma \Delta P_{lfc} + \Delta P_c\right) \tag{4.5}$$

where T_g is the time constant of the governor, R is droop parameter for primary frequency control, σ is the generator participation index ($\sigma \in \{0,1\}$ and $\sum \sigma = 1$) for the GENCOs in Area i participating in LFC while ΔP_{lfc} is the change in control signal from the secondary frequency controller and ΔP_c is the change in the set point due to deregulation. The ΔP_c for the n^{th} GENCO in the Area i can be expressed as

$$\Delta P_{c_{i,n}} = \sum_{i=1}^{N} cpf_{n,i} \Delta P_{D_i} \tag{4.6}$$

The LFC action for the restructured power system is different from the conventional power system because it takes into formulation the scheduled inter-area power flow, ΔP_{tie}^{sch}. The LFC action for Area i can be deduced from

$$\Delta P_{lfc,i} = \frac{-K_i}{s}\left(\beta_i \Delta f_i + \Delta P_{tie,i}\right) \tag{4.7}$$

where K_i and β_i are the integral gain of the LFC and frequency bias of Area i respectively, and

$$\Delta P_{tie,i}^{err} = \Delta P_{tie,i}^{sch} + \Delta P_{tie,i} \tag{4.8}$$

For the hybrid tie line interconnection considered in this study, inter area power flow to Area i from Area j is given

$$\Delta P_{tie,i} = \left(\frac{2\pi T_{ij}}{s} + \frac{K_{dc}}{1 + sT_{dc}}\right)\left(\Delta f_i - \Delta f_j\right) \tag{4.9}$$

where T_{ij} is the synchronizing coefficient of the ac tie line between Areas i and j, and K_{dc} and T_{dc} are the gain and time constant of the dc line between Areas i and j respectively [188].

With the growing share of RE systems in the modern energy mix, it is becoming expedient for RE plants to contribute to frequency control to a certain level depending on the grid code specifications. For example, the South Africa renewable energy grid code requires that grid-connected wind energy plants above 20 MW capacity reserve a fraction of their available power for primary frequency control. [**?**] This reserve power can be harnessed by adding a droop (proportional) control to the control loop of the machine-side converter of the wind energy conversion system (WECS), and it is only available for a short time. It is worth noting that this droop control strategy does not imitate the droop control in conventional generating systems but rather exploits the faster response of the WECS in providing transient power before the conventional systems respond to the frequency. [189] Also, it is important to note that the fluctuation in the RE sources can affect the frequency stability of the system when the penetration is high. To prevent digression from the scope of this work, the detailed modelling of RE systems can be found in [190]. For the i^{th} area in N interconnected control areas, the change in total output power of the RE system resulting from droop variation and source fluctuation can be derived using

$$\begin{aligned} \Delta P_{res,i} &= \sum_{j=1}^{n} \Delta P_{res_j} \\ &= \frac{1}{1+sT_{res_j}} \left(\frac{1}{K_{res_j}} \Delta f_i + \Delta P_{res}^{var} \right) \end{aligned} \tag{4.10}$$

where T_{res_j} is the time constant, K_{res_j} is the droop parameter and ΔP_{res}^{var} is the variation in output of the RE system. Finally, the change in demand in Area i that impacts the frequency response of the system is the summation of contracted and non-contracted demand can be mathematically expressed as

$$\Delta P_{D_i} = \Delta P_{D_{c,i}} + \Delta P_{D_{uc,i}} \tag{4.11}$$

The equations derived in (**??**) to (4.11) can be used to obtain the state space model for small signal stability analysis. For the i^{th} control area, we can write the state-space model as

$$\begin{aligned} \dot{X}_i &= A_i X_i + B_i U_i \\ Y_i &= C_i X_i \end{aligned} \tag{4.12}$$

where $A, B,$ and C are the system, input, and output matrices respectively with appropriate dimensions while X, U are state and input vectors respectively that are given as

$$\begin{aligned} X_i &= [\Delta f_i \ \Delta P_{m_i} \ \Delta P_{g_i} \ \Delta P_{tie,i} \ \Delta P_{res,i}]^T \\ U_i &= [\Delta P_{lfc,i} \quad \Delta P_{D_i}]^T \end{aligned} \tag{4.13}$$

4.4 Inertia Control

4.4.1 Concept of Inertia

In the traditional power system, the synchronous generators and turbines used in conventional power plants play a vital role in reducing the rate-of-change-of-frequency (RoCoF) during power imbalance because of the presence of a large amount of inertia and direct synchronous operation. During power imbalance, the total inertia is harnessed through the kinetic energy present in the rotating mass of the generating units which can be expressed as

$$J = \frac{2E_{ke}}{\omega^2} \tag{4.14}$$

where E_{ke} is the kinetic energy stored in the rotating mass in kg.m^2/s^2 and ω is the angular frequency of the machine in rad/s. The rate of change of angular speed as a result of torque imbalance between the turbine and generator is expressed as

$$\frac{d\omega}{dt} = \frac{T_m - T_e}{J} = \frac{1}{J}\left[\frac{P_m - P_e}{\omega}\right] \tag{4.15}$$

where T_m and T_e are the mechanical and electrical torque respectively while P_m and P_e are the mechanical and electrical active power respectively. The inertia constant H of the system can be defined as the ratio of the system kinetic energy and its power rating S in VA that can be mathematically represented by

$$H = \frac{E_{ke}}{S} \tag{4.16}$$

By substitution and rearrangement of (**??**) and (4.15), we can write (4.16) as:

$$\frac{d\omega}{dt} = \frac{\omega(P_m - P_e)}{2HS} \tag{4.17}$$

From (4.17), it clear that the rate of change of angular frequency is inversely proportional to the system inertia, i.e., with high system inertia, the rate of change of angular frequency is reduced during power imbalance and vice versa. As a consequence, the decommissioning of conventional generating systems due to global environmental concern and the continuous addition of RE systems (implicitly zero-inertia systems) will decrease the overall inertia of the power system, thereby making it susceptible to high-frequency deviation during power imbalance. It can be noted that the angular frequency is directly proportional to the linear frequency ($f = \frac{\omega}{2\pi}$) and the operating frequency for all GENCOs in a control area is the same as a result of synchronization, therefore, the overall inertia in a control area is a combination of all inertia present in each generating unit. It is also important to point out that the action of inertia response is the natural response of the system to frequency deviations before the activation of primary and secondary frequency control actions. To mitigate the risk of frequency instability and improve the resilience of power systems with a high penetration level of RE systems during various power system contingencies, it is important to supplement the shortage of inertia. Therefore, the concept of a virtual inertia in an RE system is introduced.

4.4.2 Virtual Inertial Control

In this subsection, the principle of inertia emulation is presented. The virtual inertia concept is proposed to emulate the damping and inertia characteristics of conventional synchronous generators, therefore maintaining or increasing the overall inertia of the system. This facilitates the increased penetration of RE systems into the energy mix without compromising the frequency stability of the system. In this work, virtual inertia control as a new ancillary service in which inertia emulation is achieved using the combination of an ESS, power electronic converter, and an appropriate control strategy, is presented. The ESS acts as an inertia unit that injects instantaneous active power into the system to reduce the RoCoF and amplitude of frequency deviation. The derivative control strategy is the kernel of the virtual inertia control, it can modify the output of the ESS depending on the RoCoF during a frequency event or disturbance. Due to the sensitivity of the derivative of the control-to-noise present in the frequency measurement (phase-locked loop of the power electronic devices), a low pass filter (LPF) is added to the control strategy. For small-signal analysis such as frequency response, the response of the LPF can be used to emulate the dynamics of the power electronics converter. [166, 191] The block diagram of the derivative-based virtual inertia control is presented in Figure 4.2. The output of the ESS is constricted between the minimum and maximum active power rating of the ESS which gives the practical operating condition of the ESS and ensure it does not behave as an infinite energy source. The equation for the dynamic inertia emulation using the derivative control strategy can be derived:

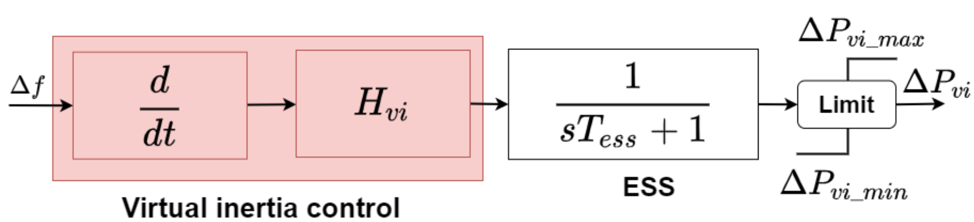

Figure 4.2 Small signal model of virtual inertia strategy.

$$\Delta P_{vi} = H_{vi} \left(\frac{1}{1 + sT_{ess}} \right) \cdot \frac{d(\Delta f)}{dt} \tag{4.18}$$

where ΔP_{vi} is the virtual power that contributes to the inertia response of the system, T_{ess} is the time constant of the low pass filter acting as an ESS, and H_{vi} is the virtual inertia gain. The choice of H_{vi} is very important because it significantly affects the response of the virtual inertia controller. Large values of H_{vi} will repress the frequency deviation with smaller overshoot and undershoot but increase the settling time of the frequency while smaller values of H_{vi} will quickly restore the frequency of the system but with high oscillation and amplitude of deviation. This makes the conventional virtual inertia control strategy with fixed inertia gain perform poorly under dynamic frequency events. Therefore, this work proposes the application of the type-II fuzzy logic system to calculate the appropriate inertia gain, thus developing an adaptive virtual inertia controller that can perform efficiently and optimally under various operating conditions.

4.4.3 Type-II Fuzzy Logic System

The basic structure of the type-II fuzzy logic control scheme is shown in Figure 4.3. The control structure has three basic stages: input processing (fuzzification) that converts the crisp input to fuzzy input; an inference engine that determines the fuzzy output based on some complex calculations and rule base; and output processing (type-reduction and defuzzification) that reduces and converts the type-II fuzzy output to crisp output. The complete control strategy can be summarised as the mapping of crisp input x into a corresponding crisp output y which can be quantitatively expressed as $y = f(x)$. The type-II fuzzy set (FS) $\tilde{F}$ where $l \in L$ and can be characterised as

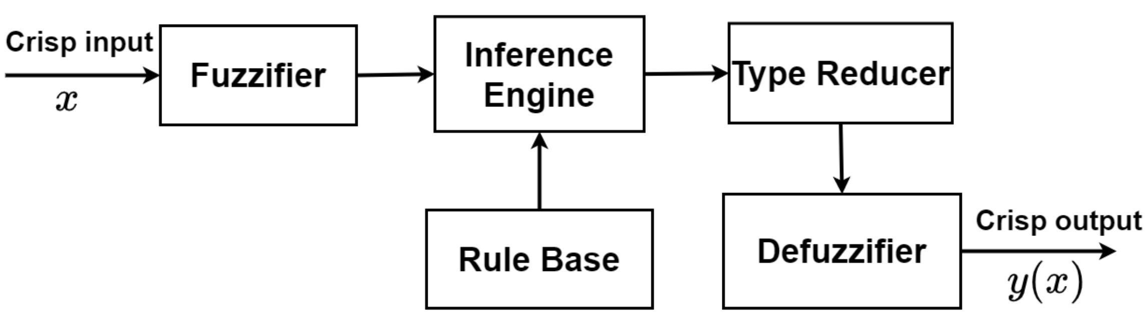

Figure 4.3 Block diagram of type-II fuzzy logic system.

$$\tilde{F} = \{((l,m), \mu_{\tilde{F}}(l,m)) \,|\, \forall l \in L, \forall m \in J_l \subseteq [0,1]\} \tag{4.19}$$

where $\mu_{\tilde{F}}(l,m)$ is a type-II membership function (MF), l is a primary variable, m is the secondary variable in which $0 \leq \mu_{\tilde{F}}(l,m) \leq 1$ and J_l is the primary membership of l. [192]

$\tilde{F}$ can also be expressed as

$$\tilde{F} = \int_{l \in L} \int_{m \in J_l} \mu_{\tilde{F}}(l,m)/(l,m) \quad J_l \subseteq [0,1] \tag{4.20}$$

where $\int\int$ denotes union over all possible l and m. When there are no uncertainties, the type-II FS reduces to a type-I FS such that the secondary variable becomes $\mu_F(l)$ and $0 \leq \mu_F(l) \leq 1$. As a corollary, the boundary of the type-II FS should correspond with the fact that the vertical slices of a MF should be between 0 and 1.

When all $\mu_{\tilde{F}}(l,m) = 1$, $\tilde{F}$ is said to be an interval type-II FS [193]. The interval type-II FS reduces (4.20) to

$$\tilde{F} = \int_{l \in L} \int_{m \in J_l} 1/(l,m) \quad J_l \subseteq [0,1] \tag{4.21}$$

or alternatively, to

$$\begin{aligned} \tilde{F} &= \int_{l \in L} \mu_{\tilde{F}}(l)/l \\ &= \int_{l \in L} \left[\int_{m \in J_l} 1/m \right] /l, \quad J_l \subseteq [0,1] \end{aligned} \tag{4.22}$$

Due to the uncertainty associated with the interval type-II FS, the boundary of uncertainty in the type-II MF is defined as the footprint of uncertainty (FOU). The outer boundary ($\overline{\mu}$) of the FOU is the upper membership function (UMF) and the inner boundary ($\underline{\mu}$) is the lower membership function (LMF) so that

$$\text{FOU}(\tilde{F}) = \bigcup_{l \in L} J_l \tag{4.23}$$

$$\overline{\mu}_{\tilde{F}}(l) \equiv \overline{\text{FOU}}(\tilde{F}) \quad \forall l \in L \tag{4.24}$$

$$\underline{\mu}_{\tilde{F}}(l) \equiv \underline{\text{FOU}}(\tilde{F}) \quad \forall l \in L \tag{4.25}$$

To determine the boundaries of the FOU, i.e., the UMF and LMF, the symmetrical triangular membership shown in Figure 4.4 is considered. The UMF and LMF of $\tilde{F}$ can be deduced from

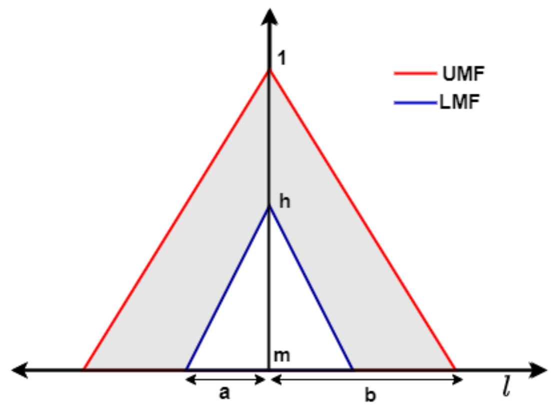

Figure 4.4 Symmetrical triangular type-II fuzzy set.

$$\bar{\mu}_{\tilde{F}}(l) = \begin{cases} 0, & l \leq m-b \\ \frac{l-m+b}{b}, & m-b < l \leq m \\ 1, & l = m \\ \frac{m+b-l}{b}, & m < l \leq m+b \end{cases} \tag{4.26}$$

$$\underline{\mu}_{\tilde{F}}(l) = \begin{cases} 0, & l \leq m-a \\ h\frac{l-m+a}{a}, & m-a < l \leq m \\ h, & l = m \\ h\frac{m+a-l}{a}, & m < l \leq m+a \end{cases} \tag{4.27}$$

Using the proof provided in [194], the uncertainty degree of the symmetrical triangular membership function can be calculated from

$$\rho_{\tilde{F}} = 1 - \left[\frac{a(2-h)}{b} + 2\frac{2ah(1-h)}{b} \ln(1-h) \right] \tag{4.28}$$

For the type-II FS, the constraint of the uncertainty degree is $0 \leq \rho_{\tilde{F}} \leq 1$. In the type-I FS where $a = b$ and $h = 1$, then $\rho_{\tilde{F}} = 0$. This points out the inability of the type-I FS to model uncertainties.

The rule structure for the type-II fuzzy logic is similar to the type-I fuzzy, for a fuzzy logic structure with a K number of rules, the n^{th} rule can be expressed in the form:

$$\begin{aligned} R_n &: \text{If } l_1 \text{ is } \tilde{F}_{1,n} \text{ and } \ldots l_i \text{ is } \tilde{F}_{i,n} \ldots \text{ and } l_I \text{ is } \tilde{F}_{I,n} \\ &\text{Then } y \text{ is } \tilde{Y}_n \end{aligned} \tag{4.29}$$

where n = (1, 2, ..., K). This type reduction block maps the type-II FLC into a type-I FLC by computing the centroid of the interval type-II FLC associated with each fired by using

$$Y_{\tilde{F}} = 1/\left\{y_p, \ldots, y_q\right\} \tag{4.30}$$

where y_p and y_q can be calculated using

$$y_p = \frac{\sum_{i=1}^{Q} y_i \bar{\mu}_{\tilde{F}}\left(y_i\right) + \sum_{i=P+1}^{N} y_i \underline{\mu}_{\tilde{F}}\left(y_i\right)}{\sum_{i=1}^{P} \bar{\mu}_{\tilde{F}}\left(y_i\right) + \sum_{i=P+1}^{N} \underline{\mu}_{\tilde{F}}\left(y_i\right)} \tag{4.31}$$

$$y_q = \frac{\sum_{i=1}^{Q} y_i \underline{\mu}_{\tilde{F}}\left(y_i\right) + \sum_{i=Q+1}^{N} y_i \bar{\mu}_{\tilde{F}}\left(y_i\right)}{\sum_{i=1}^{Q} \underline{\mu}_{\tilde{F}}\left(y_i\right) + \sum_{i=Q+1}^{N} \bar{\mu}_{\tilde{F}}\left(y_i\right)} \tag{4.32}$$

The switching point P and Q in (4.4.3) and (4.32) are iteratively determined using the Karnik-Mendel (KM) algorithm [195] The crisp output y is computed by the defuzzifier using

$$y(\mathbf{x}) = \frac{1}{2}\left[y_p(l) + y_q(l)\right] \tag{4.33}$$

4.4.4 Artificial Bee Colony Algorithm

The ABC algorithm is a heuristic optimization technique that is based on the behavior of a colony of honey bees in search of a food source position. It involves the exploration and exploitation of the available nectar positions (NPs) [152]. The colony is divided into three groups. The first group is the employed bees–they search for NPs, memorize the nectar quality of these positions, and share them with the other bees in the hive area by dancing (waggle dance), the length of dance provides the nectar quality. The second group is the onlooker bees–they wait in the hive and watch the employed bee dance, they choose the NPs based on the information shared by the employed bees; the last group is the scout bees–they are employed bees whose NPs have been neglected because of poor or low quality. Details can be found in [1, 6, 152]; the flowchart of the ABC algorithm is shown in Figure 4.5. In this paper, the ABC algorithm is used to determine the weights of the type-II fuzzy logic system.

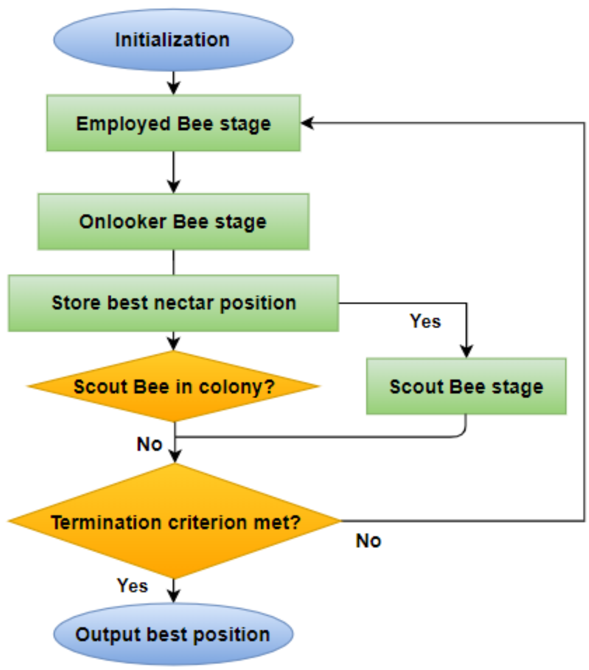

Figure 4.5 Flowchart of ABC optimization algorithm.

4.5 Adaptive Virtual Inertia Based on Type-II Fuzzy Logic Control

In this section, the proposed virtual inertia control method is developed as shown in Figure 4.6. The inputs to the type-II fuzzy logic system are the frequency deviation, Δf and its derivative, $\Delta\dot{f}$. These inputs are firstly normalized with the weights W_1 and W_2 respectively so that the final inputs to the type-II fuzzy logic system are

$$\text{Input 1} = W_1 \cdot \Delta f \tag{4.34}$$

$$\text{Input 2} = W_2 \cdot \Delta\dot{f} \tag{4.35}$$

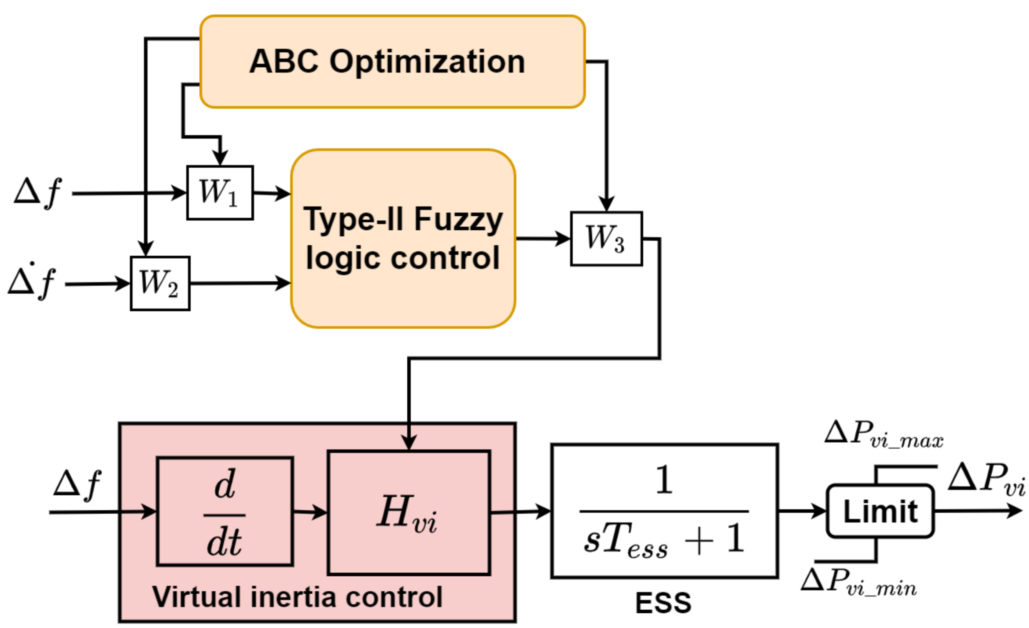

Figure 4.6 Proposed virtual inertia control strategy.

The normalized inputs are then fuzzified using the membership functions. In this work, the triangular membership function is used because of its ease of computation, few design parameters,

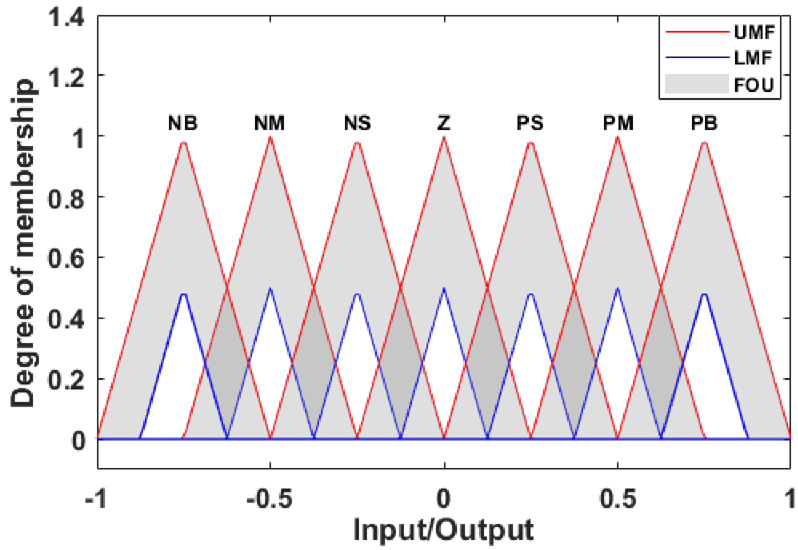

Figure 4.7 Type-II Fuzzy membership functions.

and less complexity in practical realization when compared to other types of membership functions. Due to these reasons, seven triangular membership functions are arbitrarily chosen to define the universe of discourse of the type-II fuzzy system. They are defined using the linguistic variables: Negative Big (NB), Negative Medium (NM), Negative Small (NS), Zero (Z), Positive Small (PS), Positive Medium (PM), and Positive Big (PB) as shown in Figure 4.7. The corresponding membership parameters of the seven linguistic variables are determined from (4.26) and (4.27). The fuzzified inputs which are the embedded fuzzy sets within the FOU are processed in the inference engine to generate appropriate fuzzy outputs with the aid of the fuzzy rules given in Table 4.1. The inference engine uses the min and max methods for the Meet and Join operations respectively. The Meet and Join operations map the fuzzified inputs into fuzzy outputs with the strength of the fired rule(s). The output of the inference engine is a type-II fuzzy set that cannot be directly converted to the crisp output, that is, virtual inertia gain. The type-reducer is used to convert the type-II fuzzy set to type-I fuzzy set using the KM algorithm, the smallest and largest centroids are computed using (4.4.3) and (4.32). The type-I fuzzy output is then converted to the normalized virtual

Table 4.1 Fuzzy Rule Table

		Δf						
		PB	PM	PS	Z	NS	NM	NB
	PB	NB	NB	NB	NB	NM	NS	Z
	PM	NB	NB	NB	NM	NS	Z	PS
$\Delta \dot{f}$	PS	NB	NB	NM	NS	Z	PS	PM
	Z	NB	NB	NM	Z	PM	PB	PB
	NS	NM	NS	Z	PS	PM	PB	PB
	PM	NS	Z	PS	PM	PB	PB	PB
	NB	Z	PS	PM	PB	PB	PB	PB

inertia gain using (4.33). The normalized virtual inertia gain is scaled with weight W_3 to generate the actual inertia gain, H_{vi}. The values of the input and output weights (W_1, W_2, W_3) are critical in the design and performance of the fuzzy logic system for the proposed application; therefore, the ABC optimization algorithm is employed to determine their values. The cost function used in the optimization (cost function minimization) process is a two-fold objective function that computes the derivative of the frequency deviation and absolute frequency deviation. For the i^{th} control area with virtual inertia capability, the cost function can be formulated as

$$C_{f_i} = \sum_{n=1}^{T} \left(|\Delta f_i(n)|^2 + \frac{|\Delta f_i(n) - \Delta f_i(n-1)|}{t} \right) \tag{4.36}$$

where t is the time between the actual present and previous frequency measurement. It is specified as the sample time of the controller. The values of the weights for the type-II fuzzy controller are presented in Table 4.2. The proposed optimized type-II fuzzy-based virtual inertia control system can recalculate the inertia gain to track the frequency to a zero steady-state value. Therefore, frequency deviation in Area i given in (4.3) can be written as

$$\Delta f_i = \frac{1}{2H_i s + D_i}\left(\Delta P_{m_i} + \Delta P_{res_i} - \Delta P_{tie,i} - \Delta P_{D_i} + \Delta P_{vi}\right) \tag{4.37}$$

Table 4.2 Optimal weights of the proposed strategy

Parameter	W_1	W_2	W_3
Value	11.124	0.0049	-9.562

4.6 Simulation and Discussion

In this section, the efficiency of the proposed type-II fuzzy-based virtual inertia controller is validated through extensive simulation in MATLAB. The test system for the simulation is the conventional two-area power system model that is used for frequency stability studies. [37] The model is updated to include the dynamics of modern power systems such as hybrid tie line connection, power system deregulation, and unequal area capacities. In Area 2 of the test system, one of the conventional plants has been replaced with a RE system to simulate high penetration of RE and reduced equivalent inertia; therefore, the proposed virtual inertia strategy is implemented in this area and its robustness is evaluated against the conventional and type-I fuzzy-based virtual inertia methods proposed in [41] and [5] respectively, it is important to mention that the two methods in the literature were redeveloped to satisfactorily fit the system used in this work.

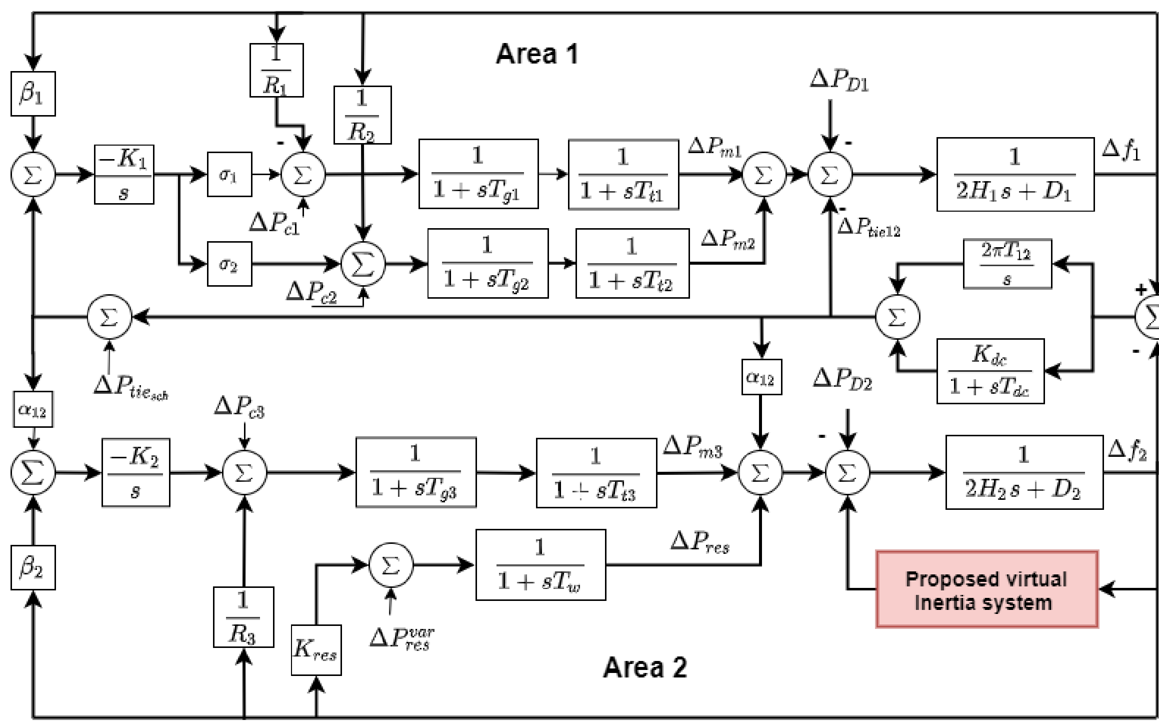

Figure 4.8 Two-area test system model.

4.6.1 Stability Analysis

In this section, the stability of the test system is analyzed by inspecting the properties of its eigenvalues. The stability analysis provides information on the model properties at initial conditions and how the model will react to small-signal disturbances outside the initial condition. Similarly, the investigation of the eigenvalue properties of the system can interpret its stability; the sign of the real parts of the eigenvalues provides sufficient information about the system stability. For a system to be stable, all the real parts of its eigenvalues have to be negative (on the left half of the complex s-plane). In Table 4.3, the eigenvalues of the closed-loop system shown in Figure 4.8 in steady-state condition (unperturbed) are presented, it can be observed that all the eigenvalues have a negative real part, therefore, indicating an asymptotically stable system. Furthermore, in small-signal analysis, a stable system will return to its equilibrium point when perturbed by small-signal disturbance. It can be seen that the modes λ_1 and λ_2 which corresponds to Δf_1 and Δf_2 respectively are in a better region of stability with high magnitudes in the real parts of their eigenvalues. The complex modes of the eigenvalues (λ_{4-7} and $\lambda_{10,11}$) indicate that the system will oscillate before reaching steady-state during small perturbations.

Table 4.3 Eigenvalues of System Model

Mode	Eigenvalue
λ_1	-17.2118
λ_2	-17.7078
λ_3	-13.0658
λ_4	-1.3063+j7.0956
λ_5	-1.3063-j7.0956
λ_6	-1.1801+j3.8124
λ_7	-1.1801-j3.8124
λ_8	-3.9736
λ_9	-3.2251
λ_{10}	-0.9941+j0.5724
λ_{11}	-0.9941+j0.5724
λ_{12}	-0.7513
λ_{13}	-0.4281
λ_{14}	-0.1033

4.6.2 Load variation

In this scenario, the effectiveness of the proposed virtual inertia control strategy is demonstrated. A step load change of $\Delta P_{D_{uc}} = 0.1$p.u in Area 2 at 10 s is simulated to illustrate the frequency response of the system during load variation. Figure 4.9(a) and (b) show the frequency deviation and derivative of frequency deviation in Area 2 under this contingency. Generally, it can be observed that the frequency response of Area 2 is improved when the virtual inertia control is incorporated into the system compared to the absence of virtual inertia in the system. More specifically, the proposed type-II fuzzy-based virtual inertia control method outperforms the type-I fuzzy-based and conventional virtual inertia control methods with the least amplitude of frequency deviation, transient excursions, and fastest recovery of the derivative of frequency deviation with damped oscillations and minimal overshoots. The performance of the proposed type-II fuzzy virtual inertia control strategy can be demonstrated by observing the change in active power of the ESS ΔP_{vi}, as shown in Figure 4.11. It can be seen that with the proposed virtual inertia strategy, the ESS is capable of injecting high instantaneous active power needed to suppress the frequency deviation when compared to other virtual inertia control methods. It is important to mention that virtual inertia elements are zero net energy devices during steady-state operation, this criteria must the considered in the design of the intelligent control systems to implement virtual inertia devices such that they do not become an infinite energy source. Due to the interconnection that exists between Areas 1 and 2, it is consequential that the perturbations in Area 2 affect Area 1 and vice versa. Therefore, it is important to observe the frequency response of Area 1 due to the contingency in Area 2 for this scenario as shown in Figure 4.10. It can be observed while the presence of virtual inertia in Area 2 helps to reduce the frequency deviation amplitudes and oscillations, the proposed type-II fuzzy-based virtual inertia achieved the least amplitude of frequency deviation with a smooth transition to zero steady-state deviation.

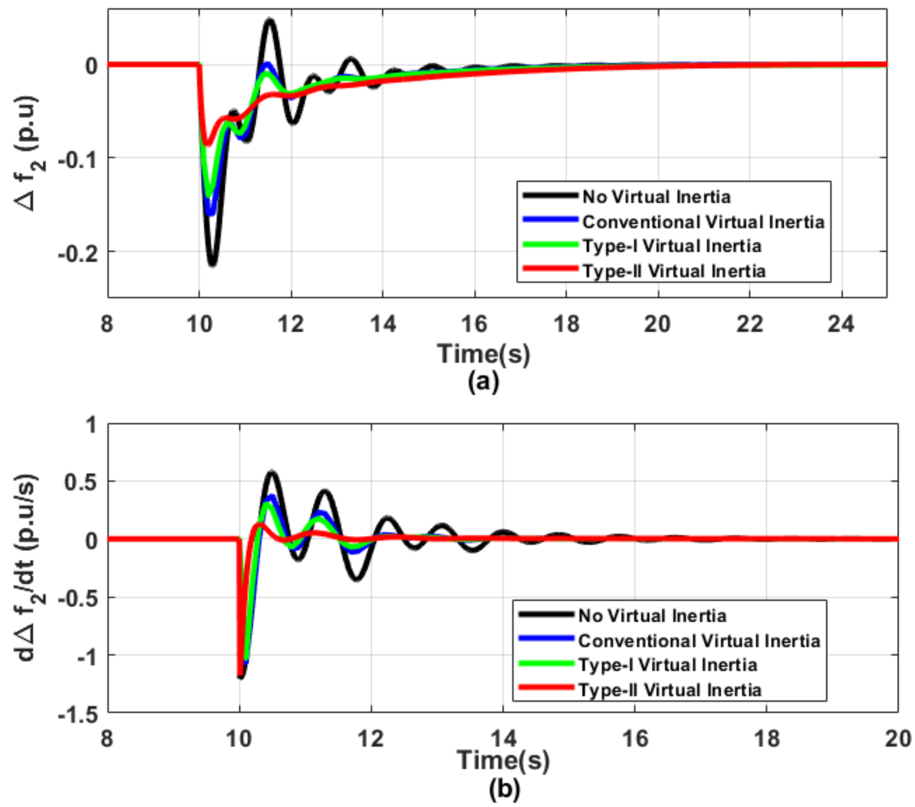

Figure 4.9 (a) Frequency deviation in Area 2 (b) rate of change of frequency deviation in Area 2 under step load variation.

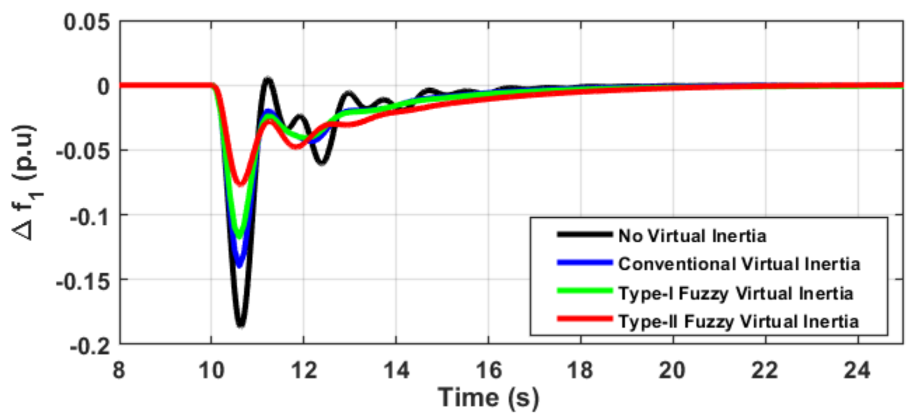

Figure 4.10 Frequency deviation in Area 1 under step load variation in Area 2.

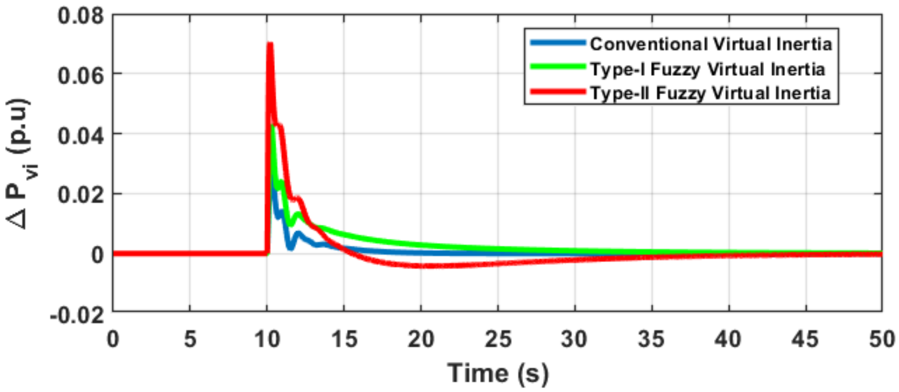

Figure 4.11 Output power of ESS under step load variation.

4.6.3 High renewable energy fluctuation

In this scenario, a more severe contingency is considered to show the robustness of the proposed virtual inertia control strategy. With the high penetration of RE systems, it is practical that the overall systems inertia and damping characteristics are affected, and with the high fluctuation of the RE sources, the frequency response of the system can be significantly affected. The high RE fluctua-

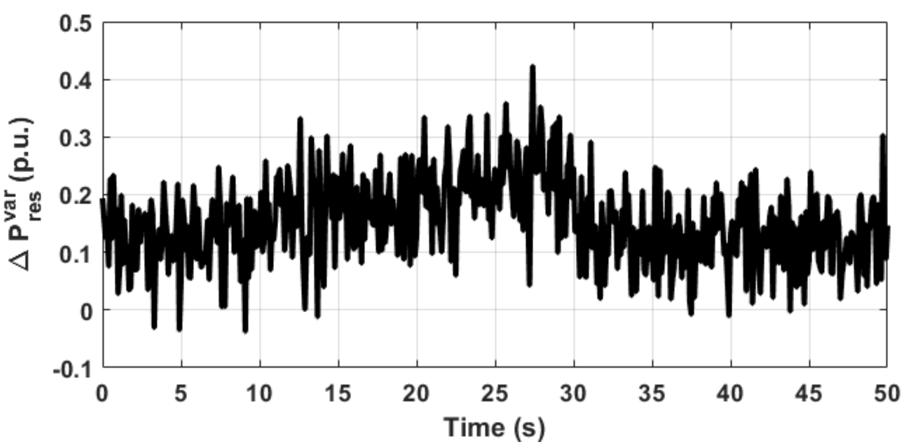

Figure 4.12 Net fluctuation in RE power in Area 2.

tion in Area 2 as shown in Figure 4.12 is used to replicate this contingency, and Figures 4.13and 4.14 show the behaviour under this contingency. From Figure 4.13(a), it is shown that the frequency deviation in Area 2 fluctuates above and below zero steady-state due to the nature of the disturbance. It shows that the proposed type-II fuzzy-based virtual inertia control strategy has the least amplitude of frequency deviation when compared to the type-I fuzzy-based and conventional virtual inertia control strategies. The derivative of the frequency deviation shown in Figure 4.13(b) shows the effectiveness of the proposed type-II fuzzy-based virtual inertia strategy in achieving faster response to keep the rate of change of frequency deviation within zero with the lowest transient excursion. This improved frequency response is a result of the rapid absorption/charging

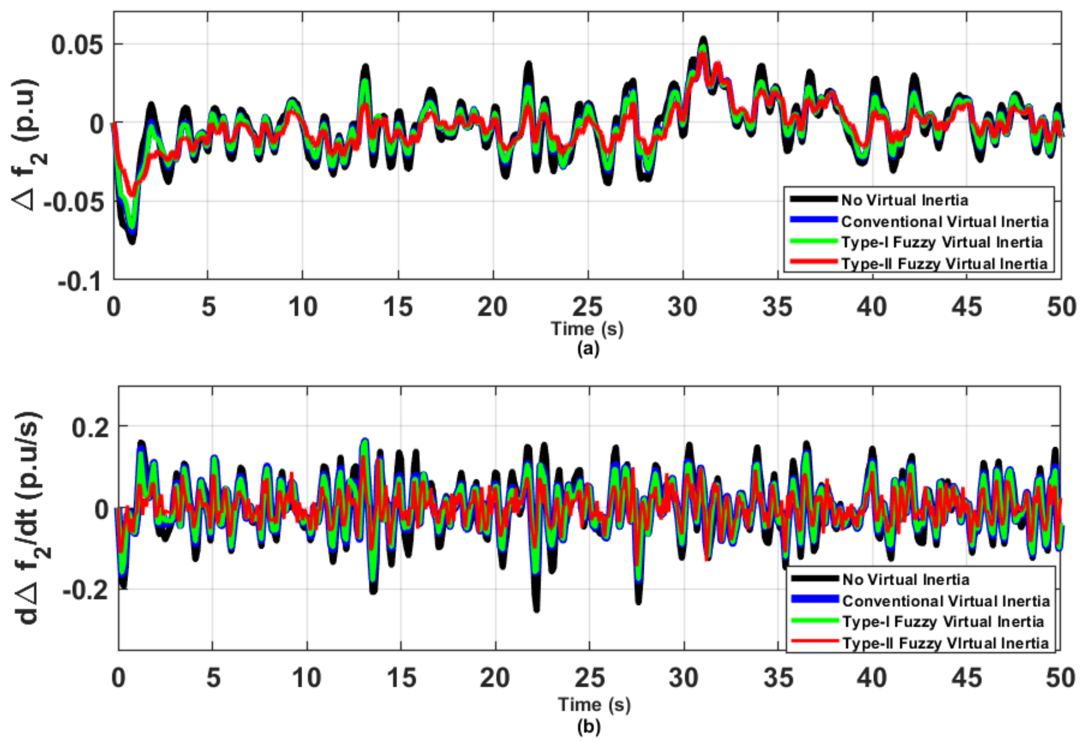

Figure 4.13 (a) Frequency deviation in Area 2 (b) rate of change of frequency deviation in Area 2 under RE fluctuation.

(negative ΔP_{vi}) and injection/discharging (positive ΔP_{vi}) by the ESS as shown in Figure 4.14(a). It shows that the proposed type-II fuzzy-based virtual inertia control strategy can efficiently adjust the virtual inertia gain, H_{vi}, to varying values as a function of the system contingency. The adjustment of the virtual inertia gain can be seen in Figure 4.14(b). While the conventional virtual inertia control strategy has a fixed gain and the type-I fuzzy-based virtual inertia control strategy adjusts the virtual inertia gain around the fixed inertia gain, the proposed type-II fuzzy-based virtual inertia strategy can adjust the virtual inertia gain to values that improve the frequency response and stability of the system.

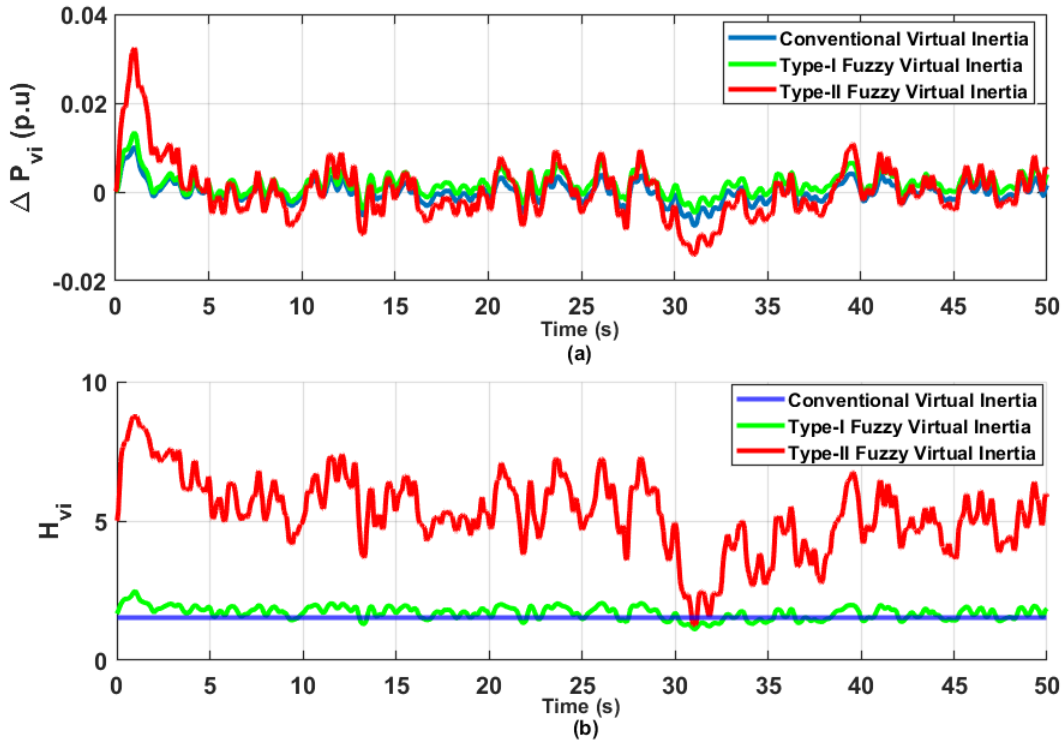

Figure 4.14 (a) Output power of ESS (b) Virtual inertia gain under RE fluctuation.

4.6.4 Parameter variation

In system design, inaccurate parameter estimations, the variation of system parameters with time, and the removal of some systems components can reduce the efficient performance of the system practically. Therefore, it is important to test the robustness of the control systems during design with parameter variations. In this scenario, the robustness of the proposed type-II fuzzy-based virtual inertia control strategy is tested by simulating the contingencies in Section 4.6.2 and 4.6.3 under these parameter variations in Area 2: $R_3 = -30\%$, $D_2 = -50\%$, $H_2 = -50\%$, $T_t = +25\%$, $T_g = +20\%$, $K_2 = -30\%$, and $\beta_2 = +25\%$. 6 It can be observed from Figure 4.15(a) that with the

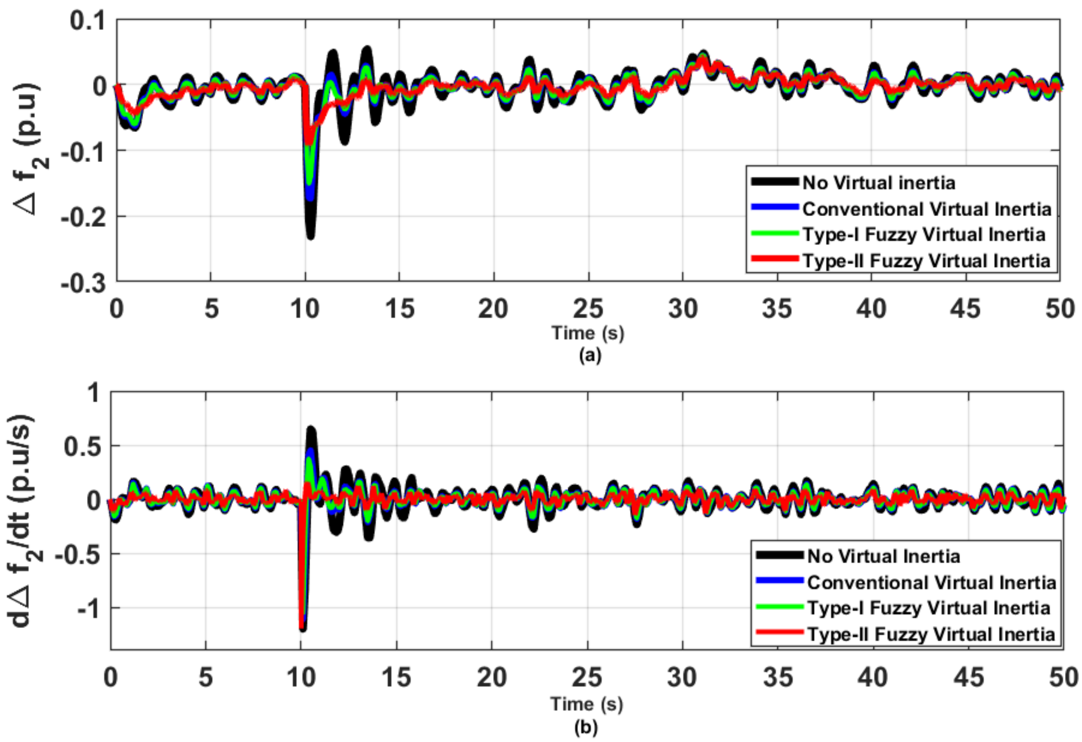

Figure 4.15 (a) Frequency deviation in Area 2 (b) rate of change of frequency deviation in Area 2 under parametric variation.

absence of virtual inertia, there is serious frequency deviation with high oscillations. With the conventional and type-I fuzzy-based virtual inertia control strategies, the frequency dip is improved by 32 % and 30 % respectively with noticeable oscillations. However, the application of the proposed type-II fuzzy-based virtual inertia control strategy significantly improves the frequency dip by approximately 70 % with damped oscillations. Furthermore, the rate of change of frequency deviation rapidly settles to zero with the proposed virtual inertia strategy when compared to other virtual inertia control strategies as seen in Figure 4.15(b).

The improved performance in the frequency response is due to the adaptive property of the type-II fuzzy controller in selecting the virtual inertia gains as shown in Figure 4.16(b) which helps to dynamically adjust the output active power of the ESS as shown in Figure 4.16(a) when compared to the conventional and type-I fuzzy-based virtual inertia control strategies. It is shown that the proposed type-II fuzzy-based virtual inertia control strategy is robust so that it efficiently performs during parameter variations and maintains the frequency stability of the system in severe scenarios.

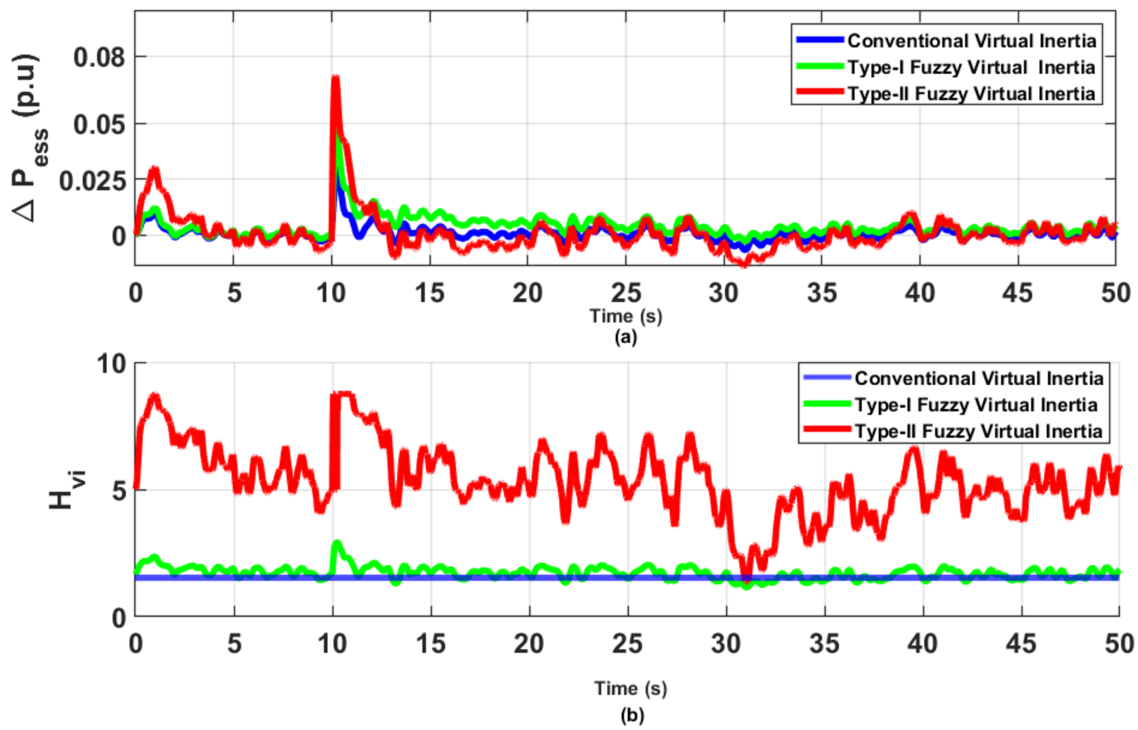

Figure 4.16 (a) Output power of ESS (b) Virtual inertia gain under parametric variation.

From the results presented in the section, it can be appreciated that a properly designed conventional virtual inertia control strategy can perform as relatively efficiently as the type-I fuzzy-based virtual inertia control strategy; however, the proposed type-II fuzzy-based virtual inertia control strategy significantly outperforms both control strategies.

4.7 Summary

This chapter presents a new virtual inertia control system using a type-II fuzzy logic control strategy. The proposed virtual inertia control strategy is used in the control loop of a dedicated ESS to improve the frequency response of a system with a high penetration of renewable energy sources in a restructured power system environment. The ABC optimization algorithm is utilized to tune the weights of the proposed controller to improve its performance. The robustness of the proposed controller is assessed under several operating scenarios and compared with the type-I fuzzy and conventional virtual inertia control strategies. The simulation results show the effectiveness of the proposed strategy to improve the frequency response of the system, thereby enhancing its stability and resilience.

Chapter 5

Robust State Estimation Method for Adaptive Load Frequency Control of Interconnected Power System in a Restructured Environment

This chapter is based on the work reported in [3].

5.1 Chapter Overview

Handling varying uncertainties in renewable energy generation and load demands are major challenges to the restructured power system environment. This chapter proposes the design of a novel control methodology using a robust unknown input observer (UIO) for dynamic state estimation and an interval type-2 fuzzy logic controller for adaptive load frequency control (LFC) of interconnected power systems with high penetration of renewable energy in a restructured power system environment. The capability of the proposed robust UIO to independently estimate the true state of the power system regardless of unknown inputs or disturbances that impact the frequency stability in real-time is demonstrated by the asymptotic zero property of the state estimation error. This is supported by using an interval type-2 fuzzy logic controller in the LFC loop of each area of the interconnected system to efficiently damp frequency oscillations, thereby, improving power system stability and resilience. The performance of the proposed methodology is evaluated using a modified two-area power system in the restructured environment. The results obtained from the stability and LFC analyses during severe operating conditions demonstrated the robustness of the proposed control framework to unknown inputs and unprecedented variations that can affect the frequency stability of the system.

5.2 Chapter Introduction

With the privatisation of many national power systems, the introduction of a free market in the energy sector, and the increasing need for economic efficiency and reliability of the electric power industry, many countries have begun to restructure the framework of their power systems [107]. Traditionally, most power system utilities were managed by the State; however, in the new restructured or deregulated environment, a transparent independent system operator (ISO) supervises the operations of the generation companies (GENCOs), transmission companies (TRANSCOs), distribution companies (DISCOs) and the new independent power producers (IPPs) [103]. In addition to deregulation, the growing penetration of renewable energy plants (REPs), energy storage systems (ESSs), and high voltage direct current (HVDC) transmission are major components in the modern power system environment [44]. Reliable transmission access and provision of timely ancillary services are two crucial concerns in a restructured environment because of the presence of different power producers. The problem of load frequency control (LFC) as an ancillary service is becoming more complex because of the increased application of power electronic devices for power generation. This reduces the overall inertia of the system. The choice of GENCOs and IPPs to participate in frequency control due to various factors such as bidding prices, reserve availability, etc, also increases [11].

To combat this problem, various approaches have been proposed and applied. These approaches are based on classical control techniques, optimal/robust control methods, heuristic optimization methods, state feedback control, and intelligent control schemes. A robust control method was presented in [196] for frequency control of a ship-based microgrid with a high share of renewable energy sources. In [132], an enhanced black hole optimization algorithm was implemented for the LFC model incorporating time delays and electric vehicles. A honey bee mating optimization fuzzy (HBMOF) controller was suggested in [197] for LFC in a deregulated power system. To mitigate the frequency deviations due to load and renewable energy fluctuations, a robust μ-synthesis approach was proposed in [198]. In [199], a robust H^{∞} method for interconnected power systems was implemented. The memory-based event-triggered H^{∞} approach was proposed in [200], this addressed LFC during the deception attack and the report in [201] considered a nonsmooth cost function in the design of a distributed LFC scheme. Online tuning of type-1 fuzzy logic control for LFC in an isolated microgrid was proposed in [202]. Authors of [203] used a type-1 FLC to tune the parameters in a set of coordinated controllers for LFC in a multi-source power system. Because of the poor uncertainty handling capability of type-1 FLC as reported in [204], the type-2 FLC has found application in engineering [193], [205]. In [182], an interval type-2 FLC was used in the vector control scheme of a doubly-fed induction generator to handle the fluctuations in wind speed and improve low voltage ride-through capability. The interval type-2 FLC was proposed in [206] to design a fault detection observer for a network control system. For LFC applications, an optimized interval type-2 FLC was proposed in [184] for secondary frequency control of a ship-board multi-microgrid, it considered communication network degradation. A detailed review of load frequency control schemes can be found in [136], [207]. At the generation level, adoption of ESSs is very important to recover the lack of inertia in the power electronic parts of generation by acting as virtual inertia sources for frequency support issues [188], [191]. Since the addition of synchronous-based wind energy conversion systems (WECS) to the energy mix can increase the system inertia response (since they have kinetic inertia), many wind farms are now expected to support in frequency regulation, mainly by providing a control mechanism for their active power as the function of the system frequency [6].

With the advancements in power system modeling and identification tools, the development of LFC methods for state estimation has received appreciable attention. However, these state estimation techniques are impractical in the new power system environment due to the inaccurate estimation of unknown inputs and model uncertainties [208]. To this effect, the unknown input observer (UIO) has proven to be efficient with negligible state estimation errors [209]. A detection and identification strategy based on UIO was proposed in [210] which identifies false data identification (FDI) due to a cyberattack on the LFC measurements. In [211], a functional observer method to design a residual generator for fault detection in an interconnected system considering unknown input was proposed. The literature does report on some studies that have harnessed the UIO for optimal LFC design schemes. In [212], a decentralized functional observer with parametric uncertainties as inputs was proposed for LFC studies. Based on UIO modeling, an optimal LFC observer was designed for unknown input estimation in [213] with a high penetration of electric vehicles. The proposed LFC approaches in the literature did not consider the unknown inputs that affect the dynamic performance for a wide range of operating conditions of the studied power systems which are very important in the restructured environment, thus, there is a need for new control schemes in the LFC computation for the complex, heterogeneous and nonlinear power system environment.

In this chapter, novel robust state estimation is proposed. This is based on an interval type-2 fuzzy logic control LFC scheme for an interconnected, multi-source power system in the restructured environment. The contributions of this chapter are

1. Design of a robust state estimation method based on UIO for online state estimation of a power system without prior knowledge of a disturbance to generate LFC signals. The simulation results corroborated the performance of the robust UIO with near-zero state estimation error.

2. To generate an appropriate control signal for the GENCOs in each area in the presence of unknown inputs, it is proposed that an interval type-2 fuzzy logic LFC method for each area is used. The robustness of the proposed LFC method is demonstrated by comparing with optimized-PI and type-1 fuzzy logic LFC methods.

3. To incorporate the complexity and topology of a modern power system, a virtual inertia-ESS is added in each area, and a hybrid HVAC/HVDC transmission network is considered in the analysis and design of the study system.

4. The proposed framework is beneficial to large and complex power systems because of the increasing RE integration where traditional LFC frameworks and control schemes cannot provide efficient performance over a wide range of unknown operating conditions.

To the best of the authors' knowledge, this is the first work that designs and implements a robust interval type-2 fuzzy logic LFC method based on UIO for a power system in the restructured environment.

The rest of this chapter is organized as follows: Section 5.3 presents detailed modeling of the power system for LFC studies in the restructured environment; Section 5.4 provides the mathematical formulation of the proposed methodology; the application of the proposed methodology to the LFC problem is presented in Section 5.5, Section 5.6 presents the simulation results that show robustness and practicability of the proposed methodology; and conclusions are drawn in Section 5.7.

5.3 System Modelling

5.3.1 Dynamics of power system restructuring

To begin the formulation of the LFC response in a restructured environment, it is important to introduce the complexities and dynamics that reflect the effect of power system restructuring in modern power systems. Firstly, the concept of a contract participation matrix (CPM) as defined in (5.1) is introduced. Each element in the matrix represents an index of contracted power generated by a DISCO and delivered to a GENCO. The sum of all elements in the column of the CPM must be equal to 1. For a power system with N control areas and n number of GENCOs, the CPM is given by [214]:

$$\text{CPM} = \begin{bmatrix} cpf_{11} & cpf_{12} & \cdots & cpf_{1N} \\ cpf_{21} & cpf_{22} & \cdots & cpf_{2N} \\ \vdots & \vdots & \ddots & \vdots \\ cpf_{n1} & cpf_{n2} & \cdots & cpf_{nN} \end{bmatrix} \tag{5.1}$$

Secondly, unlike the traditional environment, GENCOs must supply the contractual load demand of each DISCO in contract with it. This demand must be considered in the governor dynamics of each GENCO such that it responds to the total demand of all DISCO in contract with it. For a power system with N control areas, the additional dynamics for the i^{th} governor in Area j can be obtained from

$$\Delta P_{c_{i,n}} = \sum_{j=1}^{N} cpf_{ij} \Delta P_{D_j} \tag{5.2}$$

where cpf_{ij} is the contract participation factor and ΔP_{D_j} is the total demand of DISCOs in Area j.

Finally, the dynamics of the tie line power flow is formulated. For DISCOs in Area i having bilateral contract agreements with GENCOs in Area j, the scheduled inter-area power flow must be adjusted such that it follows the demand of the DISCOs from GENCOs outside their control areas. The scheduled tie line to the i^{th} control area for a large power system with N control areas can be calculated using

$$\Delta P_{tie,i}^{sch} = \sum_{\substack{j=1 \\ j\neq i}}^{N} \left(\sum_{k=1}^{n} cpf_{kj} \right) \Delta P_{D_j} \quad - \sum_{k=1}^{n} \left(\sum_{\substack{j=1 \\ j\neq i}}^{N} cpf_{jk} \right) \Delta P_{D_i} \tag{5.3}$$

5.3.2 LFC modelling in a restructured environment

Based on the deductions in the previous subsection, a new LFC model is developed which includes information that is absent in the traditional environment. For the i^{th} control area shown in Figure 5.1, the dynamics of the frequency response can be investigated by deriving sets of first-order differential equations. The frequency deviation in Area i is

$$\begin{aligned}\Delta f_i = \frac{1}{sM_i + D_i}(\Delta P_{m_{i,n}} + \Delta P_{res_i} - \Delta P_{tie,i}^{act} + \Delta P_{vi_i} \\ - \Delta P_{D_i} - \Delta P_{L_i} - \Delta P_{res,i}^{var})\end{aligned} \tag{5.4}$$

where ΔP_{m_n} is the change in mechanical output power of the n^{th} GENCO, and ΔP_{res}, ΔP_{tie}^{act}, D, ΔP_{vi}, ΔP_D, ΔP_L, and ΔP_{res}^{var} are the change in active power of renewable energy plants participating in primary frequency control, actual tie line power flow, damping, change in active power set point of virtual inertia control, total load demand contracted by DISCOs, total load demanded uncontracted, and unforecasted renewable energy variation in Area i respectively.

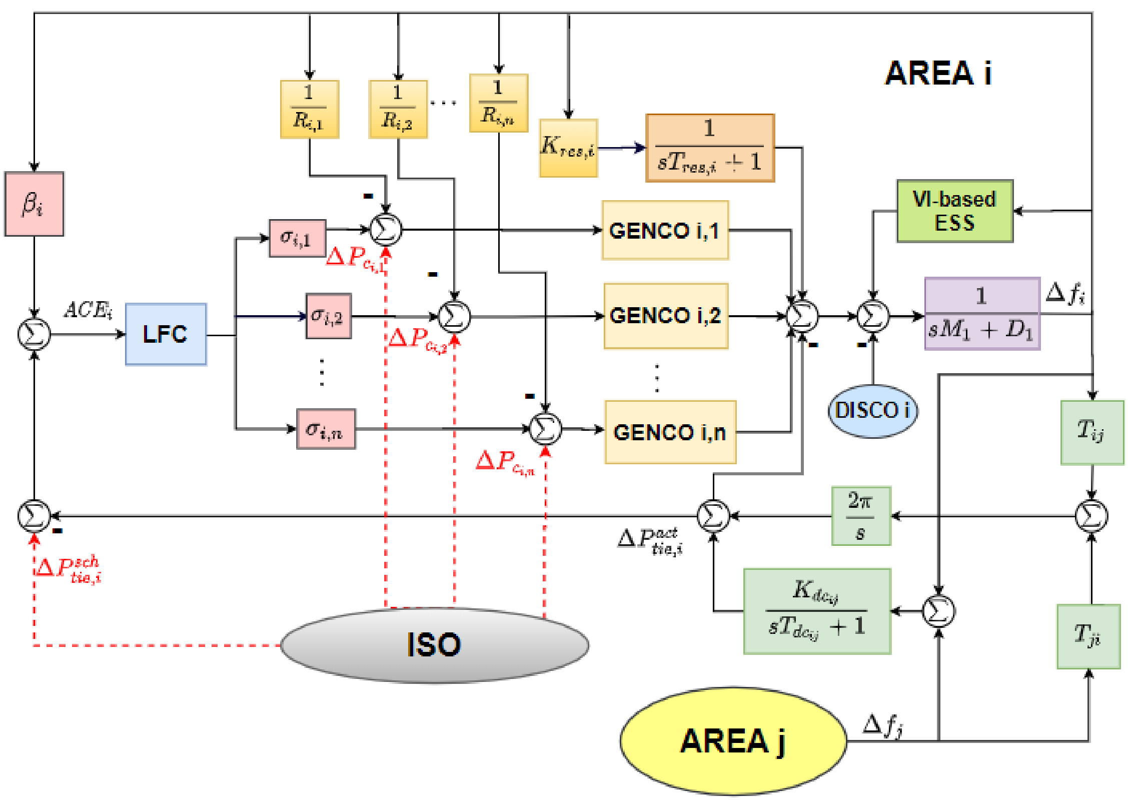

Figure 5.1 Block diagram of LFC model in a restructured environment

The turbine dynamics that change the mechanical output power of each GENCO in Area i can be obtained from

$$\Delta P_{m_{i,n}} = \frac{1}{sT_{t_{i,n}}+1}\Delta P_{g_{i,n}} \tag{5.5}$$

where $T_{t_{i,n}}$ is the turbine time constant and $\Delta P_{g_{i,n}}$ is the change in governor set point that actuates the n^{th} turbine in Area i.

As mentioned earlier, in the restructured environment, the response of each governor should factor in the total load demand of the DISCOs in contract with it. Also, for GENCOs participating in LFC regulation, it is important to define the parameter "σ" that defines the participation index of each GENCO in frequency regulation. iin contrast to the traditional environment, the computation of σ is dynamic because it is based on several factors such as bid prices, availability, operation cost, etc.

The modified change in governor set point of GENCO n in Area i can be expressed as

$$\Delta P_{g_{i,n}} = \frac{1}{sT_{g_{i,n}}+1}\left(\frac{-\Delta f_i}{R_{i,n}} + \sigma_{i,n}\Delta P_{lfc,i} + \Delta P_{c_{i,n}}\right) \tag{5.6}$$

where $T_{g_{i,n}}$ is the governor time constant, $R_{i,n}$ is speed-droop constant and $\Delta P_{lfc,i}$ is the LFC signal computed from the area control error (ACE). This regulates frequency and maintains the tie line power exchange at scheduled values.

For the ACE signal computation in the restructured environment, the tie line error, which is the difference between the actual and scheduled tie line flow, is used. For Area i, the LFC signal can be calculated from

$$\Delta P_{lfc,i} = \frac{-K_i}{s}\left(\beta_i \Delta f_i + \Delta P_{tie,i}^{error}\right) \tag{5.7}$$

where β_i is the frequency bias factor of area i, K_i is the integral gain of the load frequency controller, and $\Delta P_{tie,i}^{error}$ is the tie line error which is given by:

$$\Delta P_{tie,i}^{error} = \Delta P_{tie,i}^{act} - \Delta P_{tie,i}^{sch} \tag{5.8}$$

where

$$\Delta P_{tie,i}^{act} = \Delta P_{tie,i}^{ac} + \Delta P_{tie,i}^{dc} \tag{5.9}$$

The actual tie line is the combination of HVAC and HVDC transmission lines between different areas. The HVAC and HVDC power deviations can be expressed as:

$$\Delta P_{tie,i}^{ac} = \frac{2\pi T_{ij}}{s} \left(\Delta f_i - \Delta f_j\right) \tag{5.10}$$

and

$$\Delta P_{tie,i}^{dc} = \frac{K_{dc_{ij}}}{sT_{dc_{ij}} + 1} \left(\Delta f_i - \Delta f_j\right) \tag{5.11}$$

where T_{ij}, $T_{dc_{ij}}$ and $K_{dc_{ij}}$ are the HVAC synchronising coefficient, HVDC time constant and converter gain between Areas i and j, respectively.

With the increasing penetration of renewable energy in the energy mix, synchronous machine-based REPs are required to participate in frequency response; however, the addition of REPs introduces extra disturbance/variability to the power system. To model the effect of these variations and frequency response, the active power deviation of the REPs in Area i is

$$\Delta P_{res,i} = \frac{1}{sT_{res,i} + 1} \left(K_{res,i}\Delta f_i + \Delta P_{res,i}^{var}\right) \tag{5.12}$$

where $T_{res,i}$ is the time constant of the power electronic converter in the REP, $K_{res,i}$ is the inverse of the droop setting of the REP as usually agreed between the ISO and IPP, and $\Delta P_{res,i}^{var}$ is the variation in REP output that impacts the frequency stability of the system.

To improve frequency stability in the new power system environment, virtual inertia control has been established energy storage systems to provide short term active power during frequency imbalance [215]. Based on the derivative of the frequency deviation, the change in ESS output power that emulates the inertia process can be derives as

$$\Delta P_{vi,i} = \frac{K_{vi,i}}{sT_{vi,i} + 1}\ \Delta \dot{f}_i \tag{5.13}$$

where T_{vi} is the ESS time constant and K_{vi} is the gain of the virtual inertia controller.

To finalise the frequency response modeling, (5.4) to (5.13) are used to obtain the state-space representation for further studies. For the i^{th} control area, the state-space equations can be written in the form

$$\begin{aligned} \dot{x}_i(t) &= Ax_i(t) + Bu_i(t) + Dd_i(t) \\ y_i &= Cx_i(t) \end{aligned} \tag{5.14}$$

where A, B, C, and D are the system, input, output and disturbance matrices respectively with appropriate dimensions; $x \in \Re^l$, $u \in \Re^m$, $w \in \Re^n$ are state, input and disturbance (unknown) variables respectively given as:

$$\begin{aligned} x_i &= [\Delta f_i \; \Delta P_{m_{i,n}} \; \Delta P_{g_{i,n}} \; \Delta P_{tie,i}^{act} \; \Delta P_{res,i} \; \Delta P_{vi,}]^T \\ u_i &= [\Delta P_{lfc,i} \quad \Delta P_{D_i}] \\ d_i &= [\Delta P_{L_i} \quad \Delta P_{res,i}^{var}]^T \end{aligned} \tag{5.15}$$

5.4 Proposed Methodology

This section introduces the proposed unknown input observer model for state estimation of the LFC model described in Section 5.3. The unknown inputs $d(t)$ to the system are the uncontracted load demand and the fluctuations from REPs that are not usually available to the system in real-time but can affect the frequency stability of the system.

5.4.1 Unknown Input Observer

Considering the linear time-invariant system described in Figure 5.1, the goal of the UIO is to accurately estimate the state of the system in the presence of unknown disturbance(s). For the system described in (5.14), its observer model shown in Figure5.2 can be modeled as

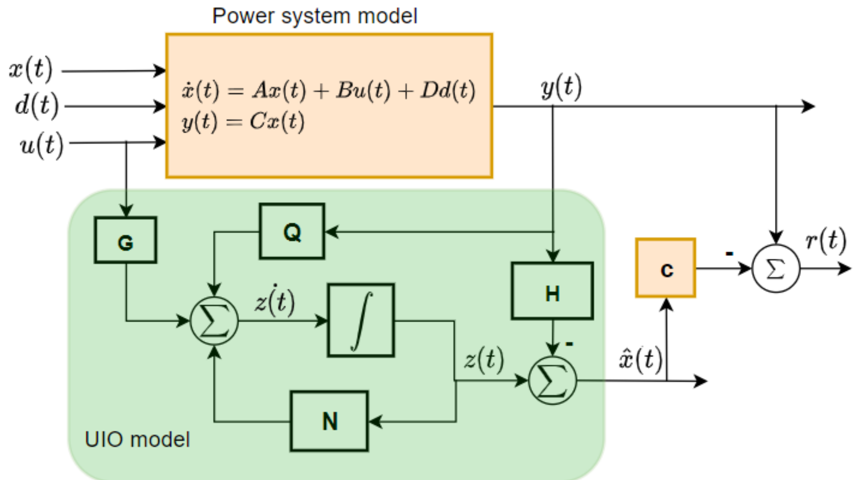

Figure 5.2 Block diagram of unknown input observer

$$\begin{aligned} \dot{z}(t) &= Nz(t) + Gu(t) + Qy(t) \\ \hat{x}(t) &= z(t) - Hy(t) \end{aligned} \tag{5.16}$$

where $z(t)$ and $\hat{x}(t)$ are the state vector of the UIO system and estimated state vector of the true system respectively. The matrices N, G, Q, and H are parameters of the UIO system that need to be formulated appropriately. It is important to mention that for (5.16) to be a reliable observer of (5.14), the state estimation error $e(t)$ given by

$$e(t) = x(t) - \hat{x}(t) \tag{5.17}$$

should asymptotically tend to zero irrespective of the unknown input $d(t)$.

Taking the derivative of (5.17), $\dot{e}(t) = \dot{x}(t) - \dot{\hat{x}}(t)$ is obtained, which can be expanded from (5.14) and (5.16) to give

$$\begin{aligned}\dot{e}(t) = (A - HCA - Q_1C)\, e(t) \\ + (N - (A - HCA - Q_1C))\, z(t) \\ + (Q_2 - (A - HCA - Q_1C))\, y(t) \\ + (G - (I - HC)B)\, u(t) \\ + (HC - I)\, Dd(t)\end{aligned} \tag{5.18}$$

For the UIO to exist, i.e, if the state estimation error asymptotically approaches zero, the following conditions which are obtained from (5.18) must hold

$$\begin{aligned} H &= (CD)^{-1}D \\ A^* &= A - HCA \\ G &= B - HCB \\ N &= A^* - Q_1C \\ Q_2 &= NH \\ Q &= Q_1 + Q_2 \end{aligned} \tag{5.19}$$

If N is stable, i.e., all its poles are located on the left-half of the complex s-plane, which means Q_1 has to be properly designed, and other conditions in (5.19) are met, then the state estimation error asymptotically approaches zero and (5.18) reduces to

$$\dot{e}(t) = Ne(t) \tag{5.20}$$

Based on linear algebra theory in [208], the lemmas of requisite conditions that make (5.16) an UIO model of the system in (5.14) can be summarised as:

Condition 1: rank (CD) = rank (D)

Condition 2: The matrix pair (C, Λ) is detectable

where

$\Lambda = A - D\Big((CD)^T CD\Big)^{-1}(CD)^T CA$

By taking the derivative of the state estimation output and rearranging it the unknown/disturbance can be estimated for the system from

$$\dot{\hat{y}}(t) = C\dot{\hat{x}}(t) \tag{5.21}$$

$$\dot{y}(t) = C[A\hat{x}(t) + Bu(t) + Dd(t)] \tag{5.22}$$

$$\hat{d} = (CD)^{\dagger}[\dot{\hat{y}} - CA\hat{x} - CBu(t)] \tag{5.23}$$

A residual function can be defined which is the difference between the true system state and estimated system where

$$r(t) = y(t) - C\hat{x}(t) \tag{5.24}$$

5.4.2 Design Procedure of Robust UIO

The design of the proposed UIO using robust control theory can be achieved with the following steps:

1. Determine the power system matrices (A, B, C and D). The disturbance matrix D must be a full column rank matrix, otherwise a matrix decomposition should be performed.

2. Check if the UIO model exists using the rank condition, i.e., rank (CD) = rank D. If this condition is not met then the output matrix C can be augmented to satisfy this condition.

3. Compute matrices $H, G,$ and Λ

4. Using the observability criterion; check if the matrix pair (C, Λ) is detectable. If this pair is undetectable, an observable canonical decomposition should be used to determine a transformation matrix that will make the new pair (C^*, Λ^*) which are detectable.

5. Determine Q_1 by solving the linear matrix inequalities (LMI) optimization problem that satisfies the condition in (5.19) using the YALMIP toolbox in MATLAB.

6. Compute $Q_2, N,$ and Q.

7. Using (5.16), formulate the robust UIO model.

5.4.3 Interval Type-2 Fuzzy Logic Control

The fuzzy logic control scheme is considered as an efficient and intelligent control scheme because of its capabilities in handling complex problems and system uncertainties. The general structure of the fuzzy logic control scheme is shown in Figure 5.3. The input processing unit (fuzzifier) converts the crisp input into a fuzzy set. Using a predefined set of rules and mathematical computations, an inference engine calculates the appropriate fuzzy output. Depending on the type of fuzzy logic used, the type-1 FLC as shown in Figure 5.3(a) converts the fuzzy output directly to crisp output while the type-2 FLC in Figure 5.3(b) uses the type-reducer block to reduce the type-2 fuzzy output into type-1 fuzzy output and the defuzzifier converts the type-1 fuzzy output into crisp outputs [195]. Regardless of the degree of the FLC scheme used, the main goal of the fuzzy logic controller is to accurately map the crisp input into a corresponding crisp output.

A type-2 fuzzy set (T2FS) denoted by $\tilde{P}$ where $x \in X$ and can be characterised by

$$\tilde{P} = \{((x,u), \mu_{\tilde{P}}(x,u)) \,|\forall x \in X, \forall u \in J_x \subseteq [0,1]\} \tag{5.25}$$

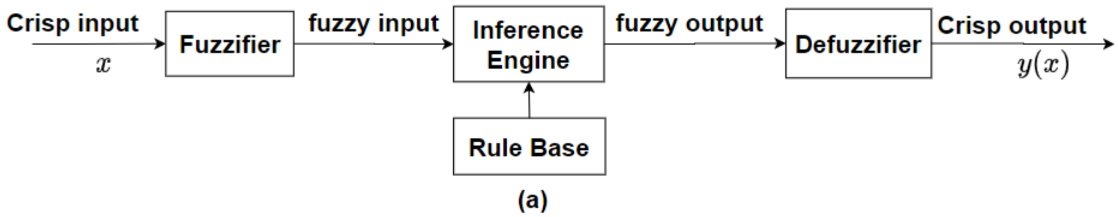

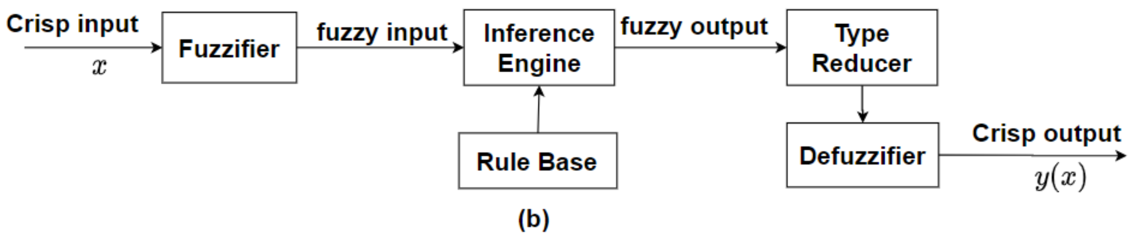

Figure 5.3 Fuzzy logic system (a) Type-1 (b) Type-2

where $\mu_{\tilde{P}}(x,u)$ is a type-2 MF, x is a primary variable, u is the secondary variable in which $0 \leq \mu_{\tilde{P}}(x,u) \leq 1$ and J_x is the primary membership of x.

$\tilde{P}$ can be expressed as

$$\tilde{P} = \int_{x \in X} \int_{u \in J_x} \mu_{\tilde{P}}(x,u)/(x,u) \quad J_x \subseteq [0,1] \tag{5.26}$$

where $\int\int$ denotes union over all possible x and u. When there are no uncertainties, the T2FS is reduced to T1FS such that the secondary variable becomes $\mu_P(x)$ and $0 \leq \mu_P(x) \leq 1$. As a corollary, the boundary of the T2FS should correspond with the fact that the vertical slices of a MF should be between 0 and 1.

When all $\mu_{\tilde{P}}(x,u) = 1$, the $\tilde{P}$ is said to be an interval T2FS (IT2FS). The IT2FS reduces (3.28) to

$$5 - \tilde{P} = \int_{x \in X} \int_{u \in J_x} 1/(x,u) \quad J_x \subseteq [0,1] \tag{5.27}$$

Due to the uncertainty associated with the IT2FS, the boundary of uncertainty in the T1FS membership functions is defined as the footprint of uncertainty (FOU). The outer boundary ($\overline{\mu}$)

of the FOU is the upper membership function (UMF) and the inner boundary ($\underline{\mu}$) is the lower membership function (LMF).

$$\mathrm{FOU}(\tilde{A}) = \bigcup_{x \in X} J_x \tag{5.28}$$

$$\bar{\mu}_{\tilde{P}}(x) \equiv \overline{\mathrm{FOU}}(\tilde{P}) \quad \forall x \in X \tag{5.29}$$

$$\underline{\mu}_{\tilde{P}}(x) \equiv \underline{\mathrm{FOU}}(\tilde{P}) \quad \forall x \in X \tag{5.30}$$

The rule structure for the T2FLC and T1FLC is the same, for a FLC structure with K number of rules, the n^{th} rule can be expressed in the form:

$$\begin{aligned} R_n : \text{if } x_1 \text{ is } \tilde{F}_{1,n} \text{ and } \ldots x_i \text{ is } \tilde{F}_{i,n} \ldots \text{ and } x_I \text{ is } \tilde{F}_{I,n} \\ \text{then } y \text{ is } \tilde{Y}_n \end{aligned} \tag{5.31}$$

where n = (1, 2, ..., K). The type reduction block maps the T2FLC into a T1FLC by computing the centroid of the IT2FLC associated with each fired by using

$$Y_{\tilde{P}} = 1/\{y_l, \ldots, y_r\} \tag{5.32}$$

where y_l and y_r can be calculated using

$$y_l = \frac{\sum_{i=1}^{L} y_i \bar{\mu}_{\tilde{P}}(y_i) + \sum_{i=L+1}^{N} y_i \underline{\mu}_{\tilde{P}}(y_i)}{\sum_{i=1}^{L} \bar{\mu}_{\tilde{P}}(y_i) + \sum_{i=L+1}^{N} \underline{\mu}_{\tilde{P}}(y_i)} \tag{5.33}$$

$$y_r = \frac{\sum_{i=1}^{R} y_i \underline{\mu}_{\tilde{P}}(y_i) + \sum_{i=R+1}^{N} y_i \bar{\mu}_{\tilde{P}}(y_i)}{\sum_{i=1}^{R} \underline{\mu}_{\tilde{P}}(y_i) + \sum_{i=R+1}^{N} \bar{\mu}_{\tilde{P}}(y_i)} \tag{5.34}$$

The switching point L and R in (5.33) and (5.34) are iteratively determined using the Karnik-Mendel algorithm. The crisp output y is computed by the defuzzifier using

$$y(x) = \frac{1}{2}\left[y_l(x) + y_r(x)\right] \tag{5.35}$$

5.5 Interval Type-2 Fuzzy-UIO in LFC problem

This section introduces the application of the proposed robust UIO and interval type-2 fuzzy logic control for dynamic state estimation and load-frequency control, respectively. The power system in the restructured environment as shown in Figure 5.4. In this chapter, the unknown inputs to the power system are the variability in the REP generation $\Delta P_{res,i}^{var}$ and unforecasted/uncontracted load demands ΔP_{L_i}. These can affect the frequency stability of the area. The contracted demands ΔP_{D_i} and LFC control signal set points $\Delta P_{lfc,i}$ are considered to be known inputs to the system. It is worth mentioning that the proposed control method is a decentralized control approach so that the disturbance of each area is decoupled from each other.

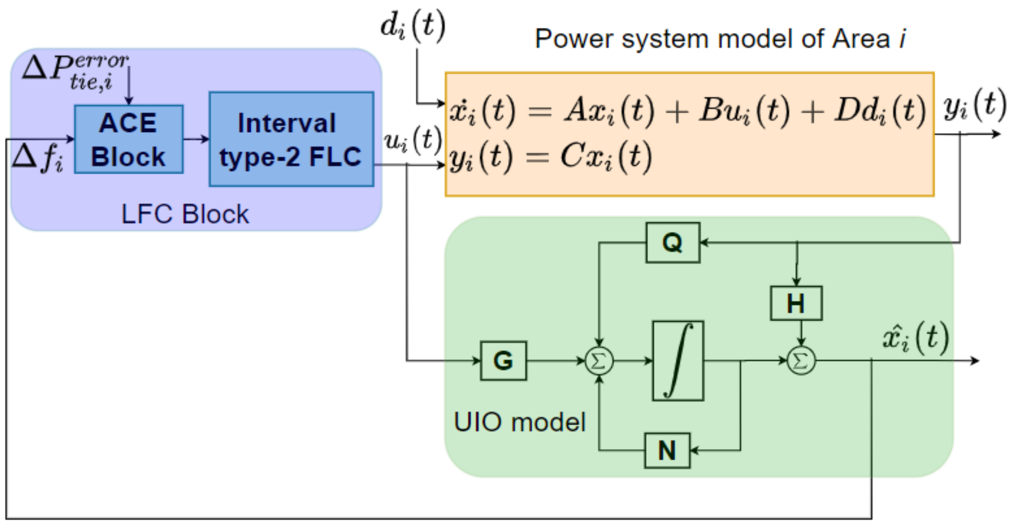

Figure 5.4 Proposed Fuzzy-based LFC for Robust UIO model

For any time-varying disturbance $d_i(t)$ in Area i, the change in area frequency Δf_i is sent to the area controller via a wireless communication channel, the time-dependent ACE is computed using

$$ACE_i(t) = \beta_i \Delta f_i(t) + \Delta P_{tie,i}^{error}(t) \tag{5.36}$$

Table 5.1 Fuzzy rules

ACE								
		NL	NM	NS	Z	PS	PM	PL
$\Delta A\dot{C}E$	NL	PL	PL	PL	PL	PM	PS	Z
	NM	PL	PL	PL	PM	PS	Z	NS
	NS	PL	PL	PM	PS	Z	NS	NM
	Z	PL	PL	PM	Z	NM	NL	NL
	PS	PM	PS	Z	NS	NM	NL	NL
	Z	PS	Z	NS	NM	NL	NL	NL
	PL	Z	NS	NM	NL	NL	NL	NL

The computed ACE and its derivative $A\dot{C}E$ are inputs to the fuzzy logic controller. To fuzzify these inputs, the triangular membership function is chosen in this chapter due to its ease of practical realization. Seven membership functions as shown in Figure 5.5 (Negative Large–NL, Negative Medium–NM, Negative Small–Ns, Zero–Z, Positive Small–PS, Positive Medium–PM, and Positive Large–PL) are chosen for both inputs to the controller. Each fuzzified input has an LMF and UMF. To process these antecedents, a set of rule firing strengths are chosen from the rule base system shown in Table 5.1. This is found by applying the min-method for the Meet operation of the LMFs and UMFs of both fuzzified inputs. Subsequently, the inference engine uses the min-method for the Meet implication in determining the appropriate type-2 fuzzy output. To reduce the type-2 fuzzy output into two type-1 fuzzy outputs (centroids), the Karnik-Mendel(KM) type reduction algorithm is used because of fast computation time and ease of implementation [216]. The output of the controller ΔP_{lfc} is the average of the centroid values.

For Area i, the computed $\Delta P_{lfc,i}$ is weighted with the area participation index $\sigma_{i,n}$ of each GENCO participating in the LFC and sent via a wireless communication channel to the governor of each

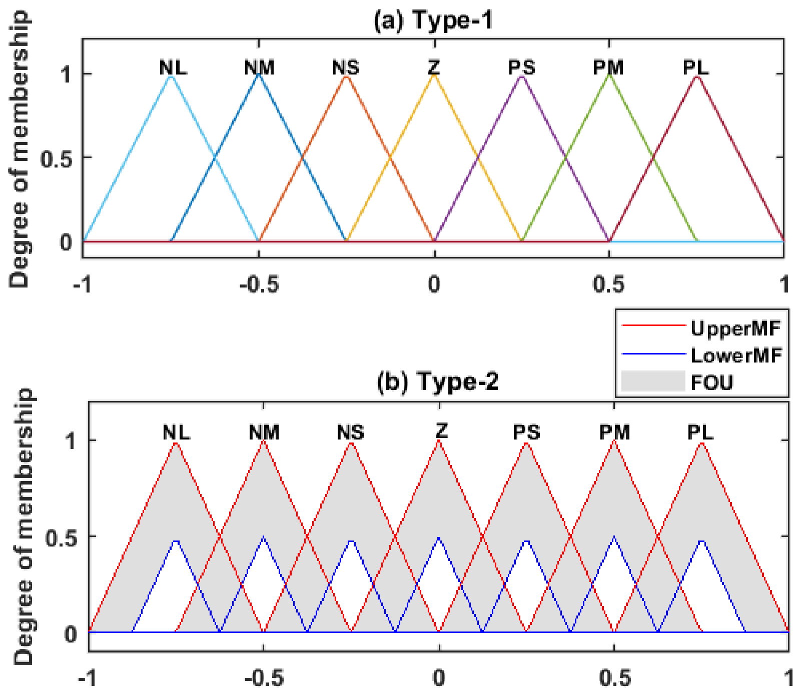

Figure 5.5 Fuzzy logic membership function (a) Type-1 (b) Type-2

GENCO for appropriate control action.

Due to the time-vary characteristics of $d(t)$, the robust UIO can efficiently observe the current state of the power system area and estimate the pattern of the disturbance for proper control measures to be taken.

5.6 Simulation

In this section, the proposed interval type-2 fuzzy controller based on robust UIO is implemented. The studied system is the established Kundur model used for LFC analysis [37]. The model has been modified to include a hybrid HVAC/HVDC transmission network, an aggregated model of a REP in each area, and a distributed virtual inertia-enabled ESS system to support frequency regulation [41]. The analysis is carried out in the restructured power system environment. The simulation is performed in the MATLAB/Simulink environment.

5.6.1 Eigenvalue analysis

To evaluate the stability of the proposed system model eigenvalue analysis is utilized. For a system to be stable, all of its eigenvalues (λ) must have negative real parts. Table 5.2 presents the eigenvalues of the proposed system model (model B), with a comparative evaluation before the addition of virtual inertia control (Model A). It can be seen that both models of the system are stable, having negative eigenvalues; however, Model B is in a better region of stability compared to Model A with two extra modes (λ_{15} and λ_{16}). This is because the virtual inertia control shifts various modes (e.g., λ_1 and λ_2) of the Model B in the negative direction. Furthermore, the results indicate that the oscillatory modes (λ_5, λ_6, λ_7 and λ_8) of Model A have a higher frequency than the modes (λ_8, λ_9, λ_{10} and λ_{11}) of Model B; this points to the ability of the virtual inertia control to damp oscillations and restore the system to stability faster than Model A. It can be stated that virtual inertia control can improve the dynamic performance of the system and strengthen its stability and Consequentially, Model B is the proposed system model used for further analysis in this chapter.

5.6.2 Demonstration of the Robust UIO Model

To demonstrate the performance of the proposed robust UIO model, its state estimation capability is investigated. For this reason, a bilateral contract scenario is considered. It is important to note

Table 5.2 Eigenvalues

Mode	Model A	Model B
λ_1	-17.2019	-102.57
λ_2	-17.2903	-102.87
λ_3	-13.0671	-16.6221
λ_4	-14.6804	-14.6205
λ_5	-0.7090+j6.5366	-12.4756
λ_6	-0.7090-j6.5366	-14.2549
λ_7	-1.0786+j3.6832	-4.8640
λ_8	-1.0786-j3.6832	-0.5043+j1.085
λ_9	-4.4422	-0.5043-j1.085
λ_{10}	-1.4856	-0.6156+j0.1427
λ_{11}	-0.7013	-0.6156-j0.1427
λ_{12}	-0.6561	-0.6588
λ_{13}	-3.2240	-2.6834
λ_{14}	-3.2256	-2.7287
λ_{15}	—	-3.2497
λ_{16}	—	-3.2471

that the bilateral scenario permits inter-area contracts between GENCOs and DISCOs, i.e, there could be an inter-area exchange of power in steady-state operation (scheduled tie line power flow) which is one of the peculiarities of the restructured environment. To this effect, it is considered that the aggregated load demand of the DISCOs in each area is $\Delta P_{D1} = \Delta P_{D2} = 0.2$ p.u from the

GENCOs based on the CPM given by

$$CPM = \begin{bmatrix} 0.25 & 0.4 \\ 0.15 & 0.1 \\ 0.15 & 0.3 \\ 0.45 & 0.2 \end{bmatrix}$$

$$\Delta P_{m1} = 0.25 \times 0.2 + 0.4 \times 0.2 = 0.13 \text{ p.u}$$

$$\Delta P_{m2} = 0.15 \times 0.2 + 0.1 \times 0.2 = 0.05 \text{ p.u}$$

$$\Delta P_{m3} = 0.15 \times 0.2 + 0.3 \times 0.2 = 0.09 \text{ p.u}$$

$$\Delta P_{m4} = 0.45 \times 0.2 + 0.2 \times 0.2 = 0.13 \text{ p.u}$$

The estimation of different system state responses to these demands is used to demonstrate the robustness of the observer. The simulation result in Figure 5.6 shows the ability of the observer to explicitly track the system states in Area 1. Figure 5.6(a) is the plot of the frequency deviation (Δf_1), while Figure 5.6(b) and 5.6(c) are the active power deviations of GENCOs 1 and 2 (ΔP_{m1} and ΔP_{m2}) respectively to meet the power demands. It is observed that ΔP_{m1} and ΔP_{m2} (true and estimated) reach the scheduled steady state values that correlate to the theoretical calculations. For Area 2, the system's true and estimated states are given in Figure 5.7. The robustness of the proposed UIO model is demonstrated with the proper tracking of the frequency deviation (Δf_2), and active power deviations of GENCOs 3 and 4 (ΔP_{m3} and ΔP_{m4}) as shown in Figure 5.7(a), (b) and (c) respectively.

To evaluate the accuracy of the proposed robust UIO model, the state estimation error, i.e, the difference between the true state and the estimated state, is used. As mentioned earlier, the state estimation error should tend towards zero for the developed UIO to be a valid observer of the system. From Figure 5.8, it is clear that the state estimation error of the area frequency deviations

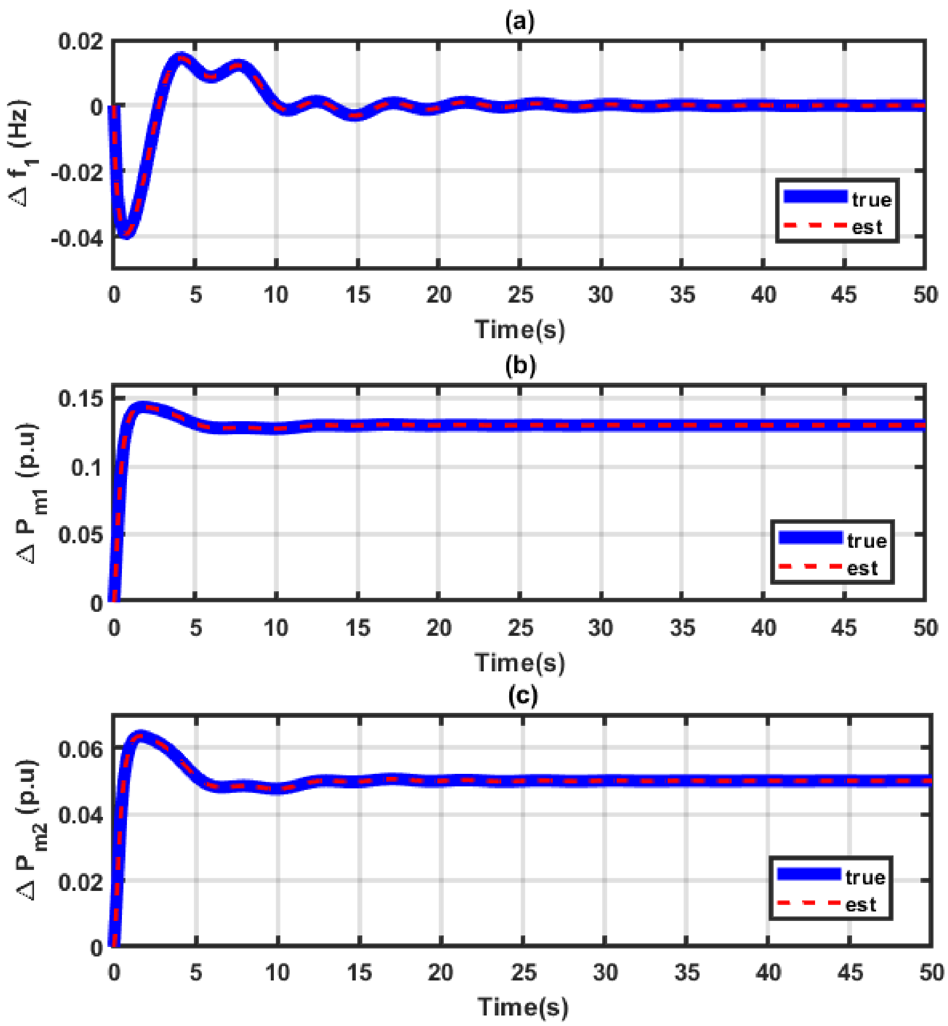

Figure 5.6 Area 1 plot (a) frequency deviation (b) active power deviation in GENCO 1 (c) active power deviation in GENCO 2

(Δf_1 and Δf_2) is approximately zero, which implies a high precision in the state estimation. From the results above, it can be inferred that the proposed robust UIO model is satisfactory for the study system.

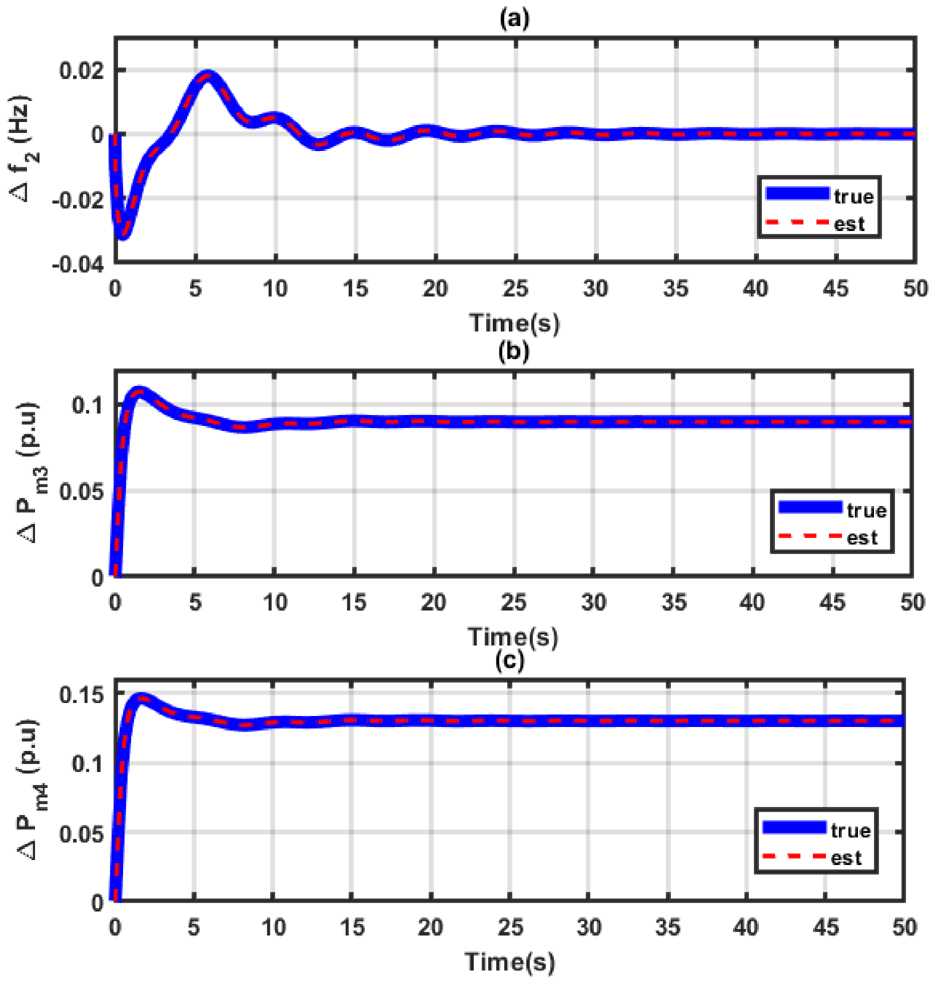

Figure 5.7 Area 2 plot (a) frequency deviation (b) active power deviation in GENCO 3 (c) active power deviation in GENCO 4

5.6.3 Estimation and Control of Unknown load variation

In this section, the efficiency of the proposed intelligent interval type-2 fuzzy logic-based load frequency controller is investigated. This provides a swift response to unknown inputs that pose a disturbance to the stability of the system. The performance of the proposed controller is evaluated against the conventional T1FLC and PI controllers.

Figure 5.9 shows the frequency response of the controllers in each area to an unknown disturbance

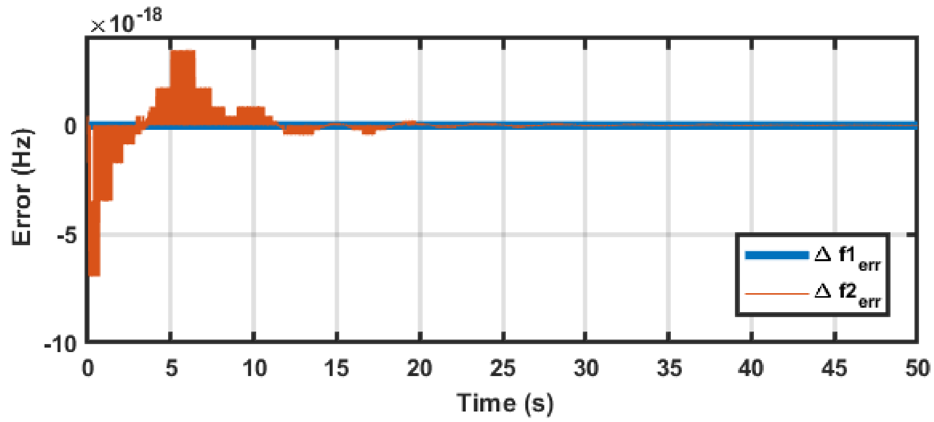

Figure 5.8 Frequency estimation error in Areas 1 and 2

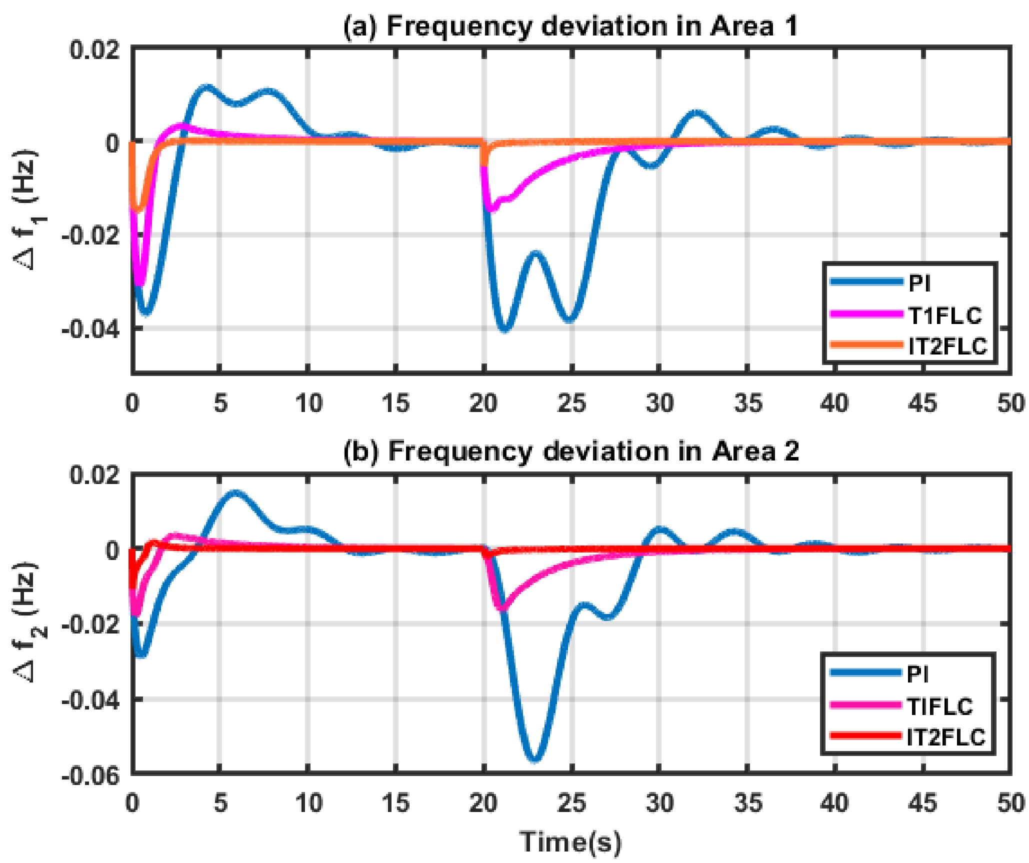

Figure 5.9 Plots of frequency deviation

at 20 s. As observed, both areas experience frequency dips at the start of the disturbance but the proposed IT2FLC controller provides the smallest undershoot when compared to the T1FLC and PI controllers. It is found that with the adoption of the proposed controller, the frequency deviation reaches zero in steady-state in the least time compared to the other controllers in Areas 1 and 2. Therefore, the proposed IT2FLC controller is efficient in restoring the system frequency to the nominal operating point despite the disturbance.

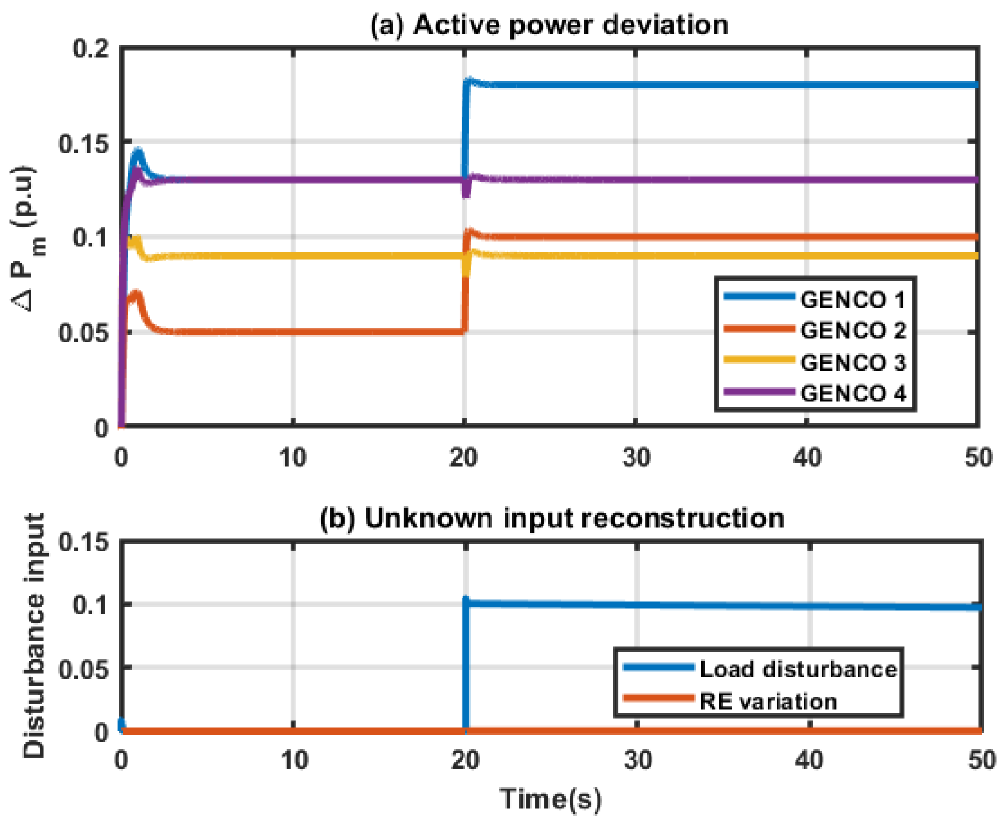

Figure 5.10 Plot of GENCOs response to unknown input

Using the proposed control scheme, the change in mechanical output power ΔP_m of each GENCO due to a sudden disturbance is shown in Figure 5.10(a). It can be observed that the responses of the GENCOs are smooth with no oscillations. This is beneficial to the health of the governors because the oscillation may trigger protective relays and sensors leading to cascading events and possible tripping of some generator units. It can also be observed that only GENCOs in Area 1, i.e, GENCOs 1 and 2, settle at a new steady-state value after the disturbance. This implies that the disturbance occurs in Area 1 and the responses of the GENCOs in this area depend on their participation index σ. GENCOs 3 and 4 also support the system during the disturbance due to the interconnection between both areas but return to their initial steady-state values after the disturbance. The ability of the proposed robust UIO model to estimate the state of the system and reconstruct the unknown input disturbance in the system is shown in Figure 5.10(b). It is worth mentioning that, with the increasing penetration level of renewable energy sources, the power system stability and resilience become more vulnerable; therefore, the estimation of this disturbance is needed to minimize forecasting errors and detect cyber attacks, etc.

To demonstrate the robustness of the proposed IT2FLC control scheme, a multiple unknown input scenario is considered. The frequency response plots of the proposed control scheme, T1FLC scheme, and PI control schemes in Area 1 are shown in Figure 5.11(a). It can be observed that the response of the PI controller is very erratic and unstable with high oscillations and undershoots; however, the T1FLC provides a better response with more stability, reduced oscillations, and undershoots. The proposed IT2FLC control scheme provides the best performance with the least undershoot, zero oscillations, and flattened steady-state operation, this shows that a desirable control input ΔP_{lfc} is attainable by adopting the suggested controller. Figure 5.11(b) shows the disturbance inputs in Area 1 of the system, it is clear that there is a fluctuation in renewable energy sources and step load disturbance that can affect the frequency stability of the system. The proposed IT2FLC controller is swift to deal with these disturbances.

It can be viewed from Figure 5.12(a) that the proposed IT2FLC controller provides the best frequency response performance when compared to other controllers in Area 2. It can be inferred

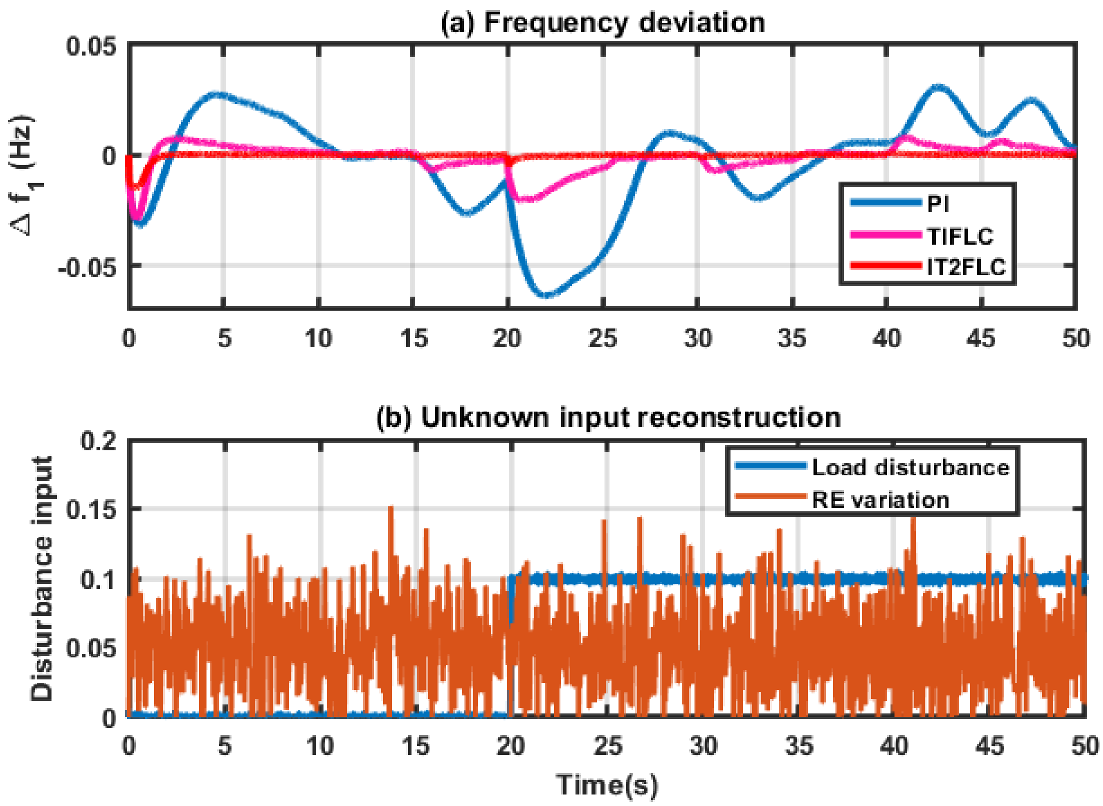

Figure 5.11 Plot of frequency response in Area 1

that the dynamic response of the system is improved with the frequency deviation returning to zero in a short settling time with no oscillations. The reconstructed unknown input in Area 2 is shown in Figure 5.12(b). It becomes clear that the disturbance in the area is a variable step load disturbance without RE fluctuation. The proposed robust UIO performs efficient estimation of the frequency states which are fed to the proposed IT2FLC controller for mitigation of frequency deviation despite the unknown inputs to the system.

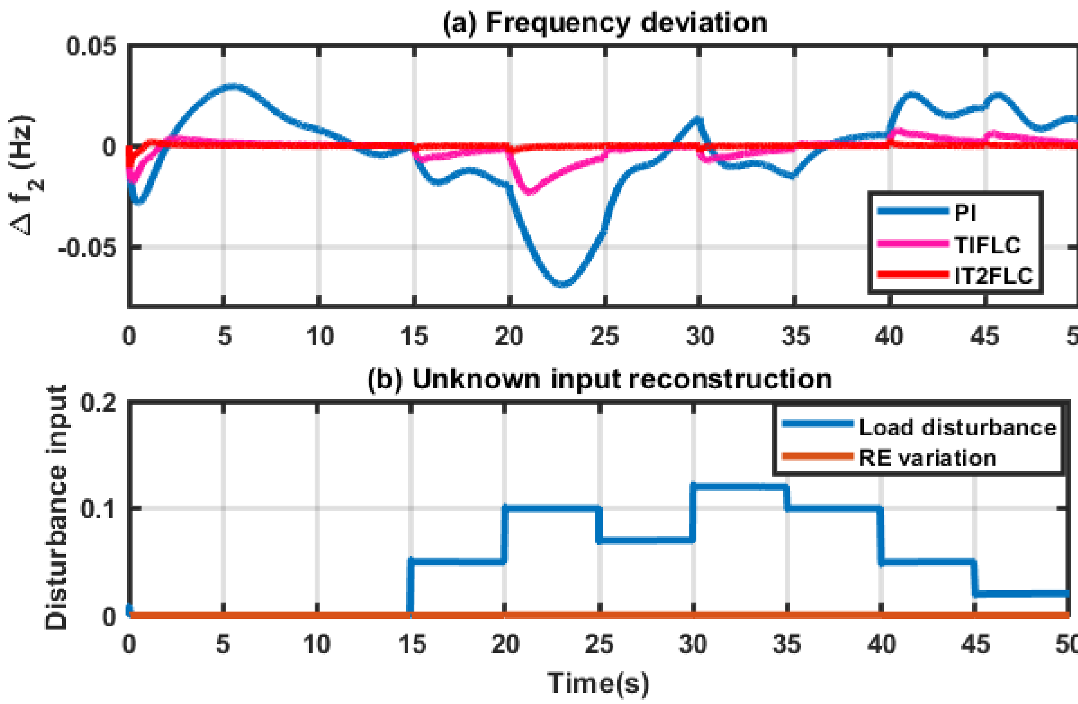

Figure 5.12 Plot of frequency response in Area 2

5.6.4 Performance during parametric variations

In this section, the robustness of the proposed IT2FLC is evaluated using parametric variations that can occur when some GENCO units are decommissioned or tripped during the excess availability of renewable energy. These variations may cause instability in the system if not handled properly. The various parameters used for the uncertainty analysis are; $M_1 = -20\%$, $M_2 = -40\%$, $D_1 = -30\%$, $D_2 = -25\%$, $R_1 = -15\%$ and $R_4 = -20\%$. Fig. 5.13 illustrates the frequency responses of the different controllers to load variations under parametric changes. It can be observed that the performance of the PI and T1FLC controllers are not satisfactory where there are severe parameter changes. In other words, the results indicate that the proposed IT2FLC method is more effective in dealing with parameter changes in terms of stable frequency response and minimal transient when compared to the other control methods. Usually, when there is a decrease in system inertia, the maximum frequency deviation increases. However, the proposed IT2FLC controller can effectively deal with the frequency deviation with the least undershoot. Hence, it is confirmed that the proposed IT2FLC scheme for frequency control is very robust in a system with high penetration of renewable energy, load variation, and diverse uncertainties.

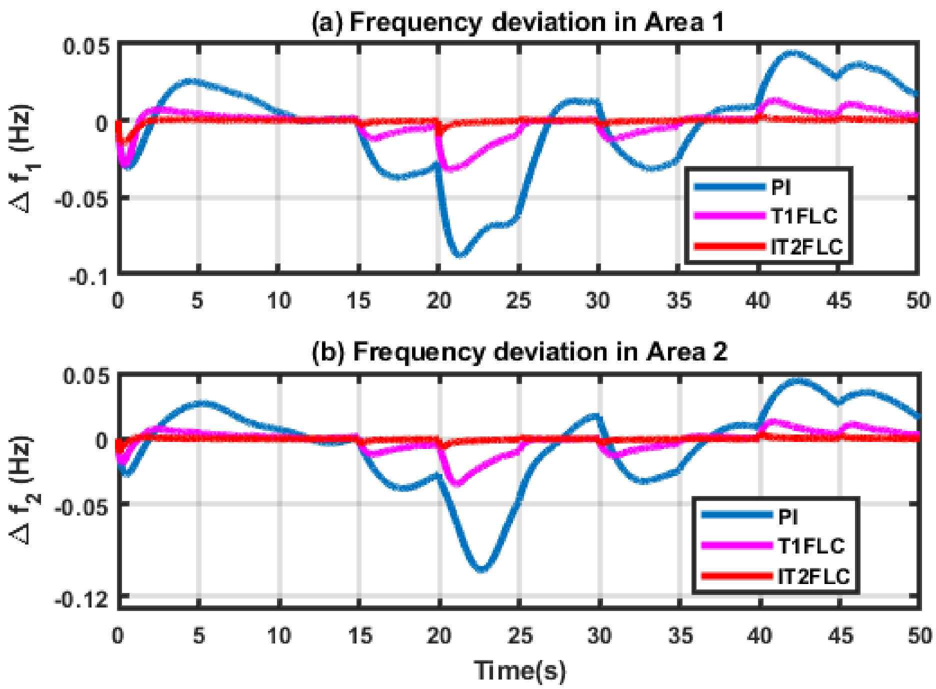

Figure 5.13 Plot of frequency response during parametric variations

5.6.5 Comparison with other control methods

The improved performance of the proposed IT2FLC control method against other existing control methods for the LFC application is illustrated in this section. The existing methods are: artificial neural networks (ANN) [131], robust control (RC) [213], T1FLC and sliding mode control (SMC) [132]. The considered performance criteria used for the comparative evaluation are nonlinearity, uncertainty, unknown input, and stability. These criteria are selected based on the analyses reported in the papers. Table 5.3 shows the comparison of the proposed IT2FLC method with other control methods using the performance criteria. Because the secondary frequency control loop in LFC schemes considers unknown inputs, existing methods such as ANN, T1FLC, and SMC will not give suitable responses if they are implemented in power systems for frequency regulation. Contrariwise, the proposed IT2FLC has been designed to consider unknown inputs using the UIO method. Regarding stability, the proposed method has given satisfactory performance when compared to other methods.

Table 5.3 Comparison of proposed method with other control methods

Performance criteria	Proposed	ANN	T1FLC	RC	SMC
Non-linearity	✓	✓	✓	×	✓
Uncertainty	✓	✓	✓	✓	✓
Unknown input	✓	×	×	✓	×
Stability	✓	×	×	×	×

5.7 Summary

The conventional LFC framework is reformulated to consider the dynamics of a restructured power system environment. The two-area model used for simulation studies is modified with hybrid HVAC/HVDC transmission, RE integration, and ESS-based virtual inertia control to adopt the transformations in modern power systems. A dynamic model observer is developed using the robust UIO method; the simulation results demonstrate that the proposed UIO model is efficient in estimating the real-time state of the system in the presence of unknown input with negligible state estimation error. Also, the IT2FLC control scheme is proposed for load frequency control.

The robustness of the control scheme is evaluated against existing control schemes. The proposed LFC controller can damp frequency oscillations and improve the stability of the system. The general control framework can be implemented at the secondary level of the hierarchical frequency control of large power systems or interconnected microgrids. For future work in this research area, the proposed observer method and control scheme will be adopted for cyber-attack detection and mitigation in smart power grids.

Chapter 6

Conclusion and Future Work

6.1 Main findings and conclusion

The main findings in this thesis are inferred from the previous chapters and summarized as follows:

1. Since the framework of the restructured power system environment would be different from the traditional one, it is important to develop appropriate small-signal models of the various additional complexities such as HVDC interconnection and tie line dynamics, renewable energy sources, the speed governor response of generators to deregulation. These models are useful to conduct proper analysis and design control strategies to improve the frequency stability of the system. To this effect, a detailed description of the fundamentals of a frequency control for interconnected power systems was developed in Chapter 2. As one of the contributions, a comprehensive mathematical model for the LFC framework considering HVAC/HVDC interconnection was developed. The small-signal model is useful for fre-

quency stability analysis with the secondary frequency control time frame. The impacts of inertia on frequency stability in the changing power system environment are also discussed.

2. With the recent grid codes becoming stringent, renewable energy plants are required to provide frequency power support to the system during contingencies. A small-signal model incorporating a wind energy conversion system with the capability to provide virtual inertia was proposed in Chapter 3. The proposed virtual inertia method is based on the derivative control strategy and implemented by operating the WECS below the maximum power point to reserve active power for frequency support. The design parameters were heuristically tuned using the artificial bee colony optimization algorithm to determine their optimal values over a wide range of operating conditions. To understand the effect of the proposed control approach on system stability, eigenvalue analysis was used to investigate the location of the poles on the complex s-plane. Based on the LFC study conducted in the deregulated environment by considering three market scenarios through simulation, it can be concluded that the designed control approach for WECS can improve the first overshoot/undershoot of the signals of interest (frequency and active power deviations) during different contingencies.

3. It is a general fact that renewable energy sources are stochastic and non-storable by nature; therefore, there is a challenge to provide reliable virtual inertia support when needed. To tackle this issue, an energy storage system was proposed to implement the virtual inertia control strategy.In addition, an advanced and intelligent control method–interval type-II fuzzy logic–was adopted for inertia emulation in place of the classical (derivative) control method used in Chapter 2. The weights of the weights/gains of the fuzzy logic controller were tuned using the ABC optimization algorithm. This novel control scheme is one of the major contributions; it is advantageous because the ESS guarantees a steady supply of active power when needed, the interval type-II fuzzy logic controller provides an adaptive and dynamic control synthesis that optimally exploits the power from the ESS depending on

the extent of frequency deviation. From the simulation results obtained, it can be concluded that the proposed control scheme is most efficient compared to the type-I fuzzy logic and derivative control schemes in improving the frequency stability of the system.

4. As mentioned in Chapter 1, this thesis aims to investigate the application of intelligent control schemes in the frequency control problem to improve the stability of interconnected systems with high penetration of renewable energy in the restructured power system environment. While virtual inertia control schemes have been proposed, a novel frequency control scheme was proposed in Chapter 5. The novel scheme is based on an unknown input observer method for dynamic state estimation and interval type-II fuzzy logic control for load frequency control. The proposed UIO model provided real-time state information of unknown inputs/disturbances such as uncontracted load demand and unpredicted renewable energy fluctuation that can affect the stability of the system. The proposed LFC scheme is decentralized for each control area to mitigate frequency deviations, restore control area frequency to nominal values, and maintain tie line power flow between interconnected areas at scheduled value. The interval type-II fuzzy logic allows for an extra degree of freedom in its modeling to handle uncertainties or unknown inputs. From the simulation results, it is found that the novel hybrid control scheme significantly improves the frequency response of the system, thereby reinforcing the stability and resilience of the system in the presence of unknown inputs.

From the studies conducted in this thesis, it can be concluded that the implementation of virtual inertia in modern power systems can improve the frequency response of the system during severe operating conditions. The results from the simulations showed the optimised virtual inertia control method has a faster response by injecting active power with damped oscillations compared to the conventional virtual inertia control method. Furthermore, the application of the interval type-II FLC for the ESS-based virtual inertia control scheme provides a better active power injection/absorption capability during power imbalance as result of load variation or renewable energy fluctuation. This work also implemented a robust LFC system using the unknown input observer and interval type-II FLC to provide accurate state estimation of the power system in the presence of unknown inputs that can impact the frequency stability of the system. The simulation results show the significance of state estimation as an important tool to maintain the resilience of power systems despite the dynamic operating conditions.

6.2 Future work

This thesis has uncovered some important aspects concerning the concept of virtual inertia and frequency control of interconnected systems in the deregulated environment. Nevertheless, taking into consideration various aspects of power systems, a great deal of research and innovation is still necessary in this area. The following can be regarded as possible future areas of research that may require investigation:

1. Application of proposed control techniques to highly complex interconnected power system models.
2. Development of alternative methods for virtual inertia emulation.
3. Development of advanced and hybrid inertia control techniques.
4. Improvement of computing techniques and measurement technologies.
5. Investigation of different ESS models for inertia emulation based on technical and economic benefits.

Bibliography

[1] Anuoluwapo O. Aluko, David G. Dorrell, Rudiren Pillay Carpanen, and Evans E. Ojo. Heuristic optimization of virtual inertia control in grid-connected wind energy conversion systems for frequency support in a restructured environment. *Energies*, 13(3):564, 2020.

[2] Anuoluwapo O. Aluko, David G. Dorrell, Rudiren Pillay Carpanen, and Evans E. Ojo. A virtual inertia control method for high renewable energy-integrated interconnected power systems. *Energy Science and Engineering*, Submitted.

[3] Anuoluwapo O. Aluko, David G. Dorrell, Rudiren Pillay Carpanen, and Evans E. Ojo. Robust state estimation method for adaptive load frequency control of interconnected power system in a restructured environment. *IEEE Systems Journal*, Early Access:1–11, 2020.

[4] Anuoluwapo O. Aluko, Rudiren Pillay Carpanen, David G. Dorrell, and Evans E. Ojo. Real-time cyber attack detection scheme for stand-alone microgrids. *IEEE Transactions on Smart Grid*, Submitted.

[5] Anuoluwapo O. Aluko, David G. Dorrell, Rudiren Pillay Carpanen, and Evans E. Ojo. Frequency control of modern multi-area power systems using fuzzy logic controller. In *IEEE PES/IAS PowerAfrica*, pages 645–649. IEEE, 2019.

[6] Anuoluwapo O. Aluko, David G. Dorrell, Rudiren Pillay Carpanen, and Evans E. Ojo.

Heuristic secondary frequency control of AC/DC interconnected power system in a deregulated environment. In *International SAUPEC/RobMech/PRASA Conference*, pages 1–6. IEEE, 2020.

[7] Anuoluwapo O. Aluko, David G. Dorrell, Rudiren Pillay Carpanen, and Evans E. Ojo. Impact assessment and mitigation of cyber attacks on frequency stability of isolated microgrid using virtual inertia control. In *2020 IEEE PES/IAS PowerAfrica*, pages 1–5, 2020.

[8] Anuoluwapo O. Aluko, David G. Dorrell, Rudiren Pillay Carpanen, and Evans E. Ojo. Vulnerability analysis of false data injection attacks on the frequency stability of isolated microgrids. In *2021 Southern African Universities Power Engineering Conference/Robotics and Mechatronics/Pattern Recognition Association of South Africa (SAUPEC/RobMech/PRASA)*, pages 1–6, 2021.

[9] Anuoluwapo O. Aluko, David G. Dorrell, Rudiren Pillay Carpanen, and Evans E. Ojo. Real-time dynamic disturbance estimation of stand-alone microgrids based on unknown input observer for frequency regulation. In *IEEE PES/IAS PowerAfrica*, pages 1–5, Submitted 2021.

[10] Elyas Rakhshani. *Analysis and Control of Multi–Area HVDC Interconnected Power Systems by Using Virtual Inertia*. Journal article, Universitat Politècnica De Catalunya, 2016.

[11] Hassan Bevrani. *Robust Power System Frequency Control*. Springer, Switzerland, second edition, 2014.

[12] Amirnaser Yazdani and Reza Iravani. *Voltage-sourced converters in power systems: Modeling, control, and applications*. John Wiley & Sons, 2010.

[13] Ahmed Selman Hadi Al-Toma. *Hybrid control schemes for permanent magnet synchronous generator wind turbines*. PhD thesis, Brunel University London, 2017.

[14] Prabha Kundur, John Paserba, Venkat Ajjarapu, Göran Andersson, Anjan Bose, Claudio Canizares, Nikos Hatziargyriou, David Hill, Alex Stankovic, Carson Taylor, et al. Definition and classification of power system stability IEEE/CIGRE joint task force on stability terms and definitions. *IEEE transactions on Power Systems*, 19(3):1387–1401, 2004.

[15] Ioannis Hadjipaschalis, Andreas Poullikkas, and Venizelos Efthimiou. Overview of current and future energy storage technologies for electric power applications. *Renewable and sustainable energy reviews*, 13(6-7):1513–1522, 2009.

[16] IEA (2019). Renewables 2019, 2019.

[17] Yuri V Makarov, Viktor I Reshetov, A Stroev, and I Voropai. Blackout prevention in the United States, Europe, and Russia. *Proceedings of the IEEE*, 93(11):1942–1955, 2005.

[18] Göran Andersson, Peter Donalek, Richard Farmer, Nikos Hatziargyriou, Innocent Kamwa, Prabhashankar Kundur, Nelson Martins, John Paserba, Pouyan Pourbeik, Juan Sanchez-Gasca, et al. Causes of the 2003 major grid blackouts in North America and Europe, and recommended means to improve system dynamic performance. *IEEE transactions on Power Systems*, 20(4):1922–1928, 2005.

[19] Majid Sanaye-Pasand. Scrutiny of the Iranian national grid. *IEEE Power and Energy Magazine*, 5(1):31–39, 2006.

[20] UCTE Investigation Committee et al. Final report of the Investigation committee on the 28 September 2003 blackout in Italy, 2004.

[21] P Kundur, DC Lee, J Bayne, and PL Dandeno. Impact of turbine generator overspeed controls on unit performance under system disturbance conditions. *IEEE Transactions on power apparatus and systems*, (6):1262–1269, 1985.

[22] B Ozer, O Arikan, G Moral, and A Altintas. Extraction of primary and secondary frequency control from active power generation data of power plants. *International Journal of Electrical Power & Energy Systems*, 73:16–22, 2015.

[23] Leonard L Grigsby. *Power system stability and control*, volume 5. CRC press, 2012.

[24] A Kurita, H Okubo, K Oki, S Agematsu, DB Klapper, NW Miller, WW Price, JJ Sanchez-Gasca, KA Wirgau, and TD Younkins. Multiple time-scale power system dynamic simulation. *IEEE Transactions on Power Systems*, 8(1):216–223, 1993.

[25] H Bevrani. Automatic generation control, ed. by H. Wayne Beaty. *Standard Handbook for Electrical engineers, 16th edn, Section*, 16:138–159, 2013.

[26] Göran Andersson. Dynamics and control of electric power systems. *Lecture notes*, pages 227–0528, 2012.

[27] Jan Machowski, Zbigniew Lubosny, Janusz W Bialek, and James R Bumby. *Power system dynamics: stability and control*. John Wiley & Sons, 2020.

[28] AS Chuang and Christine Schwaegerl. Ancillary services for renewable integration. In *2009 CIGRE/IEEE PES Joint Symposium Integration of Wide-Scale Renewable Resources Into the Power Delivery System*, pages 1–1. IEEE, 2009.

[29] Yann G Rebours, Daniel S Kirschen, Marc Trotignon, and Sbastien Rossignol. A survey of frequency and voltage control ancillary services—Part I: Technical features. *IEEE Transactions on power systems*, 22(1):350–357, 2007.

[30] John J Grainger, William D Stevenson, William D Stevenson, et al. *Power system analysis*. 2003.

[31] Dwarkadas Pralhaddas Kothari and IJ Nagrath. *Modern power system analysis*. Tata McGraw-Hill Education, 1989.

[32] Changhong Zhao, Ufuk Topcu, Na Li, and Steven Low. Design and stability of load-side primary frequency control in power systems. *IEEE Transactions on Automatic Control*, 59(5):1177–1189, 2014.

[33] Shashi Kant Pandey, Soumya R Mohanty, and Nand Kishor. A literature survey on load–frequency control for conventional and distribution generation power systems. *Renewable and Sustainable Energy Reviews*, 25:318–334, 2013.

[34] Zhixin Miao and Lingling Fan. Achieving economic operation and secondary frequency regulation simultaneously through local feedback control. *IEEE Transactions on Power Systems*, 32(1):85–93, 2016.

[35] Jianwei Li, Rui Xiong, Qingqing Yang, Fei Liang, Min Zhang, and Weijia Yuan. Design/test of a hybrid energy storage system for primary frequency control using a dynamic droop method in an isolated microgrid power system. *Applied Energy*, 201:257–269, 2017.

[36] IEEE Committee Report. Dynamic models for steam and hydro turbines in power system studies. *IEEE transactions on power apparatus and systems*, (6):1904–1915, 1973.

[37] Prabha Kundur, Neal J Balu, and Mark G Lauby. *Power system stability and control*, volume 7. McGraw-hill New York, 1994.

[38] Paul M Anderson and Aziz A Fouad. *Power system control and stability*. John Wiley & Sons, 2008.

[39] Olle Ingemar Elgerd. Electric energy systems theory: An introduction. 1982.

[40] Yong Chang, Zheng Xu, Gaihong Cheng, and Jiani Xie. Coordinate damping control of HVDC and SVC based on wide area signal. In *2006 IEEE Power Engineering Society General Meeting*, pages 7–pp. IEEE, 2006.

[41] Elyas Rakhshani, Daniel Remon, Antoni Mir Cantarellas, and Pedro Rodriguez. Analysis of derivative control based virtual inertia in multi-area high-voltage direct current interconnected power systems. *IET Generation, Transmission & Distribution*, 10(6):1458–1469, 2016.

[42] Hua Weng and Zheng Xu. Wams based robust HVDC control considering model imprecision for AC/DC power systems using sliding mode control. *Electric power systems research*, 95:38–46, 2013.

[43] Elyas Rakhshani, A Luna, Kumars Rouzbehi, P Rodriguez, and Ion Etxeberria-Otadui. Effect of VSC-HVDC on load frequency control in multi-area power system. In *2012 IEEE Energy Conversion Congress and Exposition (ECCE)*, pages 4432–4436. IEEE, 2012.

[44] Nikhil Pathak, Ashu Verma, TS Bhatti, and Ibraheem Nasiruddin. Modeling of HVDC tie links and their utilization in AGC/LFC operations of multiarea power systems. *IEEE Transactions on Industrial Electronics*, 66(3):2185–2197, 2018.

[45] Elyas Rakhshani and Javad Sadeh. Practical viewpoints on load frequency control problem in a deregulated power system. *Energy conversion and management*, 51(6):1148–1156, 2010.

[46] Hassan Bevrani and Takashi Hiyama. *Intelligent automatic generation control*. CRC press, 2017.

[47] M Prabavathi and R Gnanadass. Energy bidding strategies for restructured electricity market. *International Journal of Electrical Power & Energy Systems*, 64:956–966, 2015.

[48] H Lee Willis and Lorrin Philipson. *Understanding electric utilities and de-regulation*, volume 27. CRC Press, 2018.

[49] Jayant Kumar, Kah-Hoe Ng, and Gerald Sheble. AGC simulator for price-based operation. I. A model. *IEEE Transactions on Power Systems*, 12(2):527–532, 1997.

[50] Richard D Christie and Anjan Bose. Load frequency control issues in power system operations after deregulation. *IEEE Transactions on Power systems*, 11(3):1191–1200, 1996.

[51] Jayanth Kumar, Kah-Hoe Ng, and Gerald Sheble. AGC simulator for price-based operation. II. Case study results. *IEEE Transactions on Power Systems*, 12(2):533–538, 1997.

[52] Rakibuzzaman Shah, N Mithulananthan, RC Bansal, and VK Ramachandaramurthy. A review of key power system stability challenges for large-scale PV integration. *Renewable and Sustainable Energy Reviews*, 41:1423–1436, 2015.

[53] FW Koch, I Erlich, and F Shewarega. Dynamic simulation of large wind farms integrated in a multimachine network. In *IEEE Power Engineering Society General Meeting (IEEE Cat. No. 03CH37491)*, volume 4, pages 2159–2164. IEEE, 2003.

[54] Müfit Altin, Ömer Göksu, Remus Teodorescu, Pedro Rodriguez, Birgitte-Bak Jensen, and Lars Helle. Overview of recent grid codes for wind power integration. In *2010 12th International Conference on Optimization of Electrical and Electronic Equipment*, pages 1152–1160. IEEE, 2010.

[55] Durga Gautam, Lalit Goel, Raja Ayyanar, Vijay Vittal, and Terry Harbour. Control strategy to mitigate the impact of reduced inertia due to doubly fed induction generators on large power systems. *IEEE Transactions on Power Systems*, 26(1):214–224, 2010.

[56] Gillian Lalor, Alan Mullane, and Mark O'Malley. Frequency control and wind turbine technologies. *IEEE Transactions on Power Systems*, 20(4):1905–1913, 2005.

[57] Pieter Tielens and Dirk Van Hertem. Grid inertia and frequency control in power systems with high penetration of renewables. In *Young Researchers Symposium in Electrical Power Engineering, Date: 2012/04/16-2012/04/17, Location: Delft, The Netherlands*, 2012.

[58] M Reza Bank Tavakoli, Michael Power, Lisa Ruttledge, and Damian Flynn. Load inertia estimation using white and grey-box estimators for power systems with high wind penetration. *IFAC Proceedings Volumes*, 45(21):399–404, 2012.

[59] Gauthier Delille, Bruno Francois, and Gilles Malarange. Dynamic frequency control support by energy storage to reduce the impact of wind and solar generation on isolated power system's inertia. *IEEE Transactions on Sustainable Energy*, 3(4):931–939, 2012.

[60] Pengwei Du and Julia Matevosyan. Forecast system inertia condition and its impact to integrate more renewables. *IEEE Transactions on Smart Grid*, 9(2):1531–1533, 2017.

[61] Pádraig Daly, Damian Flynn, and Noel Cunniffe. Inertia considerations within unit commitment and economic dispatch for systems with high non-synchronous penetrations. In *2015 IEEE Eindhoven PowerTech*, pages 1–6. IEEE, 2015.

[62] Jacob Aho, Andrew Buckspan, Jason Laks, Paul Fleming, Yunho Jeong, Fiona Dunne, Matthew Churchfield, Lucy Pao, and Kathryn Johnson. A tutorial of wind turbine control for supporting grid frequency through active power control. In *2012 American Control Conference (ACC)*, pages 3120–3131. IEEE, 2012.

[63] Ioannis D Margaris, Stavros A Papathanassiou, Nikos D Hatziargyriou, Anca D Hansen, and Poul Sorensen. Frequency control in autonomous power systems with high wind power penetration. *IEEE Transactions on Sustainable Energy*, 3(2):189–199, 2012.

[64] Chi Su and Zhe Chen. Influence of wind plant ancillary frequency control on system small

signal stability. In *2012 IEEE Power and Energy Society General Meeting*, pages 1–8. IEEE, 2012.

[65] Min Hwang, Eduard Muljadi, Jung-Wook Park, Poul Sørensen, and Yong Cheol Kang. Dynamic droop–based inertial control of a doubly-fed induction generator. *IEEE Transactions on Sustainable Energy*, 7(3):924–933, 2016.

[66] Wei Zhang and Kailun Fang. Controlling active power of wind farms to participate in load frequency control of power systems. *IET Generation, Transmission & Distribution*, 11(9):2194–2203, 2017.

[67] Shinichi Nomura, Yoshihiro Ohata, Takushi Hagita, Hiroaki Tsutsui, Shunji Tsuji-Iio, and Ryuichi Shimada. Wind farms linked by smes systems. *IEEE Transactions on Applied Superconductivity*, 15(2):1951–1954, 2005.

[68] Bin Wu, Yongqiang Lang, Navid Zargari, and Samir Kouro. *Power conversion and control of wind energy systems*, volume 76. John Wiley & Sons, 2011.

[69] Jim Esch. High-power wind energy conversion systems: State-of-the-art and emerging technologies. *Proceedings of the IEEE*, 103(5):736–739, 2015.

[70] Elyas Rakhshani and Pedro Rodriguez. *Active power and frequency control considering large-scale RES*, pages 233–271. Springer Singapore, Singapore, 2014.

[71] Anuoluwapo Oluwatobiloba Aluko. Modelling and performance analysis of doubly fed induction generator wind farm. Master's thesis, Durban University of Technology, 2018.

[72] Anuoluwapo Oluwatobiloba Aluko and Kayode Timothy Akindeji. Performance analysis of grid connected SCIG and DFIG based windfarm. In *Proceedings of the 26th South African Universities Power Engineering Conference (SAUPEC)*, pages 20–25, 2018.

[73] Anuoluwapo Oluwatobiloba Aluko and Kayode Timothy Akindeji. Mitigation of low voltage contingency of doubly fed induction generator wind farm using static synchronous compensator in South Africa. In *IEEE PES/IAS PowerAfrica*, pages 13–18. IEEE, 2018.

[74] Loi Lei Lai. *Power system restructuring and deregulation: trading, performance and information technology*. John Wiley & Sons, 2001.

[75] Yogendra Arya. AGC of two-area electric power systems using optimized fuzzy PID with filter plus double integral controller. *Journal of the Franklin Institute*, 355(11):4583–4617, 2018.

[76] PH Ashmole, DR Battlebury, and RK Bowdler. Power-system model for large frequency disturbances. In *Proceedings of the Institution of Electrical Engineers*, volume 121, pages 601–608. IET, 1974.

[77] C-T Pan and C-M Liaw. An adaptive controller for power system load-frequency control. *IEEE Transactions on Power Systems*, 4(1):122–128, 1989.

[78] Elyas Rakhshani, Kumars Rouzbehi, and Sedigheh Sadeh. A new combined model for simulation of mutual effects between LFC and AVR loops. In *Asia-Pacific Power and Energy Engineering Conference*, pages 1–5. IEEE, 2009.

[79] Suryanarayana Doolla and TS Bhatti. Load frequency control of an isolated small-hydro power plant with reduced dump load. *IEEE Transactions on Power Systems*, 21(4):1912–1919, 2006.

[80] GL Kusic, JA Sutterfield, AR Caprez, JL Haneline, and BR Bergman. Automatic generation control for hydro systems. *IEEE transactions on energy conversion*, 3(1):33–39, 1988.

[81] TR Foord. Step response of a governed hydrogenerator. In *Proceedings of the Institution of Electrical Engineers*, volume 125, pages 1247–1248. IET, 1978.

[82] C Concordia and LK Kirchmayer. Tie-line power and frequency control of electric power systems [includes discussion]. *Transactions of the American Institute of Electrical Engineers. Part III: Power Apparatus and Systems*, 72(3):562–572, 1953.

[83] C Concordia and LK Kirchmayer. Tie-line power and frequency control of electric power systems-Part II [includes discussion]. *Transactions of the American Institute of Electrical Engineers. Part III: Power Apparatus and Systems*, 73(2):133–146, 1954.

[84] Ilhan Kocaarslan and Ertuğrul Çam. Fuzzy logic controller in interconnected electrical power systems for load-frequency control. *International Journal of Electrical Power & Energy Systems*, 27(8):542–549, 2005.

[85] Debirupa Hore. An analysis of two area load frequency control with different types of feedback controllers. *Int. J. Eng. Res. Technol*, 3(03), 2014.

[86] ML Kothari, J Nanda, DP Kothari, and D Das. Discrete-mode automatic generation control of a two-area reheat thermal system with new area control error. *IEEE Transactions on Power Systems*, 4(2):730–738, 1989.

[87] Rishabh Verma, Shalini Pal, et al. Intelligent automatic generation control of two-area hydrothermal power system using ANN and fuzzy logic. In *International Conference on Communication Systems and Network Technologies*, pages 552–556. IEEE, 2013.

[88] Lalit Chandra Saikia, A Bharali, O Dixit, T Malakar, B Sharma, and S Kouli. Automatic generation control of multi-area hydro system using classical controllers. In *1st International Conference on Power and Energy in NERIST (ICPEN)*, pages 1–6. IEEE, 2012.

[89] Hassan Bevrani, Fatemeh Daneshfar, and Pourya Ranjbar Daneshmand. Intelligent automatic generation control: Multi-agent Bayesian networks approach. In *IEEE International Symposium on Intelligent Control*, pages 773–778. IEEE, 2010.

[90] Hassan A Yousef, AL-Kharusi Khalfan, Mohammed H Albadi, and Nasser Hosseinzadeh. Load frequency control of a multi-area power system: An adaptive fuzzy logic approach. *IEEE Transactions on Power Systems*, 29(4):1822–1830, 2014.

[91] Mohsen Rezaei Adaryani and Hossein Afrakhte. NARMA-L2 controller for three-area load frequency control. In *19th Iranian Conference on Electrical Engineering*, pages 1–6. IEEE, 2011.

[92] Mojtaba Shiroei, Mohammad Reza Toulabi, and Ali Mohammad Ranjbar. Robust multivariable predictive based load frequency control considering generation rate constraint. *International Journal of Electrical Power & Energy Systems*, 46:405–413, 2013.

[93] K Jagatheesan, B Anand, Sourav Samanta, Nilanjan Dey, V Santhi, Amira S Ashour, and Valentina E Balas. Application of flower pollination algorithm in load frequency control of multi-area interconnected power system with nonlinearity. *Neural Computing and Applications*, 28(1):475–488, 2017.

[94] Surya Prakash and Sunil Kumar Sinha. Four area load frequency control of interconnected hydro-thermal power system by intelligent PID control technique. In *Students Conference on Engineering and Systems*, pages 1–6. IEEE, 2012.

[95] Nikolas Flourentzou, Vassilios G Agelidis, and Georgios D Demetriades. VSC-based HVDC power transmission systems: An overview. *IEEE Transactions on power electronics*, 24(3):592–602, 2009.

[96] Zaki E Al-Haiki and Ahmed N Shaikh-Nasser. Power transmission to distant offshore facilities. *IEEE Transactions on Industry Applications*, 47(3):1180–1183, 2011.

[97] B Gemmell, J Dorn, D Retzmann, and D Soerangr. Prospects of multilevel VSC technolo-

gies for power transmission. In *IEEE/PES Transmission and Distribution Conference and Exposition*, pages 1–16. IEEE, 2008.

[98] Cuiqing Du, Evert Agneholm, and Gustaf Olsson. Use of VSC-HVDC for industrial systems having onsite generation with frequency control. *IEEE Transactions on Power Delivery*, 23(4):2233–2240, 2008.

[99] KR Padiyar. *FACTS controllers in power transmission and distribution*. New Age International, 2007.

[100] Cuiqing Du, Evert Agneholm, and Gustaf Olsson. Comparison of different frequency controllers for a VSC-HVDC supplied system. *IEEE Transactions on Power Delivery*, 23(4):2224–2232, 2008.

[101] Issarachai Ngamroo. A stabilization of frequency oscillations using a power modulation control of HVDC link in a parallel AC-DC interconnected system. In *Proceedings of the Power Conversion Conference-Osaka 2002 (Cat. No. 02TH8579)*, volume 3, pages 1405–1410. IEEE, 2002.

[102] Hassan Bevrani. Decentralized robust load-frequency control synthesis in restructured power systems. 2004.

[103] Vaibhav Donde, MA Pai, and Ian A Hiskens. Simulation and optimization in an AGC system after deregulation. *IEEE Transactions on Power Systems*, 16(3):481–489, 2001.

[104] B Delfino, F Fornari, and S Massucco. Load-frequency control and inadvertent interchange evaluation in restructured power systems. *IEE Proceedings-Generation, Transmission and Distribution*, 149(5):607–614, 2002.

[105] GT Chandra Sekhar, Rabindra Kumar Sahu, AK Baliarsingh, and Sidhartha Panda. Load frequency control of power system under deregulated environment using optimal firefly algorithm. *International Journal of Electrical Power & Energy Systems*, 74:195–211, 2016.

[106] SH Hosseini and AH Etemadi. Adaptive neuro-fuzzy inference system based automatic generation control. *Electric Power Systems Research*, 78(7):1230–1239, 2008.

[107] KP Singh Parmar, S Majhi, and DP Kothari. LFC of an interconnected power system with multi-source power generation in deregulated power environment. *International Journal of Electrical Power & Energy Systems*, 57:277–286, 2014.

[108] Miguel Torres and Luiz AC Lopes. An optimal virtual inertia controller to support frequency regulation in autonomous diesel power systems with high penetration of renewables. In *Proceedings of the International Conference on Renewable Energies and Power Quality (ICREPQ 11)*, pages 13–15, 2011.

[109] Lexuan Meng, Jawwad Zafar, Shafi K Khadem, Alan Collinson, Kyle C Murchie, Federico Coffele, and Graeme Burt. Fast frequency response from energy storage systems-A review of grid standards, projects and technical issues. *IEEE Transactions on Smart Grid*, 2019.

[110] O Anaya-Lara, FM Hughes, N Jenkins, and G Strbac. Contribution of DFIG-based wind farms to power system short-term frequency regulation. *IEE Proceedings-Generation, Transmission and Distribution*, 153(2):164–170, 2006.

[111] Yujun Li, Zhao Xu, and Kit Po Wong. Advanced control strategies of PMSG-based wind turbines for system inertia support. *IEEE Transactions on Power Systems*, 32(4):3027–3037, 2017.

[112] Janaka Ekanayake and Nick Jenkins. Comparison of the response of doubly fed and fixed-

speed induction generator wind turbines to changes in network frequency. *IEEE Transactions on Energy conversion*, 19(4):800–802, 2004.

[113] FD Kanellos and ND Hatziargyriou. Control of variable speed wind turbines equipped with synchronous or doubly fed induction generators supplying islanded power systems. *IET Renewable Power Generation*, 3(1):96–108, 2009.

[114] J Driesen and K Visscher. Virtual synchronous generators. In *IEEE Power and Energy Society General Meeting-Conversion and Delivery of Electrical Energy in the 21st Century*, pages 1–3. IEEE, 2008.

[115] Ujjwol Tamrakar, Dipesh Shrestha, Manisha Maharjan, Bishnu Bhattarai, Timothy Hansen, and Reinaldo Tonkoski. Virtual inertia: Current trends and future directions. *Applied Sciences*, 7(7):654, 2017.

[116] Kalyan Chatterjee. Design of dual mode PI controller for load frequency control. *International Journal of Emerging Electric Power Systems*, 11(4), 2011.

[117] Hassan Bevrani and Takashi Hiyama. On load–frequency regulation with time delays: Design and real-time implementation. *IEEE Transactions on Energy Conversion*, 24(1):292–300, 2009.

[118] Krešimir Vrdoljak, Nedjeljko Perić, and Dino Šepac. Optimal distribution of load-frequency control signal to hydro power plants. In *IEEE International Symposium on Industrial Electronics*, pages 286–291. IEEE, 2010.

[119] Prakash K Ray, Soumya R Mohanty, and Nand Kishor. Proportional–integral controller based small-signal analysis of hybrid distributed generation systems. *Energy Conversion and Management*, 52(4):1943–1954, 2011.

[120] Milan Calovic. Linear regulator design for a load and frequency control. *IEEE Transactions on Power Apparatus and Systems*, (6):2271–2285, 1972.

[121] Wayne R Barcelo. Effect of power plant response on optimum load frequency control system design. *IEEE Transactions on Power Apparatus and Systems*, (1):254–258, 1973.

[122] Hassan Bevrani. Robust load frequency controller in a deregulated environment: A/spl mu/-synthesis approach. In *Proceedings of the 1999 IEEE International Conference on Control Applications (Cat. No. 99CH36328)*, volume 1, pages 616–621. IEEE, 1999.

[123] Balarko Chaudhuri, Bikash C Pal, Argyrios C Zolotas, Imad M Jaimoukha, and Tim C Green. Mixed-sensitivity approach to h/sub/spl infin//control of power system oscillations employing multiple FACTS devices. *IEEE Transactions on Power Systems*, 18(3):1149–1156, 2003.

[124] Ismi Rosyiana Fitri, Jung-Su Kim, and Hwachang Song. High-gain disturbance observer-based robust load frequency control of power systems with multiple areas. *Energies*, 10(5):595, 2017.

[125] Yannis Karnavas and Demetrios Papadopoulos. AGC for autonomous power system using combined intelligent techniques. *Electric Power Systems Research*, 62:225–239, 2002.

[126] Ibraheem, Prabhat Kumar, Naimul Hasan, and Nizamuddin. Sub-optimal automatic generation control of interconnected power system using output vector feedback control strategy. *Electric Power Components and Systems*, 40(9):977–994, 2012.

[127] Naimul Hasan, Prabhat Kumar, et al. Sub-optimal automatic generation control of interconnected power system using constrained feedback control strategy. *International Journal of Electrical Power & Energy Systems*, 43(1):295–303, 2012.

[128] Adeniyi Kehinde Onaolapo. *Modeling and recognition of faults in smart distribution grid using machine intelligence technique*. PhD thesis, Durban University of Technology, 2018.

[129] TS Bhatti, Ibraheem, and Nizamuddin. Agc of two area power system interconnected by AC/DC links with diverse sources in each area. *International Journal of Electrical Power and Energy Systems*, 55:297–304, 2014.

[130] Maryam Hassani Variani and Kevin Tomsovic. Distributed automatic generation control using flatness-based approach for high penetration of wind generation. *IEEE Transactions on Power Systems*, 28(3):3002–3009, 2013.

[131] Amin Safari, Farshad Babaei, and Meisam Farrokhifar. A load frequency control using a PSO-based ANN for micro-grids in the presence of electric vehicles. *International Journal of Ambient Energy*, pages 1–13, 2019.

[132] Mohammad-Hassan Khooban. Secondary load frequency control of time-delay stand-alone microgrids with electric vehicles. *IEEE Transactions on Industrial Electronics*, 65(9):7416–7422, 2017.

[133] Jiangbei Xi, Hua Geng, and Geng Yang. Adaptive VSG control of PMSG based WECS for grid frequency response. In *IEEE International Power Electronics and Application Conference and Exposition (PEAC)*, pages 1–5. IEEE, 2018.

[134] Gulshan Sharma, Ibraheem Nasiruddin, KR Niazi, and RC Bansal. Automatic generation control (AGC) of wind power system: An Least Squares-Support Vector Machine (LS-SVM) Radial Basis Function (RBF) kernel approach. *Electric Power Components and Systems*, 46(14-15):1621–1633, 2018.

[135] Rabindra Kumar Sahu, G.T. Chandra Sekhar, and Sidhartha Panda. DE optimized fuzzy

PID controller with derivative filter for LFC of multi source power system in deregulated environment. *Ain Shams Engineering Journal*, 6:511–530, 2015.

[136] Hassan Haes Alhelou, Mohamad-Esmail Hamedani-Golshan, Reza Zamani, Ehsan Heydarian-Forushani, and Pierluigi Siano. Challenges and opportunities of load frequency control in conventional, modern and future smart power systems: A comprehensive review. *Energies*, 11(10):2497, 2018.

[137] P. Rodriguez, I. Candela, and A. Luna. Control of PV generation systems using the synchronous power controller. In *IEEE Energy Conversion Congress and Exposition*, pages 993–998, 2013.

[138] Kürşat Ayan and Ulaş Kılıç. Artificial bee colony algorithm solution for optimal reactive power flow. *Applied Soft Computing*, 12(5):1477–1482, 2012.

[139] Dervis Karaboga, Beyza Gorkemli, Celal Ozturk, and Nurhan Karaboga. A comprehensive survey: Artificial bee colony (ABC) algorithm and applications. *Artificial Intelligence Review*, 42(1):21–57, 2014.

[140] C Sumpavakup, I Srikun, and S Chusanapiputt. A solution to the optimal power flow using artificial bee colony algorithm. In *International Conference on Power System Technology*, pages 1–5. IEEE, 2010.

[141] Haluk Gozde, M Cengiz Taplamacioglu, and Ilhan Kocaarslan. Comparative performance analysis of artificial bee colony algorithm in automatic generation control for interconnected reheat thermal power system. *International Journal of Electrical Power & Energy Systems*, 42(1):167–178, 2012.

[142] Dervis Karaboga and Bahriye Akay. A survey: Algorithms simulating bee swarm intelligence. *Artificial Intelligence Review*, 31(1-4):61–85, 2009.

[143] Dervis Karaboga and Bahriye Basturk. On the performance of artificial bee colony (ABC) algorithm. *Applied Soft Computing*, 8(1):687–697, 2008.

[144] Abou soufyane Benyoucef, Aissa Chouder, Kamel Kara, Santiago Silvestre, and Oussama Ait sahed. Artificial bee colony based algorithm for maximum power point tracking (MPPT) for PV systems operating under partial shaded conditions. *Applied Soft Computing*, 32:38–48, 2015.

[145] F. S. Abu-Mouti and M. E. El-Hawary. Optimal distributed generation allocation and sizing in distribution systems via artificial bee colony algorithm. *IEEE Transactions on Power Delivery*, 26(4):2090–2101, 2011.

[146] Toshio Inoue and Hiroyuki Amano. A thermal power plant model for dynamic simulation of load frequency control. In *2006 IEEE PES Power Systems Conference and Exposition*, pages 1442–1447. IEEE, 2006.

[147] Praghnesh Bhatt, Ranjit Roy, and SP Ghoshal. Optimized multi area AGC simulation in restructured power systems. *International journal of electrical power & energy systems*, 32(4):311–322, 2010.

[148] Rajesh Joseph Abraham, D Das, and Amit Patra. Load following in a bilateral market with local controllers. *International Journal of Electrical Power & Energy Systems*, 33(10):1648–1657, 2011.

[149] Wen Tan, Hongxia Zhang, and Mei Yu. Decentralized load frequency control in deregulated environments. *International Journal of Electrical Power & Energy Systems*, 41(1):16–26, 2012.

[150] Sanjeeth Sewchurran and Innocent E Davidson. Introduction to the South African Re-

newable Energy Grid Code version 2.9 requirements (Part II—Grid code technical requirements). In *IEEE Africon*, pages 1225–1230. IEEE, 2017.

[151] Thongchart Kerdphol, Fathin Rahman, and Yasunori Mitani. Virtual inertia control application to enhance frequency stability of interconnected power systems with high renewable energy penetration. *Energies*, 11(4):981, 2018.

[152] Dervis Karaboga. An idea based on honey bee swarm for numerical optimization. Report, Erciyes University, 2005.

[153] Dervis Karaboga and Bahriye Basturk. A powerful and efficient algorithm for numerical function optimization: Artificial bee colony (ABC) algorithm. *Journal of Global Optimization*, 39(3):459–471, 2007.

[154] Li Bao and Jian-chao Zeng. Comparison and analysis of the selection mechanism in the artificial bee colony algorithm. In *Ninth international conference on hybrid intelligent systems*, volume 1, pages 411–416. IEEE, 2009.

[155] Roland Burns. *Advanced control engineering*. Elsevier, 2001.

[156] Barjeev Tyagi and SC Srivastava. A decentralized automatic generation control scheme for competitive electricity markets. *IEEE Transactions on Power Systems*, 21(1):312–320, 2006.

[157] Hassan Bevrani, Yasunori Mitani, and Kiichiro Tsuji. Robust AGC: Traditional structure versus restructured scheme. *IEEJ Transactions on Power and Energy*, 124(5):751–761, 2004.

[158] Varun Kumar, AS Pandey, and SK Sinha. Grid integration and power quality issues of wind and solar energy system: A review. In *International Conference on Emerging Trends in*

Electrical Electronics & Sustainable Energy Systems (ICETEESES), pages 71–80. IEEE, 2016.

[159] Sanjeeth Sewchurran and Innocent E Davidson. Guiding principles for grid code compliance of large utility scale renewable power plant integration onto South Africa's transmission/distribution networks. In *IEEE International Conference on Renewable Energy Research and Applications (ICRERA)*, pages 528–537. IEEE, 2016.

[160] Siqi Wang and Kevin Tomsovic. Fast frequency support from wind turbine generators with auxiliary dynamic demand control. *IEEE Transactions on Power Systems*, 34(5):3340–3348, 2019.

[161] Anderson F Hoke, Mariko Shirazi, Sudipta Chakraborty, Eduard Muljadi, and Dragan Maksimovic. Rapid active power control of photovoltaic systems for grid frequency support. *IEEE Journal of Emerging and Selected Topics in Power Electronics*, 5(3):1154–1163, 2017.

[162] Mohammad Dreidy, H Mokhlis, and Saad Mekhilef. Inertia response and frequency control techniques for renewable energy sources: A review. *Renewable and Sustainable Energy Reviews*, 69:144–155, 2017.

[163] Hossam Ali, Gaber Magdy, Binbin Li, G Shabib, Adel A Elbaset, Dianguo Xu, and Yasunori Mitani. A new frequency control strategy in an islanded microgrid using virtual inertia control-based coefficient diagram method. *IEEE Access*, 7:16979–16990, 2019.

[164] Chittaranjan Pradhan, Chandrashekhar Narayan Bhende, and Anik Kumar Samanta. Adaptive virtual inertia-based frequency regulation in wind power systems. *Renewable energy*, 115:558–574, 2018.

[165] M. Datta, H. Ishikawa, H. Naitoh, and T. Senjyu. Frequency control improvement in a PV-

diesel hybrid power system with a virtual inertia controller. In *7th IEEE Conference on Industrial Electronics and Applications (ICIEA)*, pages 1167–1172, 2012.

[166] Thongchart Kerdphol, Fathin Saifur Rahman, Yasunori Mitani, Masayuki Watanabe, and Sinan Küfeoğlu. Robust virtual inertia control of an islanded microgrid considering high penetration of renewable energy. *IEEE Access*, 6:625–636, 2017.

[167] Pranjal Saxena, Navdeep Singh, and Ashok Kumar Pandey. Enhancing the dynamic performance of microgrid using derivative controlled solar and energy storage based virtual inertia system. *Journal of Energy Storage*, 31:101613, 2020.

[168] N. Sockeel, J. Gafford, B. Papari, and M. Mazzola. Virtual Inertia Emulator-Based Model Predictive Control for Grid Frequency Regulation Considering High Penetration of Inverter-Based Energy Storage System. *IEEE Transactions on Sustainable Energy*, 11(4):2932–2939, 2020.

[169] Javad Khazaei, Zhenghong Tu, and Wenxin Liu. Small-Signal Modeling and Analysis of Virtual Inertia-Based PV Systems. *IEEE Transactions on Energy Conversion*, 35(2):1129–1138, 2020.

[170] Ahmed M Othman and Attia A El-Fergany. Adaptive virtual-inertia control and chicken swarm optimizer for frequency stability in power-grids penetrated by renewable energy sources. *Neural Computing and Applications*, pages 1–14, 2020.

[171] Thongchart Kerdphol, Fathin Saifur Rahman, Masayuki Watanabe, and Yasunori Mitani. Optimization of Virtual Inertia Control Considering System Frequency Protection Scheme. In *Virtual Inertia Synthesis and Control*, pages 227–247. Springer.

[172] Sepehr Saadatmand, Pourya Shamsi, and Mehdi Ferdowsi. Adaptive critic design-based re-

inforcement learning approach in controlling virtual inertia-based grid-connected inverters. *International Journal of Electrical Power & Energy Systems*, 127:106657, 2021.

[173] V. Skiparev, J. Belikov, and E. Petlenkov. Reinforcement Learning based Approach for Virtual Inertia Control in Microgrids with Renewable Energy Sources. In *2020 IEEE PES Innovative Smart Grid Technologies Europe (ISGT-Europe)*, pages 1020–1024, 2020.

[174] F. Yao, J. Zhao, X. Li, L. Mao, and K. Qu. RBF Neural Network Based Virtual Synchronous Generator Control with Improved Frequency Stability. *IEEE Transactions on Industrial Informatics*, pages 1–1, 2020.

[175] F. J. Lin, K. H. Tan, and C. M. Shih. Distributed Generator with Virtual Inertia Using Intelligent Controller for Grid-Connected Microgrid. In *2020 IEEE International Conference on Fuzzy Systems (FUZZ-IEEE)*, pages 1–8, 2020.

[176] M. Datta and T. Senjyu. Fuzzy control of distributed PV inverters/energy storage systems/electric vehicles for frequency regulation in a large power system. *IEEE Transactions on Smart Grid*, 4(1):479–488, 2013.

[177] S. Zhang, Y. Mishra, and M. Shahidehpour. Fuzzy-logic based frequency controller for wind farms augmented with energy storage systems. *IEEE Transactions on Power Systems*, 31(2):1595–1603, 2016.

[178] H. Bevrani, F. Habibi, P. Babahajyani, M. Watanabe, and Y. Mitani. Intelligent frequency control in an AC microgrid: online PSO-based fuzzy tuning approach. *IEEE Transactions on Smart Grid*, 3(4):1935–1944, 2012.

[179] Li Yang and Zhijian Hu. Implementation of Dynamic Virtual Inertia Control of Supercapacitors for Multi-Area PV-Based Microgrid Clusters. *Sustainability*, 12(8):3299, 2020.

[180] Yazmin Maldonado and Oscar Castillo. Genetic design of an interval type-2 fuzzy controller for velocity regulation in a DC motor. *International Journal of Advanced Robotic Systems*, 9(5):204, 2012.

[181] M. Khooban, M. Gheisarnejad, N. Vafamand, and J. Boudjadar. Electric vehicle power propulsion system control based on time-varying fractional calculus: Implementation and experimental results. *IEEE Transactions on Intelligent Vehicles*, 4(2):255–264, 2019.

[182] S. Krishnama Raju and G. N. Pillai. Design and implementation of Type-2 fuzzy logic controller for DFIG-based wind energy systems in distribution networks. *IEEE Transactions on Sustainable Energy*, 7(1):345–353, 2016.

[183] Engin Yesil. Interval type-2 fuzzy PID load frequency controller using Big Bang–Big Crunch optimization. *Applied Soft Computing*, 15:100–112, 2014.

[184] Meysam Gheisarnejad, Mohammad-Hassan Khooban, and Tomislav Dragicevic. The future 5g network based secondary load frequency control in maritime microgrids. *IEEE Journal of Emerging and Selected Topics in Power Electronics*, 2019.

[185] R Vijaya Santhi, KR Sudha, and S Prameela Devi. Robust load frequency control of multi-area interconnected system including SMES units using Type-2 fuzzy controller. In *IEEE International Conference on Fuzzy Systems (FUZZ-IEEE)*, pages 1–7. IEEE, 2013.

[186] Arabinda Behera, Debashree Guha Adhya, and Sanjoy K Parida. Analysis of robust interval type-2 fuzzy PID controller for AGC in a restructured power system. In *7th International Conference on Power Systems (ICPS)*, pages 168–174. IEEE, 2017.

[187] Fahad S Abu-Mouti and ME El-Hawary. Optimal distributed generation allocation and sizing in distribution systems via artificial bee colony algorithm. *IEEE Transactions on Power Delivery*, 26(4):2090–2101, 2011.

[188] Elyas Rakhshani and Pedro Rodriguez. Inertia emulation in AC/DC interconnected power systems using derivative technique considering frequency measurement effects. *IEEE Transactions on Power Systems*, 32(5):3338–3351, 2016.

[189] Juan Manuel Mauricio, Alejandro Marano, Antonio Gómez-Expósito, and José Luis Martínez Ramos. Frequency regulation contribution through variable-speed wind energy conversion systems. *IEEE Transactions on Power Systems*, 24(1):173–180, 2009.

[190] Gerasimos Rigatos. *Intelligent renewable energy systems: modelling and control*. Springer, 2016.

[191] Thongchart Kerdphol, Masayuki Watanabe, Komsan Hongesombut, and Yasunori Mitani. Self-adaptive virtual inertia control-based fuzzy logic to improve frequency stability of microgrid with high renewable penetration. *IEEE Access*, 7:76071–76083, 2019.

[192] J. M. Mendel and R. I. B. John. Type-2 fuzzy sets made simple. *IEEE Transactions on Fuzzy Systems*, 10(2):117–127, 2002.

[193] Jerry M Mendel, Robert I John, and Feilong Liu. Interval type-2 fuzzy logic systems made simple. *IEEE transactions on fuzzy systems*, 14(6):808–821, 2006.

[194] Chengdong Li, Guiqing Zhang, Jianqiang Yi, and Ming Wang. Uncertainty degree and modeling of interval type-2 fuzzy sets: definition, method and application. *Computers & Mathematics with Applications*, 66(10):1822–1835, 2013.

[195] Qilian Liang and Jerry M Mendel. Interval type-2 fuzzy logic systems: Theory and design. *IEEE Transactions on Fuzzy systems*, 8(5):535–550, 2000.

[196] M. Khooban, M. Gheisarnejad, N. Vafamand, M. Jafari, S. Mobayen, T. Dragicevic, and J. Boudjadar. Robust frequency regulation in mobile microgrids: HIL implementation. *IEEE Systems Journal*, 13(4):4281–4291, 2019.

[197] O Abedinia, Mohammad S Naderi, and A Ghasemi. Robust lfc in deregulated environment: Fuzzy pid using hbmo. In *10th International Conference on Environment and Electrical Engineering*, pages 1–4. IEEE, 2011.

[198] Yi Han, Peter Michael Young, Abhishek Jain, and Daniel Zimmerle. Robust control for microgrid frequency deviation reduction with attached storage system. *IEEE Transactions on Smart Grid*, 6(2):557–565, 2014.

[199] Ning Chuang. Robust h^{∞} load-frequency control in interconnected power systems. *IET Control Theory & Applications*, 10(1):67–75, 2016.

[200] Engang Tian and Chen Peng. Memory-based event-triggering h^{∞} load frequency control for power systems under deception attacks. *IEEE Transactions on Cybernetics*, 2020.

[201] Zhaojian Wang, Feng Liu, Changhong Zhao, Zhiyuan Ma, and Wei Wei. Distributed optimal load frequency control considering nonsmooth cost functions. *Systems & Control Letters*, 136:104607, 2020.

[202] Hassan Bevrani, Farshid Habibi, Poya Babahajyani, Masayuki Watanabe, and Yasunori Mitani. Intelligent frequency control in an AC microgrid: Online PSO-based fuzzy tuning approach. *IEEE Transactions on Smart Grid*, 3(4):1935–1944, 2012.

[203] A. Ghafouri, J. Milimonfared, and G. B. Gharehpetian. Fuzzy-adaptive frequency control of power system including microgrids, wind farms, and conventional power plants. *IEEE Systems Journal*, 12(3):2772–2781, 2018.

[204] Hami Hagras. Type-2 FLCs: A new generation of fuzzy controllers. *IEEE Computational Intelligence Magazine*, 2(1):30–43, 2007.

[205] Matthew D Schrieber and Mohammad Biglarbegian. Hardware implementation and performance comparison of interval type-2 fuzzy logic controllers for real-time applications. *Applied Soft Computing*, 32:175–188, 2015.

[206] H. Hassani, J. Zarei, R. Razavi-Far, and M. Saif. Robust interval Type-2 fuzzy observer for fault detection of networked control systems subject to immeasurable premise variables. *IEEE Systems Journal*, 13(3):2954–2965, 2019.

[207] Ravi Shankar, SR Pradhan, Kalyan Chatterjee, and Rajasi Mandal. A comprehensive state of the art literature survey on LFC mechanism for power system. *Renewable and Sustainable Energy Reviews*, 76:1185–1207, 2017.

[208] Shreyas Sundaram and Christoforos N Hadjicostis. Delayed observers for linear systems with unknown inputs. *IEEE Transaction on Automatic Control*, 52(2):334–339, 2007.

[209] Atefe Termehchy and Ahmad Afshar. A novel design of unknown input observer for fault diagnosis in non-minimum phase systems. *IFAC Proceedings Volumes*, 47(3):8552–8557, 2014.

[210] Amir Ameli, Ali Hooshyar, Ehab F El-Saadany, and Amr M Youssef. Attack detection and identification for automatic generation control systems. *IEEE Transactions on Power Systems*, 33(5):4760–4774, 2018.

[211] H. M. Tran and H. Trinh. Distributed functional observer based fault detection for interconnected time-delay systems. *IEEE Systems Journal*, 13(1):940–951, 2019.

[212] Hassan Haes Alhelou, Mohamad Esmail Hamedani Golshan, and Nikos D Hatziargyriou. A decentralized functional observer based optimal LFC considering unknown inputs, uncertainties, and cyber-attacks. *IEEE Transactions on Power Systems*, 34(6):4408–4417, 2019.

[213] Hassan Haes Alhelou, Mohamad Esmail Hamedani Golshan, and Nikos D Hatziargyriou. Deterministic dynamic state estimation-based optimal LFC for interconnected power systems using unknown input observer. *IEEE Transactions on Smart Grid*, 2019.

[214] Oveis Abedinia, Heidarali Shayanfar, Bart Wyns, and Ali Ghasemi. Design of robust PSS to improve stability of composed LFC and AVR using ABC in deregulated environment. In *13th International conference on Artificial Intelligence (ICAI 2011)*, pages 82–88, 2011.

[215] Thongchart Kerdphol, Fathin Saifur Rahman, Masayuki Watanabe, and Yasunori Mitani. Robust virtual inertia control of a low inertia microgrid considering frequency measurement effects. *IEEE Access*, 7:57550–57560, 2019.

[216] Yang Chen, DZ Wang, and Wu Ning. Studies on centroid type-reduction algorithms for general type-2 fuzzy logic systems. *International Journal of Innovative Computing, Information and Control*, 11(6):1987–2000, 2015.

Appendix A

Simulation Parameters for Chapter 3

Table A.1 System model parameters.

Parameter	**Area 1** ($i = 1, 2$)	**Area 2** ($i = 3, 4$)
Original power system data		
Area participation factor, apf	0.5, 0.5	0.6, 0.4
Turbine time constant, T_{ti} (s)	0.32, 0.3	0.3, 0.3
Governor time constant, T_{gi} (s)	0.06, 0.08	0.06, 0.07
Droop constant, R_i (Hz/p.u MW)	2.4, 2.5	2.5, 2.7
Damping coefficient, D (p.u MW/Hz)	0.0098	0.0098
System inertia constant, H (p.u MWs)	0.098	0.1225
Frequency bias factor, β_i (p.u MW/Hz)	0.425	0.396
Synchronizing coefficient, T_{12}	0.245	
Area control error gain, K_i	0.7	0.7
Area capacity ratio, α_{12}	-1	
Additional data for the Modified system		
Wind turbine time constant, T_{wt} (s)	1.5	1.5
HVDC time constant, T_{dc} (s)	0.2	
WECS virtual inertia gain, K_w	-0.5767	-0.669

Appendix B

State Matrix for system in Chapter 3

$$A = \begin{bmatrix} A_{11} & A_{12} \\ A_{21} & A_{22} \end{bmatrix}$$

$$A_{11} = \begin{bmatrix} \frac{-D_1}{2H_1} & 0 & \frac{1}{2H_1} & \frac{1}{2H_1} & 0 & 0 & 0 & \\ 0 & \frac{-D_2}{2H_2} & 0 & 0 & \frac{1}{2H_2} & \frac{1}{2H_2} & 0 & 0 \\ 0 & 0 & \frac{-1}{T_{t1}} & 0 & 0 & 0 & \frac{1}{T_{t1}} & 0 \\ 0 & 0 & 0 & \frac{-1}{T_{t2}} & 0 & 0 & 0 & \frac{1}{T_{t2}} \\ 0 & 0 & 0 & 0 & \frac{-1}{T_{t3}} & 0 & 0 & 0 \\ 0 & 0 & 0 & 0 & 0 & \frac{-1}{T_{t4}} & 0 & 0 \\ \frac{-1}{R_1 T_{g1}} & 0 & 0 & 0 & 0 & 0 & \frac{-1}{T_{g1}} & 0 \\ \frac{-1}{R_2 T_{g2}} & 0 & 0 & 0 & 0 & 0 & 0 & \frac{-1}{T_{g2}} \end{bmatrix}$$

$$A_{12} = \begin{bmatrix} 0 & 0 & 0 & 0 & \frac{-1}{2H_1} & \frac{-1}{2H_1} & \frac{1}{2H_1} & 0 \\ 0 & 0 & 0 & 0 & \frac{-\alpha_{12}}{2H_2} & \frac{-\alpha_{12}}{2H_2} & 0 & \frac{1}{2H_2} \\ 0 & 0 & 0 & 0 & 0 & 0 & 0 & 0 \\ 0 & 0 & 0 & 0 & 0 & 0 & 0 & 0 \\ \frac{1}{T_{t3}} & 0 & 0 & 0 & 0 & 0 & 0 & 0 \\ 0 & \frac{1}{T_{t4}} & 0 & 0 & 0 & 0 & 0 & 0 \\ 0 & 0 & \frac{apf_1}{T_{g1}} & 0 & 0 & 0 & 0 & 0 \\ 0 & 0 & \frac{apf_2}{T_{g2}} & 0 & 0 & 0 & 0 & 0 \end{bmatrix}$$

$$A_{21} = \begin{bmatrix} 0 & \frac{-1}{R_3 T_{g3}} & 0 & 0 & 0 & 0 & 0 & 0 \\ 0 & \frac{-1}{R_4 T_{g4}} & 0 & 0 & 0 & 0 & 0 & 0 \\ -\beta_1 K_1 & 0 & 0 & 0 & 0 & 0 & 0 & 0 \\ 0 & -\beta_2 K_2 & 0 & 0 & 0 & 0 & 0 & 0 \\ 2\pi T_{12} & -2\pi T_{12} & 0 & 0 & 0 & 0 & 0 & 0 \\ \frac{K_{dc}}{T_{dc}} & \frac{-K_{dc}}{T_{dc}} & 0 & 0 & 0 & 0 & 0 & 0 \\ \frac{-D_1 K_{w1}}{2H_1 T_{w1}} & 0 & \frac{K_{w1}}{2H_1 T_{w1}} & \frac{K_{w1}}{2H_1 T_{w1}} & 0 & 0 & 0 & 0 \\ 0 & \frac{-D_2 K_{w2}}{2H_2 T_{w2}} & 0 & 0 & \frac{K_{w2}}{2H_2 T_{w2}} & \frac{K_{w2}}{2H_2 T_{w2}} & 0 & 0 \end{bmatrix}$$

$$A_{22} = \begin{bmatrix} \frac{-1}{T_g3} & 0 & 0 & \frac{apf_3}{T_g3} & 0 & 0 & 0 & 0 \\ 0 & \frac{-1}{T_g4} & 0 & \frac{apf_4}{T_g4} & 0 & 0 & 0 & 0 \\ 0 & 0 & 0 & 0 & -K_1 & -K_1 & 0 & 0 \\ 0 & 0 & 0 & 0 & -\alpha_{12}K_2 & -\alpha_{12}K_2 & 0 & 0 \\ 0 & 0 & 0 & 0 & 0 & 0 & 0 & 0 \\ 0 & 0 & 0 & 0 & 0 & \frac{-1}{T_dc} & 0 & 0 \\ 0 & 0 & 0 & 0 & \frac{-K_{w1}}{2H_1T_{w1}} & \frac{-K_{w1}}{2H_1T_{w1}} & \frac{-K_{w1}}{2H_1T_{w1}} - \frac{-1}{T_{w1}} & 0 \\ 0 & 0 & 0 & 0 & \frac{-\alpha_{12}K_{w2}}{2H_2T_{w2}} & \frac{-\alpha_{12}K_{w2}}{2H_2T_{w2}} & 0 & \frac{-K_{w2}}{2H_2T_{w2}} - \frac{-1}{T_{w2}} \end{bmatrix}$$